ACTA TECHNICA

ACTA TECHNICA

A JOURNAL OF THE HUNGARIAN ACADEMY OF SCIENCES

Acta Technica publishes original papers, preliminary reports and reviews in English, which contribute to the advancement of engineering sciences.
Acta Technica is published by

Subscription information

Orders should be addressed to

or to its representatives abroad

Acta Technica is indexed in Current Contents

ACTA TECHNICA

VOLUME 95 NOS 1—4

BOOK REVIEWS

ABSTRACTS

CONTENTS

BOOK REVIEWS

ABSTRACTS

ACTA
TECHNICA

ACADEMIAE SCIENTIARUM HUNGARICAE

VOLUME 95
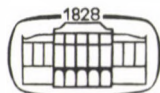
BOUNDS FOR THE BUCKLING LOAD OF A BAR
WITH ONE FIXED END

J. BARTA*

The paper deals with establishing lower and upper bounds for the buckling load of a slender elastic bar whose one end is fixed. For this purpose, two theorems are presented. For sake of generality, variable flexural rigidity, variable sectional force and elastic fixing will be considered. The elaboration of an example shows the details of computation.

Several authors have dealt with computing the buckling load of the compressed bar whose one end is fixed. Recently, this theme was discussed by P. Csonka [1]. Much has been written on finding upper bounds for buckling load but comparatively little on finding lower bounds. From the point of view of structural safety, the lower bounds are more important than the upper ones. Both lower and upper bounds will be established in the following treatment and for the sake of generality, variable flexural rigidity, variable sectional force and elastic fixing will be considered.

Description of the bar and of its load

The elastic bar is sketched in Fig. 1. It is elastically fixed at its lower end and free at its upper end. The cross section of the bar varies or its constant. l is the length of the bar and $E(x)$ is the modulus of elasticity. $I(x)$ is the moment of inertia of the cross section. Let $R(x)$ be determined by formula

$$R(x) = E(x)I(x) . \tag{1}$$

$R(x)$ is called the flexural rigidity of the bar. It is to be understood in the following sense: between curvature $y''(x)$ and bending moment $M(x)$, the relation

$$R(x)y''(x) = M(x) \tag{2}$$

exists. K is the rotational rigidity of the fixing. It is to be understood in the following sense: between rotational angle $y'(0)$ and fixing moment $M(0)$, the relation

$$Ky'(0) = M(0) \tag{3}$$

exists. The particular case $K = +\infty$ means that the fixing is perfectly rigid, (Fig. 4).

---

* Prof. Dr. J. Barta, József körút 35, H-1085 Budapest, Hungary
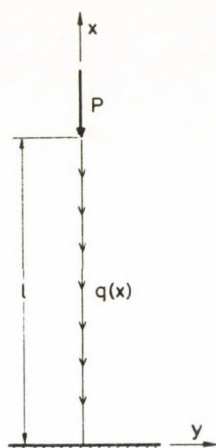
Fig. 1. Loads P and $q(x)$ are given. The stability of this straight equilibrium form is to be investigated
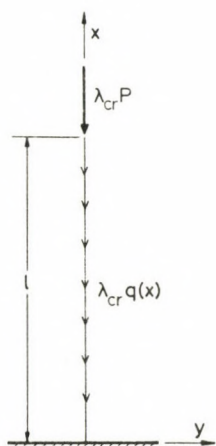
Fig. 2. Straight equilibrium form of the bar for the critical load

Two kinds of active forces act upon the bar. One acts on the upper end of the bar and has the magnitude P. The other one acts along the length of the bar and has the intensity $q(x)$. Both P and $q(x)$ are directed vertically downwards. P is a given constant and $q(x)$ is a given function. Let function $S(x)$ be defined by formula

$$S(x) = P + \int_x^l q(x)\, \mathrm{d}x \,. \tag{4}$$

It can be seen that $S(x)$ is the sectional force.
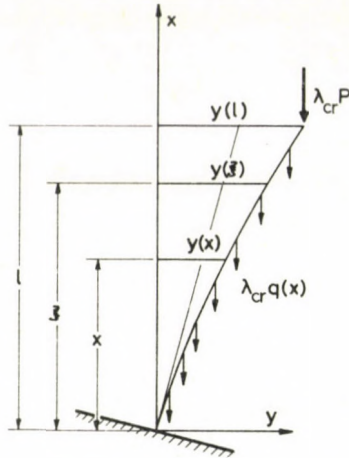
Fig. 3. Bent equilibrium form of the bar for the critical load
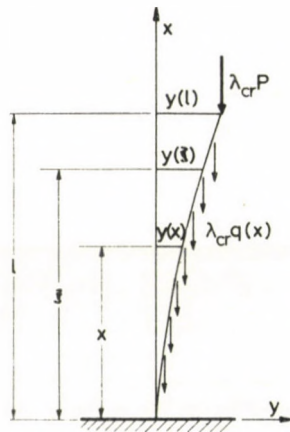
Fig. 4. Bent equilibrium form of the bar for the critical load if the fixing is perfectly rigid

In theorems I and II, $R(x)$ and $S(x)$ are to be considered as given functions, K as given positive constant.

In this paper, $[\dots]_{min}$ and $[\dots]_{max}$ denotes the smallest and the greatest value of $[\dots]$ for $0 \leq x \leq l$, respectively.

Stability problem

The structure and its loading forces

$$P \quad \text{and} \quad q(x)$$

are given in Fig. 1. We wish to investigate whether this straight equilibrium form is stable. For this purpose we shall scrutinise the equilibrium state under the action of loading forces

$$\lambda P \quad \text{and} \quad \lambda q(x).$$

Here, λ is a parameter. Let λ_{cr} denote the critical value of λ, i.e. the smallest value of λ at which not only a straight equilibrium form (Fig. 2) but also a bent equilibrium form (Fig. 3) is possible. The load consisting of loading forces

$$\lambda_{cr} P \quad \text{and} \quad \lambda_{cr} q(x)$$

is called the buckling load of the bar. For estimating λ_{cr}, one can employ either of the two following theorems.

Theorem I

≪ If $U(x)$ is a twice differentiable non-negative real function in interval $0 \leqq x \leqq l$ and satisfies the boundary conditions

$$\frac{U(0)}{U'(0)} = \frac{R(0)}{K}, \qquad U'(l) = 0 \tag{5}, (6)$$

then the relation

$$\left[-\frac{(RU')'}{SU} \right]_{\min} \leqq \lambda_{cr} \leqq \left[-\frac{(RU')'}{SU} \right]_{\max} \tag{7}$$

holds in interval $0 \leqq x \leqq l$. If the fixing is perfectly rigid ($K = +\infty$), Eq. (5) assumes the form

$$U(0) = 0. \gg \tag{8}$$

Theorem II

≪ If $V(x)$ is a differentiable real function in interval $0 \leqq x \leqq l$, and satisfies the boundary conditions

$$V(0) = \frac{-K}{R(0)}, \qquad V(l) = 0 \tag{9}, (10)$$

then the relation

$$\left[\frac{R'V+R(V'-V^2)}{S}\right]_{min} \leq \lambda_{cr} \leq \left[\frac{R'V+R(V'-V^2)}{S}\right]_{max} \tag{11}$$

holds in interval $0 \leq x \leq l$. If the fixing is perfectly rigid $(K = +\infty)$, Eq. (9) assumes the form

$$V(0) = -\infty \; . \; \gg \tag{12}$$

Units

If the unit of length is cm and the unit of force is kp, the units of quantities emerging in this paper are as follows:

$x, l, y(x)$	cm	$P, S(x)$	kp
$E(x)$	kp cm^{-2}	$q(x)$	kp cm^{-1}
$I(x)$	cm^4	$U(x)$	arbitrary unit
$R(x)$	kp cm^2	$V(x)$	cm^{-1}
$K, M(x)$	kp cm		

$Y(x)$, λ, λ_{cr} are abstract numbers.

Proof of the theorems

Let $y(x)$ denote the lateral deflection which belongs to λ_{cr}. For $y(x)$, according to (2), equation

$$R(x)y''(x) = [y(l)-y(x)]\lambda_{cr}P + \int_{\zeta=x}^{\zeta=l} [y(\zeta)-y(x)]\lambda_{cr}q(\zeta)\,d\zeta \tag{13}$$

holds. The right-hand side of (13) expresses the bending moment. By differentiating with respect to x on both sides of (13), equation

$$[R(x)y''(x)]' = -\lambda_{cr}y'(x)\left[P + \int_x^l q(x)\,dx\right] \tag{14}$$

arises. Using notation (4), symbols $R = R(x)$, $S = S(x)$ and introducing the notation $Y = Y(x) = y'(x)$, we obtain

$$(RY')' = -\lambda_{cr}YS \; . \tag{15}$$

$Y(x)$ is the rotational angle belonging to λ_{cr}. Thus $Y(x)$ satisfies the differential equation (15). Eq. (2) yields

$$R(0)Y''(0) = M(0) \; . \tag{16}$$

From (3) and (16) we obtain the relation

$$K Y(0) = R(0) Y'(0).$$ (17)

Equation

$$Y'(l) = 0$$ (18)

expresses the fact that the upper end of the bar is free. (18) follows from (13) already. Thus, $Y(x)$ satisfies not only the differential equation (15), but also the boundary conditions (17) and (18).

Making use of Eq. (15), we arrive at

$$\lambda_{cr} = -\frac{(R Y')'}{S Y}$$ (19)

Instead of (19),

$$\lambda_{cr} = -\frac{(R U')'}{S U} + \frac{[R(U'Y - U Y')]'}{S U Y}$$ (20)

can be written because after carrying out the differentiations, both (19) and (20) assume the same form.

Let us consider the last fraction of (20). We are interested in the values which this fraction assumes for $0 \leq x \leq l$. To prove theorem I, it is sufficient to demonstrate that among the values of the fraction there are both non-positive and non-negative ones. This demonstration can be performed in the following manner. The denominator does not change its sign for $0 \geq x \leq l$, (see the Appendix). Among the values of the numerator, the zero occurs because

$$\int_0^l [R(U'Y - U Y')]' dx = [R(U'Y - U Y')]_0^l = 0.$$ (21)

In (21), the boundary conditions (5), (6), (17), (18) were taken into account. With this, theorem I is proved.

The particular case $K = +\infty$ does not claim an extra proof, since the above proof refers also to this case.

In order to prove theorem II, we use theorem I. Let $V(x)$ be a differentiable function in interval $0 \leq x \leq l$, satisfying the boundary conditions (9) and (10). Consequently, a function $U(x)$ which is defined by formula

$$U(x) = \exp\left[-\int_0^x V(x)\,dx\right],$$ (22)

fulfils the premise of theorem I. Hence, (22) can be substituted to (7). In this way, (11) arises. In a similar way, also formula (12) presents itself. With this, theorem II is proved.

Example

A bar sketched in Fig. 1 has the form shown in Fig. 5. It is a slender truncated wedge. l is the length of the bar. The modulus E is constant. In the sense of formulas (1), (2), (3) and (4),

$$
\left.
\begin{aligned}
R &= \left(1 - 0.7\frac{x}{l}\right)R_0, \\
S &= \left(1 - 0.2\frac{x}{l}\right)^2 S_0, \\
K &= \frac{R_0}{l}
\end{aligned}
\right\} \tag{23}
$$

are given.

Let us establish lower and upper bounds for λ_{cr}. In order to perform this task, theorems I and II will be used.
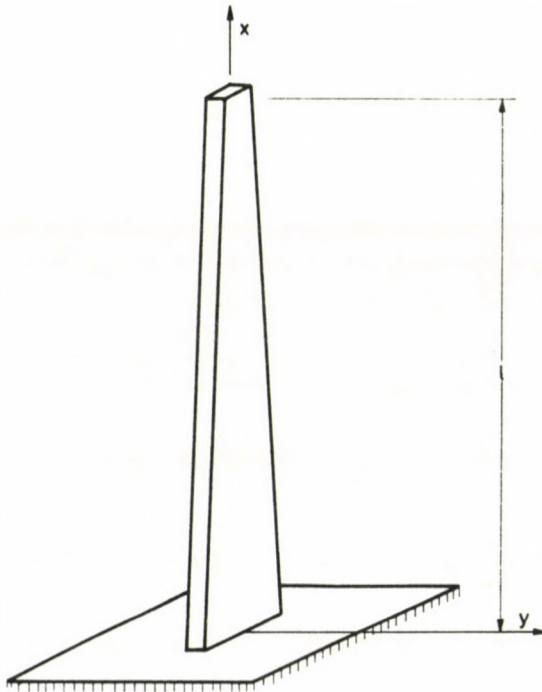
Fig. 5. In the example, the form of the bar is a slender truncated wedge

Using theorem I and data (23), relation (7) becomes

$$
\left[\frac{\frac{0.7}{l} U' - \left(1 - 0.7\frac{x}{l}\right) U''}{\left(1 - 0.2\frac{x}{l}\right)^2 U} \cdot \frac{R_0}{S_0} \right]_{\min} \leq \lambda_{\mathrm{cr}} \leq \left[\begin{array}{c} \cdots \\ \cdots \end{array} \right]_{\max}. \tag{24}
$$

Here, function $U(x)$ must be chosen. Firstly, let $U(x)$ be assumed at random, say

$$
U = 2l^2 + 2lx - x^2. \tag{25}
$$

This function is non-negative for $0 \leq x \leq l$ and satisfies conditions (5) and (6). Substituting (25) to (24), relation

$$
\left[\frac{3.4 - 2.8\frac{x}{l}}{\left(1 - 0.2\frac{x}{l}\right)^2 \left[2 + 2\frac{x}{l} - \left(\frac{x}{l}\right)^2\right]} \cdot \frac{R_0}{l^2 S_0} \right]_{\min} \leq \lambda_{\mathrm{cr}} \leq \left[\begin{array}{c} \cdots \\ \cdots \end{array} \right]_{\max} \tag{26}
$$

arises. After performing the computation, from (26), the relation

$$
0.31 \frac{R_0}{l^2 S_0} \leq \lambda_{\mathrm{cr}} \leq 1.70 \frac{R_0}{l^2 S_0}. \tag{27}
$$

follows. Thus, assumption (25) has led to bounding (27). This bounding is too loose. The reason for this is that function (25) has been assumed at random only. By attempt, the assumption

$$
U = 4l^4 + 4l^3 x - x^4 \tag{28}
$$

has been found. This assumption leads to

$$
0.70 \frac{R_0}{l^2 S_0} \leq \lambda_{\mathrm{cr}} \leq 1.01 \frac{R_0}{l^2 S_0}. \tag{29}
$$

Using theorem II and data (23), relation (11) becomes

$$
\left[\frac{-\frac{0.7}{l} V + \left(1 - 0.7\frac{x}{l}\right)(V' - V^2)}{1 - 0.2\frac{x}{l}\bigg)^2} \cdot \frac{R_0}{S_0} \right]_{\min} \leq \lambda_{\mathrm{cr}} \leq \left[\begin{array}{c} \cdots \\ \cdots \end{array} \right]_{\max}. \tag{30}
$$

The very simple assumption

$$
V = \frac{x}{l^2} - \frac{1}{l} \tag{31}
$$

leads to

$$
0.46 \frac{R_0}{l^2 S_0} \leq \lambda_{\mathrm{cr}} \leq 1.06 \frac{R_0}{l^2 S_0}. \tag{32}
$$

Assumption

$$V = -\frac{5.2}{l} - \frac{2.9x}{l^2} - \frac{3.3x^2}{l^3} + \frac{4.2}{l}\exp\frac{x}{l} \qquad (33)$$

has been found by attempt. It leads to

$$0.81\frac{R_0}{l^2 S_0} \leq \lambda_{cr} \leq 1.20\frac{R_0}{l^2 S_0}. \qquad (34)$$

From (29) and (34), the bounding

$$0.81\frac{R_0}{l^2 R_0} \leq \lambda_{cr} \leq 1.01\frac{R_0}{l^2 S_0} \qquad (35)$$

follows. One concludes from bounding (35) that the mean value

$$0.91\frac{R_0}{l^2 R_0} \qquad (36)$$

differs from the rigorous value of λ_{cr} by less than twelve per cent. By further attempts, the accuracy of the result would be increased. Meanwhile, the rigorous value of λ_{cr} is remained unknown.

Remarks on functions $U(x)$ and $V(x)$

First of all, $U(x)$ and $V(x)$ must be real and satisfy the stipulations prescribed in theorems I and II, namely
    equations (5), (6), the twofold differentiability and the non-negativity for $U(x)$,
    equations (9), (10) and the differentiability for $V(x)$.
    After having fulfilled these stipulations, one can choose $U(x)$ and $V(x)$ arbitrarily because theorems I and II remain always valid. Of course, when formula (7) or (11) will be used, one endeavours to get narrow bounds, that is, great minimum and small maximum. In the above example, suitable $U(x)$ and $V(x)$ have been chosen by attempt, although a systematic procedure (i.e. the method of iteration, [2]) is well known for the same purpose, it seemed to be not quick enough in the above example.
    The basic idea of this paper originates from the fact that both the greatest minimum and the smallest maximum equal to the rigorous value of λ_{cr}. The notions "the greatest minimum" and "the smallest maximum" occur not only in the stability problem just discussed but also in other problems [3].
    An advantage of the bounding procedure presented in this paper is expressed by the following two statements:
    1. By a suitable choice of $U(x)$, the bounding (7) becomes reasonably narrow.
    2. By a suitable choice of $V(x)$, the bounding (11) becomes reasonably narrow.
    The proof of these two statements will be performed in the following. $Y(x)$ is defined as the first eigenfunction of the eigenvalue problem (15), (17), (18). If $Y(x)$ were

chosen for $U(x)$ and $Y'(x)/Y(x)$ were chosen for $V(x)$, both (7) and (11) would become

$$-\frac{(RY')'}{SY} \leqq \lambda_{\mathrm{cr}} \leqq -\frac{(RY')'}{SY} \tag{37}$$

that is

$$-\frac{(RY')'}{SY} = \lambda_{\mathrm{cr}} \tag{38}$$

which is nothing else but equation (15).

Appendix

$S(x) U(x) Y(x)$ is a denominator in equation (20). We have to demonstrate that this denominator does not change its sign for $0 \leqq x \leqq l$. The sectional force $S(x)$ is compression and therefore we measure its magnitude by a positive number. According to premise of theorem I, $U(x)$ does not change its sign for $0 \leqq x \leqq l$. Thus we have to prove that $Y(x)$ does not change its sign for $0 \leqq x \leqq l$. We perform the proof as follows.

$Y(x)$ is the rotational angle belonging to λ_{cr}. $Y(x)$ and λ_{cr} are determined by equations (15), (17), (18) and by the stipulation that λ_{cr} is the smallest of the possible values λ. Equations

$$\begin{aligned}
(R\Phi')' &= -\lambda\Phi S \qquad \text{for} \quad 0 \leqq x \leqq l, \\
K\Phi(0) &= R(0)\Phi'(0), \\
\Phi'(l) &= 0
\end{aligned} \tag{39}$$

expresses an eigenvalue problem. $\Phi(x)$ is called the eigenfunction, λ is called the eigenvalue. Comparing (15), (17), (18) with (39), it can be seen that $\Phi = Y(x)$ is the first eigenfunction of the eigenvalue problem (39). Eigenvalue Theory [4, 5, 6] demonstrates that in the case in question, the first eigenfunction does not change its sign for $0 \leqq x \leqq l$.

References

1. Csonka, P.: Stability of a bar elastically built-in at one of its extremities. Acta Techn. Hung. 92 (1981), pp. 33—43
2. Kármán, Th. and M. A. Biot: Mathematical methods in engineering. First ed., p. 313
3. Collatz, L.: Eigenwertaufgaben mit technischen Anwendungen. Akademische Verlagsgesellschaft, Leipzig 1949, p. 126
4. Ibidem pp. 145—150
5. Kamke, E.: Differentialgleichungen. Lösungsmethoden und Lösungen. Bd. 1, Aufl. 4, pp. 231—233
6. See for ex. the article of R. Grammel in book: K. Marguerre, Neuere Festigkeitsprobleme des Ingenieurs, p. 175

A COMMENT ON THE TORSION
OF BARS HAVING A CIRCULAR CROSS-SECTION
OF VARIABLE DIAMETER

I. Ecsedi*

The paper deals with the torsion of elastic bars having a circular cross-section of variable diameter. It is proved that—considering statically equivalent loads—the minimum strain energy belongs to the surface load which develops the rotation of the end-section of the bar as a rigid body.

Symbols

r, φ, z	polar co-ordinates (Fig. 1),
$\mathbf{e}_r, \mathbf{e}_\varphi, \mathbf{e}_z$	unit vectors (Fig. 1),
$\mathbf{p} = p(r)\mathbf{e}_\varphi$	intensity of the surface load,
$\mathbf{M} = M_t\mathbf{e}_z$	torque,
T	meridian section in plane rz of the bar with a circular section of diameter variable (Fig 2),
$\partial T = \partial T_1 + \partial T_2 + \partial T_3 + \partial T_4$	boundary of range T,
$R = R(z)$ $(0 \leq z \leq 1)$	equation of ∂T_4,
$\mathbf{u} = v(r, z)\mathbf{e}_\varphi$	displacement vector,
$\tau_{r\varphi}, \tau_{z\varphi}$	shearing stresses,
$\nabla = \dfrac{\partial}{\partial r}\mathbf{e}_r + \dfrac{\partial}{\partial z}\mathbf{e}_z$	Hamilton differential operator,
" . "	sign of the scalar product of two vectors,
$\dfrac{\partial}{\partial n}$	sign of the derivative calculated in the direction of normal n of curve ∂T (Fig. 2),
s	arc co-ordinate along ∂T (Fig. 2)
U	strain energy,
G	shearing modulus of elasticity,
λ	Lagrange's multiplicator

Further symbols and quantities are defined in the text.

Basic relations

Let us consider the elastic bar having a circular cross-section of variable diameter (Fig. 1). It has a built-in end at $z = 0$ preventing any displacement of cross-section A, while the other end at $z = l$ is free and is subjected to a distributed load of intensity $\mathbf{p} = p(r)\mathbf{e}_\varphi$ in plane B. Both the surface and the inside of the bar is unloaded.

* Dr. Ecsedi I., Klapka Gy. u 36, H-3524 Miskolc Hungary
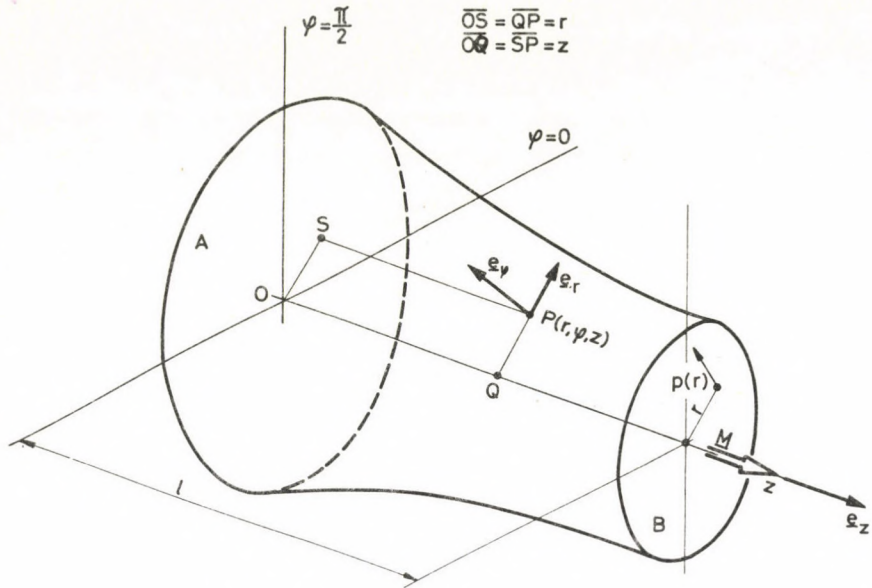
Fig. 1. Bar with a circular section of variable diameter

The distributed load acting on the plane of section B is statically equivalent to the torque defined by the vector

$$\mathbf{M} = M_t \mathbf{e}_z \tag{1.1}$$

where

$$M_t = 2\pi \int_0^{R(l)} r^2 p(r)\, \mathrm{d}r \tag{1.2}$$

The torsion of the bar having a circular cross-section of variable diameter is characterized by the following boundary value problem [1, 2]:

$$\frac{\partial^2 \psi}{\partial r^2} + \frac{3}{r}\frac{\partial \psi}{\partial r} + \frac{\partial^2 \psi}{\partial z^2} = 0, \qquad (r, z) \in T, \tag{1.3}$$

$$\psi = 0, \qquad (r, z) \in \partial T_1, \tag{1.4}$$

$$\frac{\partial \psi}{\partial n} = 0, \qquad (r, z) \in \partial T_4, \tag{1.5}$$

$$Gr\frac{\partial \psi}{\partial n} = p, \qquad (r, z) \in \partial T_3, \tag{1.6}$$

where ψ is a finite quantity at $r = 0$. $\tag{1.7}$

Figure 2 shows range T and its boundary defined by $\partial T = \partial T_1 + \partial T_2 + \partial T_3 + \partial T_4$. Making use of the function of two variables $\psi = \psi(r, z)$ in Eqs (1.3), (1.4), (1.5), (1.6), (1.7),
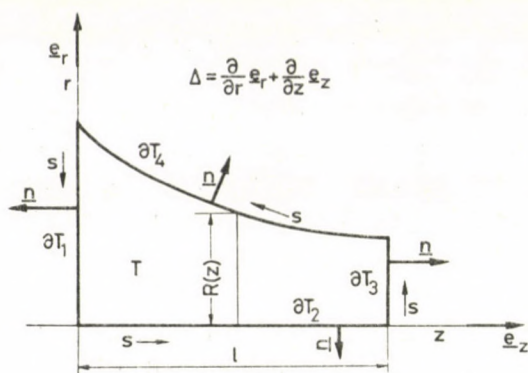
Fig. 2. Meridian section of the bar

the scalar co-ordinates of the displacement vector and those of the stress tensor, not being identically equal to zero, can be given in the following form:

$$\mathbf{u} = V(r, \varphi)\mathbf{e}_\varphi = r\psi(r, z)\mathbf{e}_\varphi , \tag{1.8}$$

$$\tau_{r\varphi} = Gr\frac{\partial\psi}{\partial r}, \qquad \tau_{z\varphi} = Gr\frac{\partial\psi}{\partial z} \tag{1.9), (1.10}$$

The strain energy of the bar can be obtained from

$$U = \frac{1}{2G}\int_V (\tau_{r\varphi}^2 + \tau_{z\varphi}^2)\,\mathrm{d}V = G\pi\int_T r^3\,|\nabla\psi|^2\,\mathrm{d}T. \tag{1.11}$$

Region V limited by the bar having a circular section of variable diameter is represented in Fig. 1. An elementary calculation proves that the relation

$$\frac{\partial^2 F}{\partial r^2} + \frac{3}{r}\frac{\partial F}{\partial r} + \frac{\partial^2 F}{\partial z^2} = \frac{1}{r^3}\nabla\cdot(r^3\nabla F) \tag{1.12}$$

holds. Combining Eqs (1.3 and (1.12) we arrive at

$$\nabla\cdot(r^3\nabla\psi) = 0, \qquad (r, z)\in T. \tag{1.13}$$

Let us consider the function of two variables $L = L(r, z)$, determined by the following equations:

$$\nabla\cdot(r^3\nabla L) = 0, \qquad (r, z)\in T, \tag{1.14}$$

$$L = 0, \qquad (r, z)\in \partial T_1 , \tag{1.15}$$

$$\frac{\partial L}{\partial n} = 0, \qquad (r, z)\in \partial T_4 , \tag{1.16}$$

$$Gr\frac{\partial L}{\partial n} = K(r), \qquad (r, z) \in \partial T_3 \tag{1.17}$$

where $L(r, z)$ is a finite function at $r = 0$. $\tag{1.18}$

In Eq. (1.17) $K = K(r)$ is a continuous function in the closed interval $0 \leq r \leq R(l)$ but otherwise is an arbitrary function of one variable. Let the function of two variable $H = H(r, z)$ be derivable continuously in the closed region $T + \partial T$, at least once, and satisfy the condition

$$H(r, 0) = 0, \qquad 0 \leq r \leq R(0).$$

According to the product-function's derivation rule and the Gauss' theorem of the transformation of integrals—making use of Eqs (1.14), (1.15), (1.16), (1.17), (1.18)—, we obtain

$$0 = \int_T H \cdot \nabla \cdot (r^3 \nabla L) \, dT = \int_T \nabla \cdot (r^3 H \nabla L) \, dT -$$

$$- \int_T r^2 \nabla H \cdot \nabla L \, dT = \int_{\partial T} r^3 H \frac{\partial L}{\partial n} \, ds -$$

$$- \int_T r^3 \nabla H \cdot \nabla L \, dT = \frac{1}{G} \int_{\partial T_3} r^3 K H \, ds - \int_T r^3 \nabla H \cdot \nabla L \, dT. \tag{1.19}$$

After some algebraic manipulation, Eq. (1.19) yields

$$\int_{\partial T_3} r^2 K H \, ds = G \int_T r^3 \nabla H \cdot \nabla L \, dT. \tag{1.20}$$

This equation will play an important role later on. Substituting $H = L = \psi$ and $K = p$ to Eq. (1.20) and making use of Eq. (1.11), we find

$$U = \pi \int_{\partial T_3} r^2 \psi p \, ds. \tag{1.21}$$

A theorem on the strain energy

Theorem. Let us consider the distributed surface loads $\mathbf{p} = p(r)\mathbf{e}_\varphi$ ($0 \leq r \leq R(l)$), which are statically equivalent. The minimum strain energy of bar U belongs to the surface load $\mathbf{p} = p(r)\mathbf{e}_\varphi$ which develops the rotation of the plane of cross-section $\mathbf{B}$ as a rigid body.

Demonstration. If the shape and the material of the bar do not vary, the strain energy U depends only on the surface load $p = p(r)$, i.e. U can be considered a functional depending on $p = p(r)$:

$$U = U[p(r)]. \tag{2.1}$$

We shall now examine how functional U varies if the surface load is modified by an increment $\partial p(r)$. Function ψ belonging to the surface load $p(r)$ is denoted by $\psi(r, z, p)$, function ψ belonging to the surface load $p + \delta p$ is denoted by $\psi(r, z; p + \delta p)$. Let the increment of function ψ be

$$\delta\psi = \psi(r, z; p + \delta p) - \psi(r, z; p) \tag{2.2}$$

The analysis of Eqs (1.13), (1.4), (1.5), (1.6), (1.7) shows that functions $\bar{\psi} = \psi(r, z; p + \partial p)$ and $\partial\psi$ are solutions of the following boundary value problems:

$$\nabla \cdot (r^3 \nabla \bar{\psi}) = 0 \qquad (r, z) \in T, \tag{2.3}$$

$$\bar{\psi} = 0 \qquad (r, z) \in \partial T_1, \tag{2.4}$$

$$\frac{\partial \bar{\psi}}{\partial n} = 0 \qquad (r, z) \in T_4, \tag{2.5}$$

$$Gr \frac{\partial \bar{\psi}}{\partial n} = p + \delta p \qquad (r, z) \in \partial T_3, \tag{2.6}$$

where $\bar{\psi}$ is a limited function at $r = 0$, $\tag{2.7}$

$$\nabla \cdot (r^3 \nabla \, \delta\psi) = 0 \qquad (r, z) \in T, \tag{2.8}$$

$$\delta\psi = 0 \qquad (r, z) \in \partial T_1, \tag{2.9}$$

$$\frac{\partial}{\partial n} \delta\psi = 0 \qquad (r, z) \in \partial T_4, \tag{2.10}$$

$$Gr \frac{\partial}{\partial n} (\delta\psi) = \delta p \qquad (r, z) \in \partial T_3, \tag{2.11}$$

where $\partial\psi$ is a limited function at $r = 0$. $\tag{2.12}$

From formula (1.21) it follows that

$$U[p + \delta p] = \pi G \int_{\partial T_3} r^2 (p + \delta p) \, [\psi(r, z; p) + \delta\psi] \, ds =$$

$$= \pi G \int_{\partial T_3} r^2 p \psi(r, z; p) \, ds + \pi G \int_{\partial T_3} r^2 \delta \, p \psi(r, z; p) \, ds +$$

$$+ \pi G \int_{\partial T_3} r^2 p \delta \, \psi \, ds + \pi G \int_{\partial T_3} r^2 \delta p \, \delta\psi \, ds =$$

$$= U[p] + \pi G \int_{\partial T_3} r^2 \delta p \, \psi(r, z; p) \, ds +$$

$$+ \pi G \int_{\partial T_3} r^2 p \, \delta\psi \, ds + \pi G \int_{\partial T_3} r^2 \delta p \, \delta\psi \, ds. \tag{2.13}$$

2

Substituting

$$K = p(r), \qquad L = \psi(r, z; p),$$ (2.14), (2.15)

$$H = \delta\psi$$ (2.16)

to formula (1.20), we find

$$\int\limits_{\partial T_3} r^2 p \, \delta\psi \, \mathrm{d}s = \int\limits_T r^3 \nabla\psi \cdot \nabla\delta\psi \, \mathrm{d}T.$$ (2.17)

Similarly, substituting

$$K = \delta p(r), \qquad L = \delta\psi$$ (2.18), (2.19)

$$H = \psi(r, z; p)$$ (2.20)

to formula (1.20), we obtain

$$\int\limits_{\partial T_3} r^2 \delta \, p\psi \, \mathrm{d}s = \int\limits_T r^3 \nabla \, \delta\psi \cdot \nabla\psi \, \mathrm{d}T$$ (2.21)

and, finally, substituting

$$K = \delta p, \qquad H = L = \delta\psi$$ (2.22), (2.23)

to formula (1.20), we arrive at

$$\int\limits_{\partial T_3} r^2 \delta p \, \delta\psi \, \mathrm{d}s = \int\limits_T r^3 \, | \, \nabla\delta\psi \, |^{\,2} \, \mathrm{d}T.$$ (2.24)

Combining the above expressions with Eq. (2.13), we have

$$U[p + \delta p] - U[p] = \pi G \nabla \int\limits_{\partial T_3} r^2 \psi \, \delta p \, \mathrm{d}s +$$

$$+ \pi G \int\limits_T r^3 \, | \, \nabla\delta\psi \, |^{\,2} \, \mathrm{d}T.$$ (2.25)

The first variant of the strain energy, a functional depending on $p = p(r)$, is obtained from Eq. (2.25):

$$\delta U = \pi G \int\limits_{\partial T_3} r^2 \psi \, \delta p \, \mathrm{d}s.$$ (2.26)

Since

$$M_t = 2\pi \int\limits_{\partial T_3} r^2 p \, \mathrm{d}s = \text{constant (of fixed value)},$$ (2.27)

we find

$$\int\limits_{\partial T_3} r^2 \psi \, \delta\varphi \, \mathrm{d}s = 0.$$ (2.28)

Let function $p = p(r)$ satisfying condition (2.27) denote the surface load which minimizes the strain energy. Making use of the well-known results of variational calculus and applying Lagrange's multiplication method to Eqs (2.26), (2.28), it can be proved that function $\psi = \psi(r, z; p)$ belonging to the surface load $p = p(r)$ and minimizing the strain energy, satisfies the following equation [3]:

$$\int_{\partial T_3} r^2(\psi - \lambda)\delta p \, ds = 0. \tag{2.29}$$

Constant λ in Eq. (2.29) is the Lagrange's multiplicator. Applying the basic lemma of variational calculus to Eq. (2.29), we obtain

$$\psi(r, z; p) = \lambda = \text{const.} \qquad (r, z) \in \partial T_3. \tag{2.30}$$

Rearranging Eq. (2.29), we find

$$\int_{\partial T_3} r^2 \psi \, \delta p \, ds = \lambda \int_{\partial T_3} r^2 \delta p \, ds = 0, \tag{2.31}$$

while Eq. (2.25) results in

$$U[p + \delta p] - U[p] =$$

$$= \pi G \int_T r^3 |\nabla \delta \psi|^2 \, dT \geq 0. \tag{2.32}$$

Equation (2.31) and inequality (2.32) show that strain energy U is minimum if condition (2.30) is satisfied. It follows from Eq. (2.30) that the displacement of cross-section B defined by co-ordinate $z = l$ caused by the surface load minimizing the strain energy can be characterized by the vector

$$\mathbf{U}(r, \varphi, z) = V(r, z)\mathbf{e}_\varphi = \lambda r \mathbf{e}_\varphi \qquad (r, z) \in \partial T_3. \tag{2.33}$$

According to Eq. (2.33), it can be stated, that the plane of cross-section B rotates around axis z by the angle of λ as a rigid body.

References

1. Arutjunjan, N. H., Abramjan, B. L.: Krucsnie uprugih tel. Fizmatgiz, Moskva (1963), 506—517
2. Timoshenko, S.—Goodier, J. J.: Theory of Elasticity. Second ed. McGraw-Hill. New York—Toronto—London 1951, 304—315
3. Schechter R. S.: The Variational Method in Engineering. McGraw-Hill. New York—Toronto—London 1967

BOUNDS FOR THE HEAT TRANSFER COEFFICIENT

I. Ecsedi*

The primary purpose of the paper is to deduce inequality relations by the application of which lower and upper bounds can be formed for the numerical value of the heat transfer coefficient.

Symbols

The symbols of major significance used in this paper are as follows.

x, y, z	orthogonal coordinates,
$\mathbf{e}_x, \mathbf{e}_y, \mathbf{e}_z$	unit vectors,
$\mathbf{r} = x\mathbf{e}_x + y\mathbf{e}_y + z\mathbf{e}_z$	position vector,
A_1	within each section even closed surface,
A_2	within each section even closed surface,
V_1	bounded space region defined by interior of A_1,
V_2	not bounded space region defined by exterior of A_2,
V	space region bounded by separate closed surfaces A_1 and A_2,
Q	heat conducted within unit of time,
T_1, T_2	temperature,
k	overall heat transfer rate,
$t = t(\mathbf{r})$	temperature field,
λ	"interior" thermal conductivity,
α_1, α_2	"exterior" thermal conductivity,
$\nabla = \dfrac{\partial}{\partial x}\mathbf{e}_x + \dfrac{\partial}{\partial y}\mathbf{e}_y + \dfrac{\partial}{\partial z}\mathbf{e}_z$	*Hamilton* differential operator,
" . "	sign of scalar product of two vectors,
$\Delta = \nabla \cdot \nabla = \dfrac{\partial^2}{\partial x^2} + \dfrac{\partial^2}{\partial y^2} + \dfrac{\partial^2}{\partial z^2}$	*Laplacian* differential operator
$\partial/\partial n$	symbol of derivative calculated in direction $\mathbf{n}$,
$\mathbf{n}$	normal unit vector of surface A_i directed outwards from region V at point $P_i (i=1,2)$ (Fig. 1),
$\varphi = \varphi(\mathbf{r}), f = f(\mathbf{r}), h = h(\mathbf{r}), g = g(\mathbf{r})$	functions of three variables,
$\mathbf{b} = \mathbf{b}(\mathbf{r})$	three dimensional vector field,
R_1, R_2	sphere radii.

Other quantities and variables are defined by the text.

1. The heat transfer coefficient

The region V_1 filled by a medium of temperature T_1 and the region V_2 filled by a medium of temperature T_2 are separated by a solid bounded by two separate closed surfaces A_1 and A_2 (Fig. 1). Through region V from the medium of higher temperature

* Dr. I. Ecsedi, Klapka Gy. u. 36, H-3524 Miskolc, Hungary
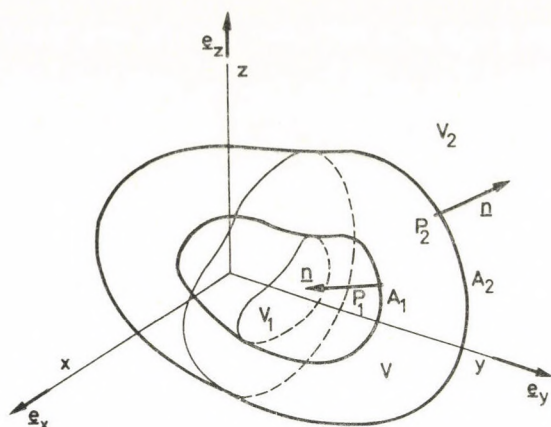
Fig. 1. Region V bounded by the closed surfaces A_1 and A_2

to that of the lower temperature heat is flowing. This process is characterized by the heat transfer coefficient k:

$$Q = k(T_1 - T_2), \quad (T_1 > T_2).$$ (1.1)

To express more exactly, k means the heat quantity transferred in *steady state* through the bounding structure, i.e., the solid filling the region V, under the effect of the unit temperature difference between the spaces separated by the bounding structure ([2], [3], [4]).

For convenience $T_1 > T_2$, further, T_1 and T_2 are, constant in time.

The field of the temperature

$$t = t(\mathbf{r}) \qquad r \in VUA_1 \, UA_2$$

of the solid lying in region V and associated with the steady state may be brought into relation with the following boundary-value problem, by making use of the Fourier-theory of heat transfer in the case where the thermal parameters λ, α_1, α_2 have a constant value ([1], [3], [5]):

$$\Delta t = 0 \qquad \mathbf{r} \in V,$$ (1.2)

$$\lambda \frac{\partial t}{\partial n} + \alpha_1 (t - T_1) = 0 \qquad \mathbf{r} \in A_1$$ (1.3)

$$\lambda \frac{\partial t}{\partial n} + \alpha_2 (t - T_2) = 0 \qquad \mathbf{r} \in A_2$$ (1.4)

In writing the boundary conditions (1.3), (1.3), the *Newtonian* law of cooling has been applied ([1], [5]).

From the solid V_1 of temperature T_1 in the unit time heat of a quantity

$$Q_1 = \lambda \int_{A_1} \frac{\partial t}{\partial n} \, dA \tag{1.5}$$

passes over the surface section A_1 to the solid of volume V. This amount of heat arrives to the surface section A_2 by "internal" thermal conduction, wherefrom it flows to the medium of temperature T_2 by "external" heat transfer. The numerical value of the amount of heat leaving may be determined by making use of the formula

$$Q_2 = \lambda \int_{A_2} \frac{\partial t}{\partial n} \, dA . \tag{1.6}$$

With the aid of Eq. (1.2) it may readily be pointed out that

$$Q_1 + Q_2 = 0 ,$$

in agreement with the principle of the conservation of energy. This may be proved as follows:

$$0 = \lambda \int_V \Delta t \, dV = \lambda \int_{A_1} \frac{\partial t}{\partial n} \, dA + \lambda \int_{A_2} \frac{\partial t}{\partial n} \, dA = Q_1 + Q_2 . \tag{1.8}$$

In the following, new formulae will be deduced for the calculaion of the quantity of heat $Q = Q_1$ in order to obtain the explicit expression of the heat transfer coefficient k.

From the equation

$$t \Delta t + (\Delta t)^2 = \nabla \cdot (t \nabla t) \tag{1.9}$$

by integration and by the application of the Gaussian theorem of integral transformation one obtains Eq. (1.10) also taking Eq. (1.2) into consideration:

$$\int_V (\nabla t)^2 \, dV = \int_{A_1} t \frac{\partial t}{\partial n} \, dA + \int_{A_2} t \frac{\partial t}{\partial n} \, dA . \tag{1.10}$$

Eq. (1.10) may again be transformed by making use of the boundary conditions (1.3), (1.4):

$$\lambda \int_V |\nabla t|^2 \, dV = -\frac{\lambda^2}{\alpha_1} \int_{A_2} \left(\frac{\partial t}{\partial n} \right)^2 \, dA - \frac{\lambda^2}{\alpha_2} \int_{A_2} \left(\frac{\partial t}{\partial n} \right)^2 \, dA + \lambda (T_1 - T_2) \int_{A_1} \frac{\partial t}{\partial n} \, dA . \tag{1.11}$$

In writing down Eq. (1.11) we also made use of the relationship (1.8). By the combination of formula (1.5) and Eq. (1.11) one obtains the formula (1.12):

$$Q = \frac{1}{T_1 - T_2} \left\{ \lambda \int\limits_V |\nabla t|^2 \, dV + \frac{\lambda^2}{\alpha_1} \int\limits_{A_1} \left(\frac{\partial t}{\partial n}\right)^2 dA + \frac{\lambda^2}{\alpha_2} \int\limits_{A_2} \left(\frac{\partial t}{\partial n}\right)^2 dA \right\}. \tag{1.12}$$

It may easily be pointed out that the formula (1.12) can also be written in the following form, by making use of the boundary conditions (1.3) and (1.4):

$$Q = \frac{1}{T_1 - T_2} \left\{ \lambda \int\limits_V |\nabla t|^2 \, dV + \alpha_1 \int\limits_{A_1} (t - T_1)^2 \, dA + \alpha_2 \int\limits_{A_2} (t - T_2)^2 \, dA \right\}. \tag{1.13}$$

It the following, it will be proved that the value of the heat transfer coefficient k does not depend on the difference of temperatures $T_1 - T_2$, the value of k is the function of the thermal parameters λ, α_1, α_2 and the "shape" of region V.

Let us consider the function of three variables

$$\varphi = \varphi(\mathbf{r}), \qquad \mathbf{r} \in VU A_1 \, U A_2$$

unequivocally by the following prescriptions:

$$\Delta\varphi = 0 \qquad \mathbf{r} \in V \tag{1.14}$$

$$\lambda \frac{\partial\varphi}{\partial n} + \alpha_1 (\varphi - 1) = 0, \qquad \mathbf{r} \in A_1, \tag{1.15}$$

$$\lambda \frac{\partial\varphi}{\partial n} + \alpha_2 \varphi = 0, \qquad \mathbf{r} \in A_2. \tag{1.16}$$

By elementary calculation it may be pointed out that with knowledge of the solution to the boundary-value problem defined by Eqs (1.2), (1.3), (1.4) may be produced in the following way:

$$t(\mathbf{r}) = (T_1 - T_2)\varphi(\mathbf{r}) + T_2 \qquad \mathbf{r} \in VU A_1 \, U A_2. \tag{1.17}$$

By the combination of formulae (1.12) and (1.17) one obtains the formula (1.18):

$$Q = \left\{ \lambda \int\limits_V |\nabla\varphi|^2 \, dV + \frac{\lambda^2}{\alpha_1} \int\limits_{A_1} \left(\frac{\partial\varphi}{\partial n}\right)^2 dA + \frac{\lambda^2}{\alpha_2} \int\limits_{A_2} \left(\frac{\partial\varphi}{\partial n}\right)^2 dA \right\} (T_1 - T_2). \tag{1.18}$$

From the formula (1.18), by comparing it with Eq. 1.1 it may be read that

$$k = \lambda \int\limits_V |\nabla\varphi|^2 \, dV + \frac{\lambda^2}{\alpha_1} \int\limits_{A_1} \left(\frac{\partial\varphi}{\partial n}\right)^2 dA + \frac{\lambda^2}{\alpha_2} \int\limits_{A_2} \left(\frac{\partial\varphi}{\partial n}\right)^2 dA. \tag{1.19}$$

On the basis of the above formula it can readily be seen that the value of k is indeed the only function of the thermal parameters α, λ_1, λ_2 and the shape of the region

V. By the combination of formula (1.19) and the boundary conditions (1.15), (1.16) one arrives to the following formula for k:

$$k = \lambda \int_V |\nabla\varphi)^2 \, dV + \alpha_1 \int_{A_1} (\varphi - 1)^2 \, dA + \alpha_2 \int \varphi^2 \, dA. \tag{1.20}$$

From the above relationships it ensues that k is always positive, $k > 0$.

The primary purpose of this paper is to derive such inequality relations by the application of which lower and upper bounds may be performed for k. The exact (strict) value of the heat transfer coefficient might be given only with the knowledge of the solution to the boundary-value problem defined by Eqs (1.14), (1.15), (1.16). The solution of the explicit form of the boundary-value problem defined by Eqs (1.14), (1.15), (1.16) is known only with regions V of very simple shapes [5], wherefore such principles and methods are of great significance with the application of which lower and upper bounds may be produced to the numerical value of the heat transfer coefficient k.

2. Upper bound

Proposition 2.1. Be $f = f(r)$ continuous in region $VUA_n \, UA_2$, and in region V at least once continuously derivable, otherwise an arbitrary function of three variables. The inequality relation

$$k \leqq \lambda \int_V |\nabla f|^2 \, dV + \alpha_1 \int_{A_1} (f - 1)^2 \, dA + \alpha_2 \int_{A_2} f^2 \, dA \tag{2.1}$$

is valid.

Demonstration. Consider the function of three variables defined by the prescription

$$h(\mathbf{r}) = f(\mathbf{r}) - \varphi(\mathbf{r}), \qquad \mathbf{r} \in VUA_1 \, UA_2. \tag{2.2}$$

By a lengthy but elementary calculation the following relationship may be deduced:

$$\lambda \int_V (\nabla f)^2 \, dV + \alpha_1 \int_{A_1} (f - 1)^2 \, dA + \alpha_2 \int_{A_2} f^2 \, dA =$$

$$= \lambda \int |\nabla\varphi|^2 \, dV + \alpha_1 \int_{A_1} (\varphi - 1)^2 \, dA + \alpha_2 \int_{A_2} \varphi^2 \, dA +$$

$$+ 2\lambda \int_V \nabla h \cdot \nabla\varphi \cdot dV + \alpha_1 \int_{A_1} h(\varphi - 1) \, dA + 2\alpha_2 \int_{A_2} h\varphi \, dA + \lambda \int_V |\nabla h|^2 \, dV + \alpha_1 \int_{A_1} h^2 \, dA +$$

$$+ \alpha_2 \int_{A_2} h^2 \, dA = k + \lambda \int_V |\nabla h|^2 \, dV + \alpha_1 \int_{A_1} h^2 \, dA + \alpha_2 \int_{A_2} h^2 \, dA. \tag{2.3}$$

By deducing Eq. (2.3) the following relationship has been used

$$\lambda \int_V \nabla h \cdot \nabla \varphi \, dV + \alpha_1 \int_{A_1} h(\varphi - 1) \, dA + \alpha_2 \int_{A_2} h\varphi \, dA =$$

$$= \lambda \int_V \nabla \cdot (h\nabla \varphi) \, dV - \lambda \int_V h\Delta \varphi \, dV + \alpha_1 \int_{A_1} h(\varphi - 1) \, dA + \alpha_2 \int_{A_2} h\varphi \, dA =$$

$$= \int_{A_1} \left[\lambda \frac{\partial t}{\partial n} + \alpha_1 (\varphi - 1) \right] h \, dA + \int_{A_2} \left[\lambda \frac{\partial \varphi}{\partial n} + \alpha_2 \varphi \right] h \, dA - \lambda \int_V h\Delta \varphi \, dV = 0 . \quad (2.4)$$

In proving Eq. (2.4), Eqs (1.14), (1.15), (1.16) being in connection with the function $\varphi = \varphi(\mathbf{r})$ have been applied.

From formula (2.3) the correctness of the proposition may directly be read and it is even evident that in the inequality relation (2.1) the sign of equality is only valid if

$$h \equiv 0 \qquad \mathbf{r} \in VUA_1 \, UA_2 ,$$

that is if

$$f \equiv \varphi \qquad \mathbf{r} \in VUA_1 \, UA_2$$

Proposition 2.2. Let us have $f = f(\mathbf{r})$ continuous in a closed region $VUA_1 \, UA_2$, and in an open region V at least once continuously derivable function of one variable, non-identically equal to zero. The inequality relation

$$k \leqq \alpha_1 A_1 - \frac{\left(\alpha_1 \int_{A_1} f \, dA \right)^2}{\lambda \int_V | \nabla f |^2 \, dV + \alpha_1 \int_{A_1} f^2 \, dA + \alpha_2 \int_{A_2} f^2 \, dA} \quad (2.5)$$

is valid.

Demonstration. Applying the inequality relation (2.1) to the function $f(\mathbf{r}) = pf(\mathbf{r})$, wherein p is an arbitrary real parameter, yields the following relationship

$$k \leq p^2 D_0 - 2pD_1 + D_2 , \quad (2.6)$$

wherein

$$D_0 = \int_V | \nabla f |^2 \, dV + \alpha_1 \int_{A_1} f^2 \, dA + \alpha_2 \int_{A_2} f^2 \, dA , \quad (2.7)$$

$$D_1 = \alpha_1 \int_{A_1} f \, dA , \quad (2.8)$$

$$D_2 = \alpha_1 A_1 , \qquad \left(A_1 = \int_{A_1} dA \right) . \quad (2.9)$$

The inequality relation (2.6) is valid to any value of the real parameter p. By an appropriate selection of p the right-hand side of (2.6) might be reduced to the minimum

and, on the basis of the minimum obtained, one arrives directly to the proof of the proposition 2.2.

It can easily be pointed out that in relation (2.5) the sign of equality is only valid if

$$f = a\varphi , \tag{2.10}$$

wherein a is an arbitrary real constant differing from zero.

Lower bound

Proposition 3.1. In the closed region $V U A_1 U A_2$ the continuous vector field $\mathbf{b} = \mathbf{b}(\mathbf{r})$ differing from the identically zero vector should satisfy the differential equation

$$\nabla \cdot \mathbf{b} = 0 \qquad \mathbf{r} \in V . \tag{3.1}$$

The following inequality relation is valid:

$$k \geqslant \frac{\left(\int\limits_{A_1} \mathbf{b} \cdot \mathbf{n} \, dA \right)^2}{\dfrac{1}{\lambda} \int\limits_{V} \mathbf{b}^2 \, dV + \dfrac{1}{\alpha_1} \int\limits_{A_1} (\mathbf{b} \cdot \mathbf{n})^2 \, dA + \dfrac{1}{\alpha_2} \int\limits_{A_2} (\mathbf{b} \cdot \mathbf{n})^2 \, dA} . \tag{3.2}$$

Demonstration. Let us have

$$E(\mathbf{c}, \mathbf{d}) = \lambda \int\limits_{V} \mathbf{c} \cdot \mathbf{d} \, dV + \frac{\lambda^2}{\alpha_1} \int\limits_{A_1} (\mathbf{c} \cdot \mathbf{n})(\mathbf{d} \cdot \mathbf{n}) \, dA + \frac{\lambda^2}{\alpha_2} \int\limits_{A_2} (\mathbf{c} \cdot \mathbf{n})(\mathbf{d} \cdot \mathbf{n}) \, dA , \tag{3.3}$$

wherein:

$$\mathbf{c} = \mathbf{c}(\mathbf{r}) \quad \text{and} \quad \mathbf{d} = \mathbf{d}(\mathbf{r})$$

defined in the closed region $V U A_1 U A_2$ are two arbitrary continuous vector fields. On the basis of the Schwarz-inequality it may be written that

$$E(\mathbf{c}, \mathbf{c}) \, E(\mathbf{d}, \mathbf{d}) \geqslant |(\mathbf{c}, \mathbf{d})|^2 \tag{3.4}$$

In the inequality relation (3.4) let us use the following notation:

$$\mathbf{c}(\mathbf{r}) = \nabla \varphi, \qquad \mathbf{d}(\mathbf{r}) = \mathbf{b}(\mathbf{r}) \tag{3.5), (3.6}$$

wherein the vector field $\mathbf{b} = \mathbf{b}(\mathbf{r})$ satisfied the differential equation (3.1). It can easily be understood that

$$k = E(\nabla \varphi, \nabla \varphi) . \tag{3.7}$$

The relationship

$$E(\nabla\varphi, \mathbf{b}) = \lambda \int_V \nabla\varphi \cdot \mathbf{b} \, dV + \frac{\lambda^2}{\alpha_1} \int_{A_1} \frac{\partial\varphi}{\partial n} (\mathbf{b} \cdot \mathbf{n}) \, dA + \frac{\lambda^2}{\alpha_2} \int_{A_2} \frac{\partial\varphi}{\partial n} (\mathbf{b} \cdot \mathbf{n}) \, dA =$$

$$= \lambda \int_V \nabla \cdot (\varphi\mathbf{b}) \, dV - \lambda \int_V \varphi \nabla \cdot \mathbf{b} \, dV + \frac{\lambda^2}{\alpha_1} \int \frac{\partial\varphi}{\partial n} (\mathbf{b} \cdot \mathbf{n}) \, dA +$$

$$+ \frac{\lambda^2}{\alpha_2} \int \frac{\partial\varphi}{\partial n} (\mathbf{b} \cdot \mathbf{n}) \, dA = \lambda \int_{A_1} \left(\varphi + \frac{\lambda}{\alpha_1} \frac{\partial\varphi}{\partial n} \right) (\mathbf{b} \cdot \mathbf{n}) \, dA +$$

$$+ \lambda \int_{A_2} \left(\varphi + \frac{\lambda}{\alpha_2} \frac{\partial\varphi}{\partial n} \right) (\mathbf{b} \cdot \mathbf{n}) \, dA = \lambda \int_{A_1} (\mathbf{b} \cdot \mathbf{n}) \, dA \qquad (3.8)$$

further, the inequality (3.4) and formulae (3.5), (3.6), (3.7) by their combination directly yield the inequality relation (3.2) to be proved. In deriving the relationship (3.8) the rule of differentation of the product function as well as the Gaussian integration theorem, the equations (1.15), (1.16) and (3.1) have been applied.

By some discussion it may be pointed out that in relation (3.2) the sign of equality is valid only in the case where

$$\mathbf{b} = a\nabla\varphi \qquad (3.9)$$

differs from zero, however, otherwise being an arbitrary real constant.

Proposition 3.2. The three-variable, non-identically constant in the closed region VUA_1UA_2 continuous function $g = g(\mathbf{r})$ should satisfy the partial differential equation

$$\Delta g = 0 \qquad \mathbf{r} \in V \qquad (3.10)$$

The inequality relation

$$k \geqslant \frac{\left(\int_{A_1} \frac{\partial g}{\partial n} \, dA \right)^2}{\frac{1}{\lambda} \int_V |\nabla g|^2 \, dV + \frac{1}{\alpha_1} \int_{A_1} \left(\frac{\partial g}{\partial n} \right)^2 dA + \frac{1}{\alpha_2} \int_{A_2} \left(\frac{\partial g}{\partial n} \right)^2 dA} \qquad (3.11)$$

is valid.

Demonstration. The correctness of the inequality relation (3.11) ensues directly from the inequality relation (3.2) in case where the replacement

$$\mathbf{b} = \nabla g \qquad (3.12)$$

is applied. It is evident that vector $\mathbf{b}$ of the above form satisfies the differential equation (3.1) in case where $\mathbf{g}$ is harmonic in region V. It can easily be proved that the sign of equality in the relation (3.1) is only valid if

$$g = a\varphi + b \tag{3.13}$$

wherein a and b are arbitrary real constants excepting the restriction $a \neq 0$.

Examples

4.1. Let us have in the inequality relation (2.1) $f = 0$.
By an elementary calculation one obtains the result

$$k \leqslant \alpha_1 A_1 \tag{4.1}$$

which can also directly be read from the inequality relation (2.5).

4.2. Let us have in the inequality relation (2.1) $f = 1$.
By calculating with this function one obtains the result

$$k \leqslant \alpha_2 A_2 \tag{4.2}$$

4.3. The three-variable function $F = F(\mathbf{r})$ continuously differentiable in sections, in the closed region $V U A_1 U A_2$, should satisfy the following boundary conditions:

$$F(\mathbf{r}) = 1, \qquad \mathbf{r} \in A_1, \tag{4.3}$$

$$F(\mathbf{r}) \doteq 0, \qquad \mathbf{r} \in A_2. \tag{4.4}$$

Replacement of the function $F = F(\mathbf{r})$ defined by the above prescriptions into the inequality relation 2.1 yields the following upper bound:

$$k \leqslant \int_V |\nabla F|^2 \, dV. \tag{4.5}$$

From Dirichlet's minimum-principle it ensues that the upper bound of the form (4.5) is the sharpest if the function $F = F(\mathbf{r})$ is harmonic in region V.

4.4. In the inequality relation (2.5) be

$$f = c = \text{constant}, \qquad (c \neq 0). \tag{4.6}$$

With the help of the elementary calculation the following upper bound of very simple structure might be deducted to the heat transfer coefficient k:

$$k \leqslant \cfrac{1}{\cfrac{1}{\alpha_1 A_1} + \cfrac{1}{\alpha_2 A_2}} \tag{4.7}$$

4.5. In the inequality relation (2.5) be $f = F$ wherein $F = F(\mathbf{r})$ denotes the three-variable function entering in the formula (4.5). With the help of a short calculation one
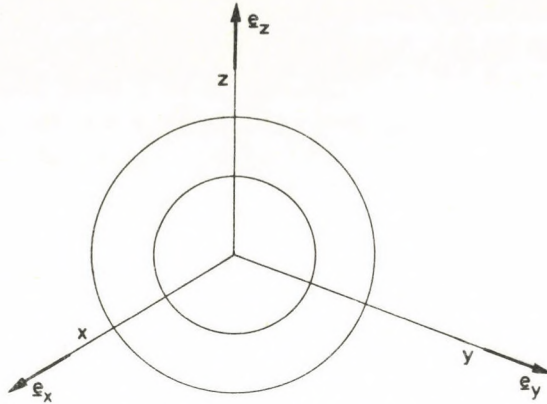
Fig. 2. Spherical hollow region

obtains to the numerical value of the coefficient k the following upper bound:

$$k \leqslant \frac{1}{\dfrac{1}{\alpha_1 A_1} + \dfrac{1}{\lambda} \dfrac{1}{\int\limits_V |\nabla F|^2 \, \mathrm{d}V}} \, . \tag{4.8}$$

Obviously, the upper bound of type (4.8) is the sharpest in case where $F = F(\mathbf{r})$ is harmonic in region V.

4.6. Consider the hollow region of spherical form represented by Fig. 2.

Let us have in the inequality relation (2.5) for $f(\mathbf{r})$ the following expression

$$f(\mathbf{r}) = \alpha_2 \frac{R_2^2}{r} + \lambda - \alpha_2 R_2, \qquad (r = |\mathbf{r}| = \sqrt{x^2 + y^2 + z^2}). \tag{4.9}$$

By a lengthy, however, by an elementary calculation, one obtains the result

$$k \leqslant \frac{4\pi}{\dfrac{1}{\alpha_1 R_1^2} + \dfrac{1}{\lambda}\left(\dfrac{1}{R_1} - \dfrac{1}{R_2}\right) + \dfrac{1}{\alpha_2 R_2^2}} \tag{4.10}$$

4.7. Into the inequality relation (3.11) the harmonic function

$$g(\mathbf{r}) = \frac{1}{r}, \qquad (r = \sqrt{x^2 + y^2 + z^2}) \tag{4.11}$$

is replaced. By this replacement one arrives to the following lower bound:

$$k \geqslant \frac{\left(\int\limits_{A_1} \dfrac{\mathbf{r} \cdot \mathbf{n}}{r^3}\, dA\right)^2}{\dfrac{1}{\alpha_1}\int\limits_{A_1}\dfrac{(\mathbf{r} \cdot \mathbf{n})^2}{r^3}\, dA + \dfrac{1}{\lambda}\int\limits_V \dfrac{dV}{r^4} + \dfrac{1}{\alpha_2}\int\limits_{A_2}\dfrac{(\mathbf{r} \cdot \mathbf{n})^2}{r^6}\, dA} \tag{4.12}$$

In connection with the formula deduced, it should be noted that the origin of the system of coordinates xyz is within the closed surface A_1 in the region V_1.

4.8. Let us apply the formula (4.12) to the spherical hollow region V. The following result will be obtained:

$$k \geqslant \frac{4\pi}{\dfrac{1}{\alpha_1 R_1^2} + \dfrac{1}{\lambda}\left(\dfrac{1}{R_1} - \dfrac{1}{R_2}\right) + \dfrac{1}{\alpha_2 R_2^2}} \tag{4.13}$$

4.9. Comparing formulae (4.10) and (4.13) yields the exact value of the heat transfer coefficient of the spherical hollow solid, in agreement with the data of the literature on the subject ([2], [3]), is as follows:

$$k = \frac{4\pi}{\dfrac{1}{\alpha_1 R_2^2} + \dfrac{1}{\lambda}\left(\dfrac{1}{R_1} - \dfrac{1}{R_2}\right) + \dfrac{1}{\alpha_2 R_2^2}}\,. \tag{4.14}$$

References

1. Jakab, M.: Heat Transfer, Vol. 1 Wiley, New York 1959
2. Mihajev, M. A.: Basic Principles of the Practical Calculation of Heat Transfer. Tankönyvkiadó, Budapest 1953
3. Pattantyús: Manual of Mechanical and Electrical Engineers, Vol. 2. Basic Knowledge — Knowledge of Materials. General Editor: I. Sályi. Műszaki Könyvkiadó, Budapest, 1961. Heat Transfer. Pp. 1 184—1222.
4. Gereben, Z.: Building Physics for Practising Architects. Műszaki Könyvkiadó, Budapest, 1981 pp. 41—61
5. Frank–Mises: Differential and Integral Equations of Mechanics and Physics. Vol. II (Physics) Műszaki Könyvkiadó. Budapest 1967, pp. 577—680

SOME COMMENTS ON THE TORSION
OF BARS HAVING AN ANNULUS CROSS-SECTION
OF VARIABLE SIZE SUPPORTED ELASTICALLY
ALONG ITS ENTIRE LENGTH

I. Ecsedi*

The paper deals with the torsion of elastic bars with a continuous elastic support. The section of the bars is an annulus of variable size. Due to the elastic support, the intensity of the continuous load on the surface of the bars is proportional to the displacement of the points of the surface of the bars. The boundary value problem of torsion as well as the formula of the torsional rigidity are presented. Making use of inequalities, lower and upper bounds are given for the torsional rigidity. Approximate values are obtained in this way for the torsional rigidity without using—even knowing—the solution of the boundary value problem of torsion.

Symbols

r, φ, z	polar co-ordinates,
$\mathbf{e}_r, \mathbf{e}_\varphi, \mathbf{e}_z$	unit vectors,
$\mathbf{u} = v(r, z)\mathbf{e}_\varphi$	displacement vector,
ϑ	angle of rotation,
$\mathbf{V} = \dfrac{\partial}{\partial r}\mathbf{e}_r + \dfrac{\partial}{\partial z}\mathbf{e}_z$	*Hamilton* differential operator,
".."	sign of the scalar product of two vectors,
" $\times$ "	sign of the vectorial product of two vectors,
a, b	co-ordinates denoting the end sections of the bar,
T	planar range defined by the meridian section of the bar,
$\partial T = \partial T_1 \cup \partial T_2 \cup \partial T_3 \cup \partial T_4$	boundary of range T,
$\mathbf{n}$	unit vector belonging to the "outer" normal of boundary curve ∂T,
$\mathbf{e}$	unit vector belonging to the tangent of boundary curve ∂T,
s	arc co-ordinate along boundary curve ∂T,
$R_3 = R_3(z) \quad a \leq z \leq b$	equation of curve ∂T_3,
$R_4 = R_4(z) \quad a \leq z \leq b$	equation of curve ∂T_4,
G	shear rigidity of elasticity of the bar,
k	constant characterizing the elastic support ($k > 0$),
M	torque,
$\partial/\partial n$	sign of the derivative in the direction of $\mathbf{n}$,
$\partial/\partial s$	sign of the derivative in the direction of e,
$\psi = \psi(r, z), f = f(r, z),$	
$H = H(r, z), h = h(r, z)$	auxiliary functions,
$\mathbf{c} = \mathbf{c}(r, z) = c_r(r, z)\mathbf{e}_r + c_z(r, z)\mathbf{e}_z$	planar vector field,
$p = p(z), P = P(z), \hat{p} = \hat{p}(z), \hat{P} = \hat{P}(z)$	auxiliary functions,
S	torsional rigidity.

Further symbols and variables are defined in the text.

* Ecsedi I., Klapka Gy. u. 36, H-3524 Miskolc, Hungary

2. Introduction, basic relations

Let us consider the elastic bar having an annulus cross-section of variable size shown in Fig. 1. The bar is subjected to distributed loads of intensity

$$\mathbf{p}_3 = p_3(r, z)\mathbf{e}_\varphi, \qquad \mathbf{p}_4 = p_4(r, z)\mathbf{e}_\varphi$$

both on its inner and outer surfaces. It has a built-in end at $z = a$ preventing any displacement of that cross-section, while the displacement of the other end at $z = b$ is defined by

$$\mathbf{u}_b = \vartheta r \mathbf{e}_\varphi$$

The volume of the bar is unloaded. The usual assumption of elasticity are valid, i.e.:
— displacements are small,
— the problem is a quasistatic one,
— the effect of heat, initial stresses and imperfections is negligible,
— the material of the bar is homogeneous, isotropic and linearly elastic.

The torsion of the elastic bar shown in Fig. 1 is characterized by the following boundary value problem [1, 2, 3]:

$$\nabla \cdot (r^3 \nabla \psi) = 0 \qquad (r, z) \in T, \tag{2.1}$$

$$Gr \frac{\partial \psi}{\partial n} = p_3 \qquad (r, z) \in \partial T_3, \tag{2.2}$$

$$Gr \frac{\partial \psi}{\partial n} = p_4 \qquad (r, z) \in \partial T_4 \tag{2.3}$$

$$\psi = 0 \qquad (r, z) \in \partial T_1 \tag{2.4}$$

$$\psi = \vartheta \qquad (r, z) \in \partial T_2 \tag{2.5}$$

Range T and its boundary defined by ∂T are represented in Fig. 2.

Making use of the function of two variables $\psi = \psi(r, z)$, the displacement vector $\mathbf{u} = \mathbf{u}(r, \varphi, z)$ can be given in the following form:

$$\mathbf{u} = v(r, z)\mathbf{e}_\varphi = r\psi(r, z)\mathbf{e}_\varphi \tag{2.6}$$

The scalar co-ordinates of the stress tensor, not being identically equal to zero, are obtained from relations

$$\tau_{r\varphi} = Gr \frac{\partial \psi}{\partial r}, \tag{2.7}$$

$$\tau_{z\varphi} = Gr \frac{\partial \psi}{\partial z}. \tag{2.8}$$

If the bar has continuous elastic supports, the load functions are as follows:

$$p_3 = -kv(r, z) = -kr\psi(r, z) \qquad (r, z) \in \partial T_3 \tag{2.9}$$
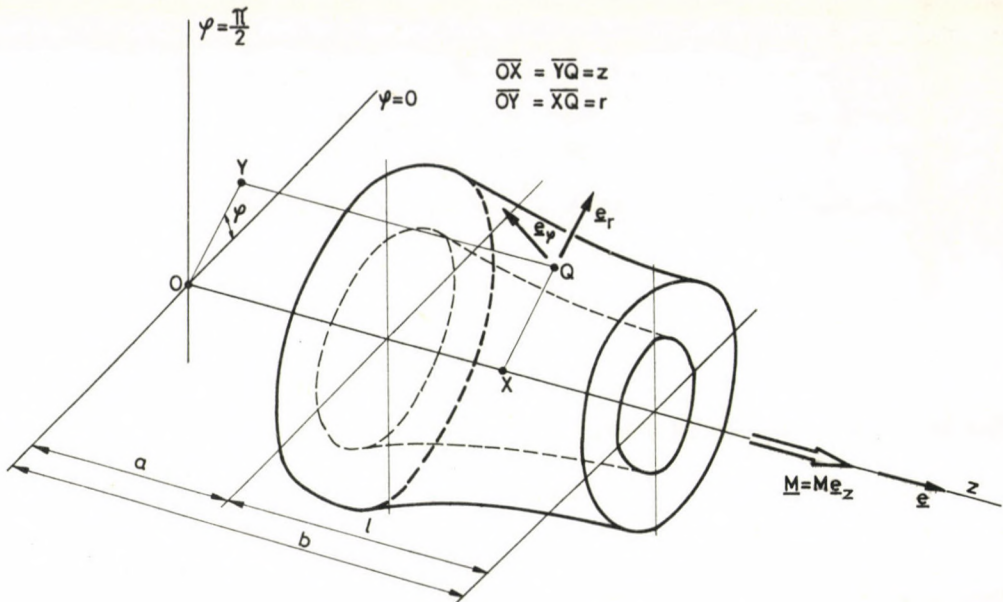
Fig. 1. Bar with an annulus of variable section
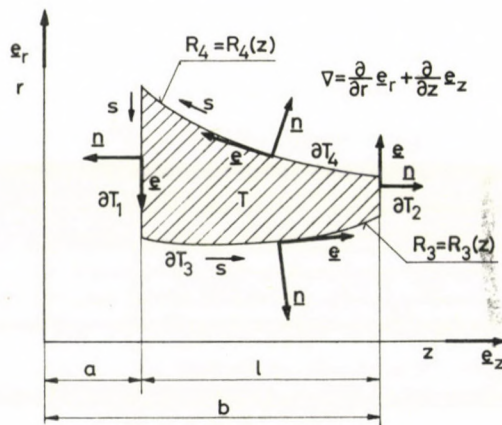
Fig. 2. Meridian section of the bar

$$p_4 = -kv(r, z) = -kr\psi(r, z) \qquad (r, z) \in \partial T_4 . \tag{2.10}$$

Let us introduce the notation

$$f = f(r, z) = \frac{\psi(r, z)}{\vartheta} \tag{2.11}$$

Making use of Eqs (2.1), (2.2), (2.3), (2.4), (2.5), (2.9), (2.10), (2.11), the torsional problem of the bar having an annulus cross-section of variable size supported elastically along

3*

its entire length can now be presented. Taking into account the fact that the bar has a built-in end at $z = a$ preventing any displacement there, while the displacement vector at $z = b$ is $\mathbf{u}_b = \vartheta r \mathbf{e}_\varphi$, the following boundary value problem can be set up:

$$\nabla \cdot (r^3 \nabla f) = 0 \qquad (r, z) \in T, \tag{2.12}$$

$$G \frac{\partial f}{\partial n} + kf = 0 \qquad (r, z) \in \partial T_3 \cup \partial T_4, \tag{2.13}$$

$$f = 0 \qquad (r, z) \in \partial T_1, \tag{2.14}$$

$$f = 1 \qquad (r, z) \in \partial T_2. \tag{2.15}$$

Making use of function $f = f(r, z)$, the displacement vector u and the shearing stresses $\tau_{r\varphi}$ and $\tau_{z\varphi}$ assume the form

$$\mathbf{u} = v(r, z)\mathbf{e}_\varphi = \vartheta r f(r, z)\mathbf{e}_\varphi, \tag{2.16}$$

$$\tau_{r\varphi} = G\vartheta r \frac{\partial f}{\partial r}, \tag{2.17}$$

$$\tau_{z\varphi} = G\vartheta r \frac{\partial f}{\partial z}. \tag{2.18}$$

The cross-section of the bar at $z = b$ is subjected to the torque [1]:

$$M = 2\pi \int\limits_{\partial T_2} r^2 \tau_{\varphi z}\, \mathrm{d}s = \vartheta 2\pi G \int\limits_{\partial T_2} r^3 \frac{\partial f}{\partial n}\, \mathrm{d}s. \tag{2.19}$$

The torsinal rigidity S of the bar having an annulus cross-section of variable size elastically supported is defined by the formula

$$S = \frac{M}{\vartheta}. \tag{2.20}$$

Some relations concerning the torsional rigidity S will now be introduced. According to the product-function's derivation rule and the Gauss' theorem of the transformation of integrals—making use of Eqs (2.12), (2.13), (2.14), (2.15)—, we obtain

$$\int\limits_T f\nabla \cdot (r^3 \nabla f)\, \mathrm{d}T = \int\limits_T \nabla \cdot (r^3 \nabla f)\, \mathrm{d}T - \int\limits_T r^3 |\nabla f|^2\, \mathrm{d}T = \int\limits_{\partial T} r^3 f \frac{\partial f}{\partial n}\, \mathrm{d}s -$$

$$-\int\limits_T r^3 |\nabla f|^2\, \mathrm{d}T = \int\limits_{\partial T_2} r^3 \frac{\partial f}{\partial n}\, \mathrm{d}s + \int\limits_{\partial T_3 \cup \partial T_4} r^3 f \frac{\partial f}{\partial n}\, \mathrm{d}s - \int\limits_T r^3 |\nabla f|^2\, \mathrm{d}T = \int\limits_{\partial T_2} r^3 \frac{\partial f}{\partial n}\, \mathrm{d}s -$$

$$- \int\limits_T r^3 |\nabla f|^2\, \mathrm{d}T - \frac{G}{k} \int\limits_{\partial T_3 \cup \partial T_4} r^3 \left(\frac{\partial f}{\partial n}\right)^2\, \mathrm{d}s \tag{2.21}$$

Combining Eqs (2.19), (2.20), (2.21), we have

$$S = 2\pi G \int_{\partial T_2} r^3 \frac{\partial f}{\partial n} \, ds , \qquad (2.22)$$

$$S = 2\pi G \left(\int_{T} r^3 |\nabla f|^2 \, dT + \frac{G}{k} \int_{\partial T_3 \cup \partial T_4} r^3 \left(\frac{\partial f}{\partial n} \right)^2 \, ds \right). \qquad (2.23)$$

Substituting Eq. (2.13) in to Eq. (2.23), we arrive at

$$S = 2\pi G \int_{T} r^3 |\nabla f|^2 \, dT + 2\pi k \int_{\partial T_3 \cup \partial T_4} r^3 f^2 \, ds . \qquad (2.24)$$

Formulas (2.23), (2.24) and equations (2.12), (2.13), (2.14), (2.15) show that the torsional rigidity S is always a positive quantity, i.e. $S > 0$.

The application of the Gauss' theorem of the transformation of integrals to Eq. (2.12) leads to

$$\int_{T} \nabla \cdot (r^3 \nabla f) \, dT = \int_{\partial T_1} r^3 \frac{\partial f}{\partial n} \, ds + \int_{\partial T_2} r^3 \frac{\partial f}{\partial n} \, ds + \int_{\partial T_3 \cup \partial T_4} r^3 \frac{\partial f}{\partial n} \, ds = 0 . \qquad (2.25)$$

Making use of Eqs (2.2) and (2.25), we find

$$S = -2\pi G \left(\int_{\partial T_1} r^3 \frac{\partial f}{\partial n} \, ds + \int_{\partial T_3 \cup \partial T_4} r^3 \frac{\partial f}{\partial n} \, ds \right). \qquad (2.26)$$

Finally, introducing Eq. (2.13) to Eq. (2.26), the formula for the torsional rigidity turns out to be

$$S = -2\pi G \int_{\partial T_1} r^3 \frac{\partial f}{\partial n} \, ds + 2\pi k \int_{\partial T_3 \cup \partial T_4} r^3 f \, ds . \qquad (2.27)$$

The primary aim of this paper is to derive inequalities enabling us to establish lower and upper bounds for the torsional rigidity S defined by formula (2.20) belonging to bars having an annulus cross-section of variable size. The exact value of the torsional rigidity could be obtained by solving the boundary value problem defined by Eqs (2.12), (2.13), (2.14), (2.15). In several cases, however, the exact solution of this problem is not known and, therefore, we abandon the idea of trying to find the exact value for the torsional rigidity. Instead, we will show how the value of the torsional rigidity can be set between lower and upper bounds.

3. Upper bound

3.1 Theorem. Let the function of two variables $H = H(r, z)$ be continuous in the closed region $T \cup \partial T$ and be continuously derivable in the open region T at least once and satisfying the conditions

$$H(r, z) = 0 \qquad (r, z) \in \partial T_1 \tag{3.1}$$

$$H(r, z) = H_2 = \text{constant} \qquad (r, z) \in \partial T_2 \tag{3.2}$$

It should be proved that the inequality

$$S \leqslant \frac{2\pi G \displaystyle\int_T r^3 \, |\nabla \cdot H|^2 \, dT + 2\pi k \displaystyle\int_{\partial T_3 \cup \partial T_4} r^3 H^2 \, ds}{H_2^2} \tag{3.3}$$

holds.

Demonstration. To prove inequality (3.3), we rely on the Schwarz inequality

$$D(f, f) D(H, H) \geqslant |D(f, H)|^2 \tag{3.4}$$

where

$$D(f, f) = 2\pi G \int_T r^3 \, |\nabla f|^2 \, dT + 2\pi k \int_{\partial T_3 \cup \partial T_4} r^3 f^2 \, ds, \tag{3.5}$$

$$D(H, H) = 2\pi G \int_T r^3 (\nabla H)^2 \, dT + 2\pi k \int_{\partial T_3 \cup \partial T_4} r^3 H^2 \, ds, \tag{3.6}$$

$$D(f, H) = 2\pi G \int_T r^3 \nabla f \cdot \nabla H \, dT + 2\pi k \int_{\partial T_3 \cup \partial T_4} r^3 f H \, ds. \tag{3.7}$$

According to the product-function's derivation rule and the Gauss' theorem of the transformation of integrals—making use of Eqs (2.12), (2.13), (2.24), (3.1), (3.2)—, we obtain

$$2\pi G \int_T r^3 \nabla f \cdot \nabla H \, dT + 2\pi k \int_{\partial T_3 \cup \partial T_4} r^3 f H \, ds = 2\pi G \int_T \nabla \cdot (r^3 H \nabla f) \, dT -$$

$$- 2\pi G \int_T H \nabla \cdot (r^3 \nabla f) \, dT + 2\pi k \int_{\partial T_3 \cup \partial T_4} r^3 H f \, ds = 2\pi G \int_{\partial T_1} r^3 H \frac{\partial f}{\partial n} \, ds +$$

$$+ 2\pi G H_2 \int_{\partial T_2} r^3 \frac{\partial f}{\partial n} \, ds + 2\pi \int_{\partial T_3 \cup \partial T_4} H r^3 \left[G \frac{\partial f}{\partial n} + k f \right] ds = H_2 S. \tag{3.8}$$

Combining the evident formula

$$S = D[f, f] \tag{3.9}$$

with equation (3.8) and inequality (3.4), we arrive directly at inequality (3.3).

4. Lower bound

4.1. Theorem. Let the vector

$$\mathbf{c} = \mathbf{c}(r, z) = c_r(r, z)\mathbf{e}_r + c_z(r, z)\mathbf{e}_z$$

be different from zero in the vector field rz and satisfying the partial differential equation

$$\nabla \cdot (r^3 \mathbf{c}) = 0 \qquad (r, z) \in T. \tag{4.1}$$

It should be proved that inequality

$$S \geqslant 2\pi G \frac{\left(\int\limits_{\partial T_2} r^3 \mathbf{c} \cdot \mathbf{n}\, ds\right)^2}{\int\limits_{T} r^3 \cdot \mathbf{b}^2\, dT + \dfrac{G}{k} \int\limits_{\partial T_3 \cup \partial T_4} r^3 (\mathbf{b} \cdot \mathbf{n})^2\, ds} \tag{4.2}$$

holds.

Demonstration. The basis of the demonstration is the Schwarz inequality

$$E[\nabla f, \nabla f] E[\mathbf{c}, \mathbf{c}] \geqslant (E[\nabla f, \mathbf{c}])^2 \tag{4.3}$$

where

$$E[\nabla f, \nabla f] = 2\pi G \int\limits_{T} r^3 \lfloor \nabla f \rfloor^2\, dT + 2\pi \frac{G^2}{k} \int\limits_{\partial T_3 \cup \partial T_4} r^3 (\nabla f \cdot \mathbf{n})^2\, ds, \tag{4.4}$$

$$E[\mathbf{c}, \mathbf{c}] = 2\pi G \int\limits_{T} r^3 \mathbf{c}^2\, dT + 2\pi \frac{G^2}{k} \int\limits_{\partial T_3 \cup \partial T_4} r^3 (\mathbf{c} \cdot \mathbf{n})^2\, ds, \tag{4.5}$$

$$E[\nabla f, \mathbf{c}] = 2\pi G \int\limits_{T} r^3 \nabla f \cdot \mathbf{c}\, dT + 2\pi \frac{G^2}{k} \int\limits_{\partial T_3 \cup \partial T_4} r^3 (\nabla f \cdot \mathbf{n})(\mathbf{c} \cdot \mathbf{n})\, ds. \tag{4.6}$$

It goes without saying that

$$S = E[\nabla f, \nabla f]. \tag{4.7}$$

Applying the product-function's derivation rule and the Gauss' theorem of the transformation of integrals and making use of Eqs (2.12), (2.14), (4.1), quantity $E[\nabla f, \mathbf{c}]$ can be transfered into the following form:

$$E[\nabla f, \mathbf{c}] = 2\pi G \int_T r^3 \nabla f \cdot \mathbf{c} \, dT + 2\pi \frac{G^2}{k} \int_{\partial T_3 \cup \partial T_4} r^3 (\nabla f \cdot \mathbf{n})(\mathbf{c} \cdot \mathbf{n}) \, ds =$$

$$= 2\pi G \int_T \nabla \cdot (r^3 \mathbf{c} f) \, dT - 2\pi G \int_T f \nabla \cdot (r^3 \mathbf{c}) \, dT +$$

$$+ 2\pi \frac{G}{k} \int_{\partial T_3 \cup \partial T_4} r^3 \frac{\partial f}{\partial n}(\mathbf{c} \cdot \mathbf{n}) \, ds = 2\pi G \int_{\partial T_1} r^3 f \mathbf{c} \cdot \mathbf{n} \, ds + 2\pi G \int_{\partial T_2} r^3 f \mathbf{c} \cdot \mathbf{n} \, ds +$$

$$+ 2\pi G \int_{\partial T_3 \cup \partial T_4} r^3 (\mathbf{c} \cdot \mathbf{n}) \left[f + \frac{G}{k} \frac{\partial f}{\partial n} \right] ds = 2\pi G \int_{\partial T_2} \mathbf{c} \cdot \mathbf{n} \, ds . \tag{4.8}$$

The combination of inequality (4.3) and equations (4.7), (4.8) directly results in inequality (4.2) which had to be proved.

   4.2 Theorem. Let the function of two variables $h = h(r, z)$ be continuously derivable, at least twice, and not identically equal to a constant in the closed region $T \cup \partial T$. The inequality to be proved is

$$S \geq 2\pi G \frac{(h_4 - h_3)^2}{\int_T \frac{|\nabla h|^2}{r^3} \, dT + \frac{G}{k} \int_{\partial T_3 \cup \partial T_4} \frac{1}{r^3} \left(\frac{\partial h}{\partial s} \right)^2 ds} \tag{4.9}$$

where

$$h_3 = h(R_3(b), b), \tag{4.10}$$

$$h_4 = h(R_4(b), b). \tag{4.11}$$

Demonstration. Making use of the substitution

$$\mathbf{c} = \frac{1}{r^3} \nabla h \times \mathbf{e}_\varphi \tag{4.12}$$

inequality (4.2) yields the verification of (4.9). It is obvious that vector $\mathbf{c} = \mathbf{c}(r, z)$ of the above form satisfies partial differential equation (4.1). After some algebraic manipulation, we have

$$\int_{\partial T_3 \cup \partial T_4} r^3 (\mathbf{c} \cdot \mathbf{n})^2 \, ds = \int_{\partial T_3 \cup \partial T_4} \frac{1}{r^3} [(\nabla h \times \mathbf{e}_\varphi) \cdot \mathbf{n}]^2 \, ds =$$

$$= \int_{\partial T_3 \cup \partial T_4} \frac{1}{r^3} [\nabla h \cdot (\mathbf{e}_\varphi \times \mathbf{n})]^2 \, ds = \int_{\partial T_3 \cup \partial T_4} \frac{1}{r^3} (\nabla h \cdot \mathbf{e})^2 \, ds = \int_{\partial T_3 \cup \partial T_4} \frac{1}{r^3} \left(\frac{\partial h}{\partial s} \right)^2 ds , \tag{4.13}$$

$$\int_{\partial T_2} r^3(\mathbf{c} \cdot \mathbf{n}) \, ds = \int_{\partial T_2} (\nabla h \times \mathbf{e}_\varphi) \cdot \mathbf{n} \, ds =$$

$$= \int_{\partial T_2} \nabla h \cdot (\mathbf{e}_\varphi \times \mathbf{n}) \, ds = \int_{\partial T_2} \nabla h \cdot \mathbf{e} \, ds = \int_{\partial T_2} \frac{\partial h}{\partial s} \, ds = h_4 - h_3 \, . \tag{4.14}$$

Eqs (4.13), (4.14) show that inequality (4.9) holds.

5. Supplementary remarks

5.1 A short discussion on inequalities (3.3) and (4.2) shows that the sign of equality in (3.3), (4.2) holds only if

$$H(r, z) = \alpha f(r, z) \, , \tag{5.1}$$

$$\mathbf{c}(r, z) = \alpha \nabla f \tag{5.2}$$

where α is a real, arbitrary constant which is different from zero.

5.2 Let consider the function of two variables $F = F(r, z)$ which, apart from a real additive constant, is unambiguously defined by

$$\nabla F = r^3(\mathbf{e}_\varphi \times \nabla f) \tag{5.3}$$

Making use of Eq. (5.3), it is easy to see that function $F = F(r, z)$ satisfies the following elliptic partial differential equation

$$\nabla \cdot \left(\frac{1}{r^3} \nabla F \right) = 0 \qquad (r, z) \in T. \tag{5.4}$$

Combining Eqs (2.22) and 5.3), we have

$$S = 2\pi G(F_4 - F_3) \tag{5.5}$$

since

$$\int_{\partial T_2} r^3 \frac{\partial f}{\partial n} \, ds = \int_{\partial T_2} r^3 \nabla f \cdot \mathbf{n} \, ds =$$

$$= \int_{\partial T_2} \nabla F \cdot (\mathbf{n} \times \mathbf{e}_\varphi) \, ds = \int_{\partial T_2} \nabla F \cdot \mathbf{e} \, ds = F_4 - F_3 \tag{5.6}$$

where

$$F_3 = F(R_3(b), b) \, , \tag{5.7}$$

$$F_4 = F(R_4(b), b) \, . \tag{5.8}$$

A derivation involving formula (2.26) yields the same result.

Finally, making use of formulas

$$|\nabla F|^2 = r^6 |\nabla f|^2, \tag{5.9}$$

$$\left(\frac{\partial F}{\partial s}\right)^2 = r^6 \left(\frac{\partial f}{\partial n}\right)^2 \tag{5.10}$$

which we obtained from Eq. (5.3), we arrive at

$$S = 2\pi G \left(\int_T \frac{|\nabla F|^2}{r^3} \, dT + \frac{G}{k} \int_{\partial T_3 \cup \partial T_4} \frac{1}{r^3} \left(\frac{\partial F}{\partial s}\right)^2 \, ds \right). \tag{5.11}$$

In addition to the above results, a short discussion can be carried out concerning inequality (4.9). The discussion shows that the sign of equality in (4.9) is valid only if

$$h(r, z) = \alpha F(r, z) + \beta \tag{5.12}$$

where α and β are arbitrary, real constants excluding the case $\alpha = 0$.

6. Applications

6.1 Let function $H(r, z)$ in inequality (3.1) assume the form

$$H(r, z) = P(z). \tag{6.1}$$

Let the function of one variable $P = P(z)$ satisfy the boundary conditions

$$P(a) = 0, \tag{6.2}$$

$$P(b) = 1. \tag{6.3}$$

A simple calculation yields

$$\int_T r^3 |\nabla P|^2 \, dT = \int_a^b A(z)(P'(z))^2 \, dz, \tag{6.4}$$

$$\int_{\partial T_3 \cup \partial T_4} r^3 P^2 \, dT = \int_a^b B(z)(P(z))^2 \, dz \tag{6.5}$$

where

$$A(z) = \frac{G}{2} [(R_4(z))^4 - (R_3(z))^4]\pi, \tag{6.6}$$

$$B(z) = 2k[(R_3(z))^3 \sqrt{1 + (R_3'(z))^2} + (R_4(z))^3 \sqrt{1 + (R_4'(z))^2}]\pi \tag{6.7}$$

The above expressions together with inequality (3.3) result in the following upper bound

$$S \leqslant \int_a^b [A(P')^2 + BP^2] \, dz. \tag{6.8}$$

6.2. Let quantities a, b, P in inequality (6.8) assume the following values

$$a=0, \, b=l \quad \text{and} \quad P=\frac{z}{l} \tag{6.9}$$

Substituting expressions (6.9) into inequality (6.8), we arrive at an upper bound for the torsional rigidity:

$$S \leqslant \frac{1}{l^2} \int_0^l [A(z)+z^2 B(z)] \, dz . \tag{6.10}$$

6.3 Let functional I take the form

$$I[P(z)] = \int_a^b [A(P')^2 + BP^2] \, dz . \tag{6.11}$$

Making use of the elementary results of variational calculus, it can be shown that, concerning functions $P = P(z)$ satisfying conditions (6.2), (6.3), functional I is minimum at a function $\hat{P} = \hat{P}(z)$ which is a solution of the boundary value problem

$$-\frac{d}{dz}\left(A(z)\frac{d\hat{P}}{dz}\right) + B(z)\hat{P} = 0 \qquad a < z < b \tag{6.12}$$

$$\hat{P}(a) = 0, \tag{6.13}$$

$$\hat{P}(b) = 1 . \tag{6.14}$$

For functions $\hat{P} = \hat{P}(z)$ satisfying conditions (6.12), (6.13), (6.14), inequality

$$I[\hat{P}(z)] \leqslant I[P(z)] \tag{6.15}$$

holds.

On the basis of relation

$$I[\hat{P}(z)] = \int_a^b [A(\hat{P}')^2 + B\hat{P}^2] \, dz =$$

$$= \int_a^b (A\hat{P}'\hat{P})' \, dz + \int_a^b [(-A\hat{P}')' + B\hat{P}] \, dz = [A\hat{P}'\hat{P}]_a^b = A(b)\hat{P}'(b) \tag{6.16}$$

and inequalities (6.10), (6.15), we obtain

$$S \leqslant A(b)\hat{P}'(b) \tag{6.17}$$

The above results show that, considering upper bounds in the form of (6.8), the best approximation for the torsional rigidity emerges if $P(z) = \hat{P}(z)$.

6.4 Let us apply inequality (4.9) to function

$$h = h(r, z) = r^4 p(z) \tag{6.18}$$

A long but elementary calculation results in

$$S \geqslant \frac{2\pi G}{i[p(z)]} \tag{6.19}$$

where

$$i[p(z)] = \int\limits_a^b [A_2(p')^2 + 2A_1 p'p + A_0 p^2] \, dz , \tag{6.20}$$

$$A_2 = \frac{(R_4(z))^6 - (R_3(z))^6}{6} + \frac{G}{k} \left[\frac{(R_4(z))^5}{\sqrt{1+(R'_4(z))^2}} + \frac{(R_3(z))^2}{\sqrt{1+(R'_3(z))^2}} \right] , \tag{6.21}$$

$$A_1 = 4 \frac{G}{k} \left[\frac{(R_4(z))^4 R'_4(z)}{\sqrt{1+(R'_4(z))^2}} + \frac{(R_3(z))^2 R'_3(z)}{\sqrt{1+(R'_3(z))^2}} \right] , \tag{6.22}$$

$$A_0 = 4[(R_4(z))^4 - (R_3(z))^4 + 4 \frac{G}{k} \left(\frac{(R_3(z))^3 (R'_3(z))^2}{\sqrt{1+(R'_3(z))^2}} + \right.$$

$$\left. + \frac{(R_4(z))^3 (R'_4(z))^2}{\sqrt{1+(R'_4(z))^2}} \right)] . \tag{6.23}$$

The function of one variable $p = p(z)$ in formula (6.20) satisfies the boundary condition

$$p(b) = \frac{1}{(R_4(b))^4 - (R_3(b))^4} . \tag{6.24}$$

6.5 Let function $p(z)$ in inequality (6.19) be constant in the form

$$p(z) = \frac{1}{(R_4(b))^4 - (R_3(b))^4} = \text{constant} . \tag{6.25}$$

After a short calculation, the lower bound for the torsional rigidity emerges as

$$S \geqslant 2\pi G \frac{\{[R_4(b)]^4 - [R_3(b)]^4\}^2}{\int\limits_a^b A_0(z) \, dz} . \tag{6.26}$$

6.6 Making use of the elementary results of variational calculus, it can be shown that

$$\min_{p(z)} i[p(z)] = i[\hat{p}(z)] \tag{6.27}$$

where function $\hat{p} = \hat{p}(z)$ is the solution of the following boundary value problem

$$-(A_2 \hat{p}')' + (A_0 - A'_1)\hat{p} = 0 \qquad a < z < b , \tag{6.28}$$

$$A_2(a)\hat{p}'(a) + A_1(a)\hat{p}(a) = 0 \tag{6.29}$$

$$\hat{p}(b) = \frac{1}{(R_4(b))^4 - (R_3(b))^4} . \tag{6.30}$$

Applying the above results to functions $h = h(r, z)$ defined by Eq. (6.18), it can be proved that the best lower bound belongs to

$$h(r, z) = r^4 \hat{p}(z) \tag{6.31}$$

The application of function $h = h(r, z)$ in the form of (6.31) results in

$$S \geq \frac{2\pi G}{i[\hat{p}(z)]}.$$ (6.32)

We will now transform the right-hand side of the lower bound (6.32) into a more explicit form:

$$i[\hat{p}(z)] = \int_a^b [A_2(\hat{p}')^2 + 2A_1 \hat{p}\hat{p}' + A_0 \hat{p}^2] \, dz = \int_a^b (A_2 \hat{p}'\hat{p})' \, dz -$$

$$- \int_a^b [(-A_2 \hat{p}')'\hat{p} + (A_1 \hat{p}^2)' + A_0 \hat{p}^2] \, dz = [A_2 \hat{p}'\hat{p}]_a^b + \int_a^b [(-A_2 \hat{p}')' + (A_1 \hat{p}^2)' -$$

$$- A_1' \hat{p}^2 + A_0 \hat{p}^2] \, dz = [A_2 \hat{p}'\hat{p} + A_1 \hat{p}^2]_a^b + \int_a^b \hat{p}[(-A_2 \hat{p}')' + (A_0 - A_1')\hat{p}] \, dz =$$

$$= [A_2(b)\hat{p}'(b) + A_1(b)\hat{p}(b)]\hat{p}(b) =$$

$$= \frac{A_2(b) \, [(R_4(b))^4 - (R_3(b))^4]\hat{p}'(b) + A_1(b)}{(R_4(b))^4 - (R_3(b))^4}.$$ (6.33)

The formula of the torsional rigidity (6.32) can now be written as

$$S \geq \frac{2\pi G[(R_4(b))^4 - (R_3(b))^4]^2}{[(R_4(b))^4 - (R_3(b))^4]A_2(b)\hat{p}'(b) + A_1(b)}$$ (6.34)

6.7 The exact value of the torsional rigidity is not known even in the special case when

$$R_3 = R_3(z) = \text{constant},$$ (6.35)

$$R_4 = R_4(z) = \text{constant}.$$ (6.36)

In this case the quantities necessary for the calculation of the upper bound (6.17) are as follows:

$$A = \frac{G}{2}(R_4^4 - R_3^4)\pi = \text{constant},$$ (6.37)

$$B = 2k\pi(R_4^3 + R_3^3) = \text{constant}.$$ (6.38)

Introducing the notation

$$\alpha^2 = \frac{4k(R_3^3 + R_4^3)}{G(R_4^4 - R_3^4)},$$ (6.39)

differential equation (6.12) turns into

$$\hat{P}'' - \alpha^2 \hat{P} = 0$$ (6.40)

The solution satisfying this differential equation and boundary conditions (6.13), (6.14) runs accordingly

$$\hat{P}(z) = \frac{\text{sh } \alpha z}{\text{sh } \alpha l} \,. \tag{6.41}$$

Substituting the above function to (6.17) and making use of formula (6.39), we arrive at

$$S \leqslant \frac{G\pi}{4} (R_4^4 - R_3^4) \sqrt{\frac{(R_3^4 + R_3^3)k}{(R_4^4 - R_3^4)G}} \text{ cth } 2 \sqrt{\frac{(R_4^3 + R_3^3)k}{R_4^4 - R_3^4 G}} \, l \,. \tag{6.42}$$

6.8 The lower bound for a bar limited by circular cylinders can be obtained from inequality (6.34). The quantities necessary for the calculation in the case of $a = 0$, $b = 0$ are the following:

$$A_2 = \frac{1}{6} (R_4^6 - R_3^6) + \frac{G}{k} (R_4^5 + R_3^5) = \text{constant} \,, \tag{6.43}$$

$$A_1 = 0 \,, \tag{6.44}$$

$$A_0 = 4(R_4^4 - R_3^4) = \text{constant} \,. \tag{6.45}$$

Introducing the notation

$$\beta^2 = \frac{4(R_4^4 - R_3^4)}{\dfrac{1}{6} (R_4^6 - R_3^6) + \dfrac{G}{k} (R_4^5 + R_3^5)} \,, \tag{6.46}$$

the differential equation (6.28) turns into

$$\hat{p}'' - \beta^2 \hat{p} = 0 \,. \tag{6.47}$$

The solution satisfying this equation as well as boundary conditions (6.29), (6.30) at $a = 0$ and $b = l$ reads as

$$\hat{p}(z) = \frac{1}{R_4^4 - R_3^4} \frac{\text{ch } \beta z}{\text{ch } \beta l} \,. \tag{6.48}$$

Making use of (6.34), (6.46), (6.48), the lower bound for the torsional rigidity becomes

$$S \geqslant \frac{2\pi G(R_4^4 - R_3^4)^2}{\left[\dfrac{1}{6} (R_4^6 - R_3^6) + \dfrac{G}{k} (R_4^5 + R_3^5) \right] \beta \text{ th } \beta l} \,. \tag{6.49}$$

6.9 Figure 3 shows the meridian cross-section of a bar limited by cones. The basic data are as follows:

$$\gamma_4 = 1 \qquad \gamma_3 = 0,8, \qquad k = 2 \cdot 10^6 \text{ N} \cdot \text{mm}^{-3},$$

$$G = 10^5 \text{ N} \cdot \text{mm}^{-2}, \qquad l = 90 \, mm,$$

$$a = 10 \text{ mm}, \qquad b = 100 \text{ mm}$$

$$R_3(z) = \gamma_3 z = 0.8 \, z \quad [\text{mm}] \,,$$

$$R_4(z) = \gamma_4 z = z \qquad [\text{mm}] \,.$$
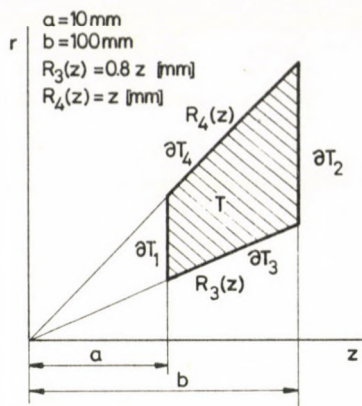
Fig. 3. Meridian section of the bar limited by cones

Making use of inequalities (6.10), (6.26), the lower and upper bounds for the torsional rigidity emerge as

$$10.8 \times 10^{11} \ \text{Nmm} < S < 12.9 \times 10^{11} \ Nmm.$$

References

1. Arutjujan, N. H.—Abramjan, B. L.: Krucsenie uprugih tel. Izd. Lit. Fiz.—Mat. Moskva 1963, 506—516
2. Timpe, A.: Die Torsion von Umdrehungskörpern. Math. Ann. Leipzig. 71 (1911), 480—509
3. Willers, Fr.: Die Torsion eines Rotationskörpers um seine Achse. Zeitschr. f. Math und Phys. 55 (1907), 225—263

PROPOSED CONTINUUM MODEL FOR SIMULATING THE BEHAVIOUR OF GRANULAR MATERIALS

J. Füzy*—J. Vas**

The paper presents a possible way to simulate the very special behaviour of granular materials. Applying the well-known micro-elastic continuum theory for the problem a continuum theory with intrinsic volume-change was elaborated. The basic equations include the following unknown kinematic functions: the displacement vector and the intrinsic volume-change as a scalar function. The consitutive equation consists of six new elastic material constants, to evaluate them requires further investigations

Introduction

The theories proposed for the calculation of the inner stress distribution and deformation of a considerable part of shell structures, such as the shells of revolution, are so accurate that even the special behaviour of the material used for construction can modify in no considerable degree the statics of storage tanks or silos [1].

In view of this fact it seems highly superfluous to improve the accuracy of these theories any further as long as the functions and distribution of the outer load do not attain an approximately similar accuracy. The materials most frequently stored in such types of tanks or silos are granular materials, grain, gravel, etc. The accuracy of computing the pressure exerted on the inner surface of the shell by the statics and dynamics of the stored material leaves in these cases much to be desired.

To promote the solution of this topical design problem in this particular field of engineering we try to show in this paper a possibility of simulating the behaviour of granular materials by a continuum mechanical model.

Summary of the general equations of linear microelasticity

As is well known, in classical linear elasticity there occurs only one kinematic variable as the basic unknown function, namely the displacement vector field. In micro-elasticity the kinematic freedom of the elementary point of continuum was extended by a tensor field, which means an intrinsic micro-deformation tensor of the elementary

* Dr. J. Füzy, Scientific Adviser, Hungarian Institute for Building Science, ÉTI, David F. u. 6, H-1113 Budapest, Hungary
** J. Vas, Senior Researcher, Hungarian Institute for Building Science, ÉTI, Dávid F. u. 6, H-1113 Budapest, Hungary

4

point as a new independent kinematic variable besides the displacement vector field [2].

It is not necessary to clarify the full physical background and reality of such continua, all the more because the literature on that particular branch of science leaves no doubt in this respect [3, 5, 6], especially in the case of the so-called Cosserat continua which are a degenerate type of the theory [4].

The micro-deformation tensor d_{ij} is taken to be homogeneous at the elementary point which is a finite micro-volume, and non-homogeneous in the macro-medium. The symmetric part of d_{ij} is the micro-strain: $d_{(ij)}$ and the antisymmetric part is the micro-rotation: $d_{[ij]}$.

An alternative interpretation is that the quantities d_{ij} are proportional to the components of the displacement of the tips of the deformable directors [7], in that case $d_{[ij]}$ are the components of the displacement of the tips of the Cosserat "trièdre".

We define the usual strain (now the macro-strain):

$$D_{(ij)} = \frac{1}{2} (\partial_i u_j + \partial_j u_i) \tag{1}$$

and also the so-called relative deformation which is the difference between the macro-displacement gradient and the micro-deformation:

$$\gamma_{ij} = \partial_i u_j - d_{ij} \tag{2}$$

and the micro-deformation gradient (the macro-gradient of the micro-deformation):

$$\kappa_{ijk} = \partial_i d_{jk} \tag{3}$$

The basic kinematic unknown functions u_i and d_{ij} are assumed to be single valued functions of the coordinates of the macro-space, leading to the compatibility equations:

$$e_{mik} e_{nlj} \partial_i \partial_j D_{kl} = 0, \qquad \text{a.)}$$

$$e_{mij} \partial_i \kappa_{jkl} = 0, \qquad \text{b.)}$$

$$\partial_i (D_{(jk)} + D_{[jk]} - \gamma_{jk}) = \kappa_{ijk} \qquad \text{c.)} \tag{4}$$

where $D_{[ij]}$ is the macro-rotation and e_{ijk} is the alternating tensor.

In view of the variation of potential energy W, we define the Cauchy stress tensor:

$$S_{(ij)} = \frac{\partial W}{\partial D_{(ij)}} = S_{(ji)} \tag{5}$$

the relative stress tensor:

$$\sigma_{ij} = \frac{\partial W}{\partial \gamma_{ij}} \tag{6}$$

and the double stress tensor:

$$\mu_{ijk} = \frac{\partial W}{\partial \kappa_{ijk}} \tag{7}$$

From the variational equation of motion, there follow immediately the twelve equations of motion [2]:

$$\partial_i(S_{(ij)} + \sigma_{ij}) + f_j = \rho\ddot{u}_j, \qquad \text{a.)}$$

$$\partial_i\mu_{ijk} + \sigma_{jk} + \varphi_{jk} = -\frac{1}{3}\rho'L_{ij}^2 d_{1k}, \text{b.)} \qquad (8)$$

Thus f_i is the body force per unit volume, φ_{jk} is to be interpreted as a double force per unit volume, ρ is the mass density of the material per unit macro-volume, ρ' is the mass density of micro-material and the dot means differentiation with respect to time. The expression L_{ij}^2 represents a kind of inertia tensor depending on the measures of the unit cell (micro-volume) [2].

3. Proposed continuum model for simulating the behaviour of granular materials

One of the most interesting and significant features of the behaviour of granular materials is that the continuum may change in volume without isotropic pressure. This means for instance, that a unit volume of granular material under shear deformation will be compacted if the initial state of the pattern was loose, and it will relax if it was originally compact. This phenomenon definitely influences the dynamics of granular materials and so we want to focus our analysis on that.

In our opinion the theory of micro-elasticity expounded above should be remarkably suitable for that purpose. It is only necessary to take the isotropic part of the micro-deformation tensor as an intrinsic volume change into account, which means a scalar function "e" as an independent variable besides the displacement vector:

$$d_{[ij]} = 0 \quad \text{and} \quad d_{(ij)} = e\delta_{ij} \qquad (9)$$

In that case the relative deformation will take the following form:

$$\gamma_{ij} = u_{j,i} - e\delta_{ij} \qquad (10)$$

using the conventional abbreviation $\partial_j u_i = u_{i,j}$ and δ_{ij} designating the Kronecker symbol.

Based on this assumption the micro-deformation gradient will reduce to a vector:

$$\kappa_i = e_{,i} \qquad (11)$$

and as a consequence, the double-stress tensor reduces to a vector μ_i also.

We try to find the constitutive equation in the following linearized form:

$$S_{(ij)} = c_1 D_{(ij)} + c_2 D_{kk}\delta_{ij} + c_3 e\delta_{ij}, \qquad \text{a.)}$$

$$\sigma_{ij} = c_4 D_{(ij)} + c_5 D_{kk}\delta_{ij} + c_6 D_{[ij]} + c_7 e\delta_{ij}, \qquad \text{b.)}$$

$$\mu_i = c_8 e_{,i} \qquad \text{c.)} \qquad (12)$$

4*

The constants c_1 and c_2 do not represent new constitutive constants, they are linear combinations of the Lamé's constitutive moduli, but $c_3 - c_8$ are new ones.

Introducing a new general stress tensor by the following definition:

$$\tilde{S}_{ij} = S_{(ij)} + \sigma_{ij} \qquad \text{a.)}$$

$$\tilde{S}_{ij} = (c_1 + c_4)D_{(ij)} + (c_2 + c_5)D_{kk} + c_6 D_{[ij]} + (c_3 + c_7)e\delta_{ij} \qquad \text{b.)} \quad (13)$$

the first equation of motion (8/a) will take the form of the classical continuum:

$$\tilde{S}_{ij,i} + f_j = \rho\ddot{u}_j \qquad (14)$$

The second equation of motion (8/b) can be simplified by using Eqs (12/b) and (12/c) and finally we get the following form:

$$c_8 e_{,ii} + (c_4 + 3c_5)u_{i,i} + 3c_7 e = \rho\,\frac{L^2}{6}\,\ddot{e} \qquad (15)$$

having taken into account that $D_{(ij)}\delta_{ij} = u_{i,i}$. In the equation the double force per unit volume is neglected and the global-mass ρ and the micro-mass ρ' are assumed to be identical. The micro-volume (unit-cell) is regarded to be cubic and so it has only one significant dimension: "L" and, as a consequence, the inertia tensor reduces to a constant as is the case in the Cosserat theory. The meaning of "L" in our case must be the smallest possible volume that still contains a sufficient number of grains for the phenomenon to take place.

4. Conclusion

The geometric equation $D_{ij} = u_{j,i}$ and the constitutive equation (13/b) together with the two equations of motion (14) and (15) form the basic system of equations of the proposed continuum model. These equations include a new variable: "e", which means the intrinsic volume change superposed on the dilatation u_{ii} of the medium. For the new variable which is a scalar function we have a new equation (15), the other equations are very similar to the ones of the classical elastic continua, they differ only in the isotropic term on the right side of the constitutive equation (14).

A problem to be invesigated in the future follows from the undefined new constitutive constants: $c_3 - c_8$. The main purpose of working out such continuum models should be to elaborate the algorithm of the system—by finite elements for instance—and obtain in this way a very effective scientific tool to investigate the behaviour of granular materials.

In that case there is a possibility to change the values of the new constants systematically—especially in connection of c_8—and so to determine their actual values for different materials.

It will be possible to follow the tracks of the whole process using this method by displaying the numerical solutions of the system of equations at equidistant time lags.

In this way we could improve our knowledge of the behaviour of granular media, for instance in the course of the discharge of silos, etc.

References

1. Füzy, J.: The Influence of Heretogeneous Concrete Character on the Moment Distribution in the Edge-Effect of Membrane Shells. IASS Bulletin, n. 68. pp. 39—42
2. Mindlin, R. D.: Micro-Structure in Linear Elasticity. Arch. Rational Mech. Anal. 16, pp. 51—78
3. Eringen, A. Cemal: Theory of Micropolar Elasticity. A Fracture and Advanced Treatment. Ed. Liebowitz, Academic Press, New York. Vol. 7
4. Schijve: Note on Couple Stresses. Journ. Mech. Phys. Sol. 14, pp. 113—120
5 Koh, S. L.: A special Theory of Microelasticity. Int. J. Engng. Sci. 8, pp. 583—593.
6. Kröner, E.: On the Physical Reality of Torque Stresses in Continuum Mechanics. Int. J. Engng. Sci. 1, pp. 261—278
7. Ericksen, J. L., Truesdell, C.: Exact Theory of Stress and Strain in Rods and Shells. Arch. Rational Mech. Anal. 21, pp. 295—308

STABILITY OF VISCOELASTIC STRUCTURES

GY. IJJAS*

The critical state of a viscoelastic structure—i.e. when the velocity of the deformation of the structure is infinite—can be characterized by the singularity of a Hesse matrix. This Hesse matrix contains the second derivatives of the difference of the free energy of the structure and the work of the loads with respect to the outer parameters. In the case of viscoelastic structures the Hesse matrix usually is the function of the initial imperfections, the loads and the inner parameters (creep).

1. Introduction

Reports on creep stability problems have been published from the end of the forties. But until 1978 solutions of single problems were only presented. Some of them are excellent, but others are only acceptable.

Hayman [2], [3] gave the first general discussion of the creep stability problems on the base of the bifurcation theory and cleared up some false ideas.

The most important thesises of his articles are as follows.

Let us leave the creep of the structure out of consideration, that is be the structure elastic. The modulus of elasticity of the structure is the same as that of the short time modulus of the original structure. If the structure has no unstable equilibrium state at a prescribed load level, the velocity of the deformation of the original (viscoelastic) structure will not be infinite at that load level. Naturally the load of the structure has to be less than the lowest critical load of the elastic structure. It follows, that the structure has no finite critical time at that load level. Hayman showed it in the case of statically determinate structures.

If the elastic structure has at least one unstable equilibrium state at a prescribed load level, then there is the possibility of infinitely large velocity of deformation at finite deformation. It follows that the structure may have finite critical time.

There is the hypothetical possibility, that a structure originally has a stable equilibrium path and this stable equilibrium path is becoming unstable during creep. However, we have not met any research activity presenting this kind of structure.

Hayman's papers [2], [3] are excellent, but they give only a phenomenological description, without rigorous mathematical base. So his results are not of general nature.

* Ijjas György, Öv u. 165, H-1147-Budapest, Hungary

The aim of this paper is to present the criterion of the loss of stability of viscoelastic structures on a rigorous mathematical base. We will examine structures with finite degree of freedom only with finite critical time. We will not take into account the aging and plastic deformations. We will prove that at the critical time the determinant of the Hesse matrix of the structure vanishes. This is the generalization of the energy criterion of the elastic stability.

2. The demonstration of the general criterion of viscoelastic stability

The Lagrange equation of the small vibration of dissipative structures was probably set up at the end of the thirties [4], [5]. If we do not take into account the kinetic energy, the remaining part of the equation is the static equilibrium equation of dissipative structures. Biot [6] was the first who derived this equation from thermodynamic principles for the case of linear viscoelasticity. This equation reads

$$\frac{\partial V}{\partial q_i} + \frac{\partial D}{\partial \dot{q}_i} = P_i, \tag{1}$$

where V is the free energy of the structure,
   D is the dissipation function,
   q_i are the generalized coordinates (components of displacement),
   $\dot{q}_i$ are the velocity components of displacement,
   P_i are the components of the generalized force vector.

If we have conservative loads, then making use of equation $Q = V - W$, where their works is W, Eq. (1) takes the form:

$$\frac{\partial Q}{\partial q_i} + \frac{\partial D}{\partial \dot{q}_i} = 0. \tag{2}$$

One of our basic assumption is that the displacement of the structure is always the sum of the elastic and the creep displacement. We will name the sum of these displacements external parameters, and the creep displacements internal parameters.

Since Q depends on the displacements only, and D depends on the velocity of the internal parameters, the system of equations (2) can be divided into two parts:

$$\frac{\partial Q}{\partial q_i} = 0, \qquad (i = 1, \ldots, m) \tag{3a}$$

$$\frac{\partial Q}{\partial q_j} + \frac{\partial D}{\partial \dot{q}_j} = 0, \qquad (j = m+1, \ldots, m+n) \tag{3b}$$

where m is the number of the independent external parameters, n is the number of the independent internal parameters. Equations (3a) will be called external equilibrium equations, and equations (3b) will be called internal equilibrium equations (W is the function of the external parameters only, so Eqs (3a) contain the loads).

We will postulate that the velocity of the internal parameters tends to infinity only in the case of infinite forces. This statement seems plausible, if we examine the equation of Newton, Bailey, Ludwik or Nadai viscous flow [7].

So we have to examine only the velocity of external parameters. Let's differentiate Eqs (3a) with respect to time. (In the following the double indexes indicate summation convention):

$$\frac{d}{dt}\left[\frac{\partial Q}{\partial q_i}\right] = \frac{\partial^2 Q}{\partial q_i \partial q_l} \dot{q}_l = 0 . \quad (l=1, \ldots, m+n) \tag{4}$$

$$(i=1, \ldots, m)$$

Let us divide the equations of the system of equations (4) into two parts. The first part contains the velocity of the external parameters as multipliers, the second part contains the velocity of internal parameters as multipliers. The system of equations (3) thus assumes the form

$$\frac{\partial^2 Q}{\partial q_i \partial q_l} \dot{q}_l + \frac{\partial^2 Q}{\partial q_i \partial q_j} \dot{q}_j = 0, \quad (i=1, \ldots, m) \tag{5a}$$

$$(l=1, \ldots, m)$$

$$\frac{\partial Q}{\partial q_j} + \frac{\partial D}{\partial \dot{q}_j} = 0, \quad (j=m+1, \ldots, m+n) \tag{5b}$$

where $\dot{q}_l$ is the velocity of the external parameters. However, the system of equations (5a) is linear for the velocity of the external parameters $\dot{q}_l$. Since we have postulated that $\dot{q}_j$ is infinite only in the case of infinite forces, formula

$$\left|\frac{\partial^2 Q}{\partial q_i \partial q_l}\right| = 0 \tag{6}$$

represents the necessary condition for at least one of the velocities: $\dot{q}_l = \infty$. (Q is a continuous function and its derivatives are continuous too).

In other words, the velocity of at least one of the external parameters (the velocity of full displacements) is infinite, if the determinant of the Hesse matrix of the function of the difference of the free energy and the work of external forces vanishes. (The Hesse matrix contains only derivatives with respect to the external parameters!). This Hesse matrix is the matrix of the coefficients of the system of equations (5a). This criterion is the generalization of the energy criterion of the stability of elastic structures (In the case of elasticity we have no internal parameters.)

The above derivation was based on the Lagrange equation of linearly viscoelastic system. This results, however, can easily be extended to the case of nonlinear creep.

Namely, the external equilibrium equations (3a) can be derived from the elastic potential (the free energy) of the structure and from the work of external forces. It

follows that they express the equilibrium of external forces and the internal (elastic) forces (stresses). The internal parameters are only parameters in these equations. So these equations do not give any information about the type of creep (linear or nonlinear). This information can only be obtained from the internal equilibrium equations. It can easily be seen that in the case of nonlinear creep (i.e. the system of equations (3b) are nonlinear) the earlier derivations hold.

The derivation in this form holds only in the case of constant loads. If the loads are not constant, Eqs (4) and (5) contain an element which is the function of the velocity of loading. Since we examine only statically loaded structures, the velocity of loading is not infinite, so the conditions of the earlier deduction do not change.

If the system of equations (3) has a solution, this solution is the system of displacements of the structure (the external and internal parameters) in the function of time. Introducing this system of parameters into (6), we obtain an equation for time. If Eq. (6) has positive real solutions, then the smallest one is the critical time.

3. Illustrative examples

Let us analyse some simple examples to illustrate the previous derivation and to show some important new relations.

A statically indeterminate structure is shown in Fig. 1. The rigidity of the bar of length L is infinite. K_1 and K_2 are linear springs and can deform without restriction. The constitutive equations of the springs are

$$F = K_2(\Delta - \Delta_0), \tag{7a}$$

$$M = K_1(\Theta - \Theta_0), \tag{7b}$$

where $\Delta_0 = L \sin \Theta_0$ represents the initial stress-free state. (If Δ_0 relates to the structural imperfections, then condition $\Delta_0 = 0$—i.e. the bar is vertical—means the structure
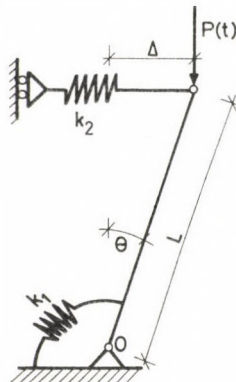
Fig. 1.

without initial imperfection). The equilibrium condition of the structure is that the moment at point 0 is zero. Taking into consideration equation (7), this condition results in

$$PL \sin \Theta - K_2 L^2 (\sin \Theta - \sin \Theta_0) \cos \Theta - K_1 (\Theta - \Theta_0) = 0, \tag{8}$$

The structure is in critical state when $\partial P / \partial \Theta = 0$. (This is equivalent to the singularity of the Hesse matrix of the potential energy.) Expressing P from (8) and differentiating with respect to Θ, we obtain a fraction. The left-hand side of Eq.

$$K_2 L^2 (\sin \Theta_0 - \sin^3 \Theta) + K_1 [\sin \Theta - (\Theta - \Theta_0) \cos \Theta] = 0 \tag{9}$$

is the numerator of this fraction. Condition $\partial P / \partial \Theta = 0$ is equivalent to Eq. (9). Equation (9) yields the critical deformation in the function of initial imperfect state.

Let us analyse the structure shown in Fig. 2. The condition of equilibrium in this case reads

$$PL \sin \Theta - FL \cos \Theta - M = 0 \tag{10}$$

where

$$F = K_2 (\Delta - \Delta_0) = K_2 (L \sin \Theta - \Delta_0). \tag{11}$$

The constitutive equation of the spring-dashpot model on Fig. 2. reads

$$K_1 b_1 \dot{\Theta} = K_1 M^n + b_1 \dot{M} \tag{12}$$

where n is a constant. This is the Norton law. Making use of (11) and expressing M from (10), Eq. (12) becomes

$$\dot{\Theta} = \frac{K_1 [PL \sin \Theta - K_2 (L \sin \Theta - \Delta_0) L \cos \Theta]^n + b_1 \dot{P} \sin \Theta}{K_1 + K_2 L \Delta_0 \sin \Theta + K_2 L^2 \cos 2\Theta - PL \cos \Theta}. \tag{13}$$

If we use

$$K_1 b_1 \dot{\Theta} = K_1 M + b_1 \dot{M} \tag{14}$$

instead of (12) which is the constitutive equation of the Maxwell modell, then we obtain again a fraction form for $\dot{\Theta}$. Its denominator and the denominator of Eq. (13) are the same.

Let us define the change of energy of the system in Fig. 2. as

$$Q = \frac{1}{2} K_1 (\Theta - \Theta_d - \Theta_0)^2 + \frac{1}{2} K_2 (\Delta - \Delta_0)^2 - PL(\cos \Theta_0 - \cos \Theta). \tag{15}$$

In this equation Θ_d means the displacement of the piston in the b_1 dashpot. (Θ_d is the internal parameter). If we differentiate (15) with respect to Θ twices (regarding Θ_d as an independent variable), we arrive at

$$\frac{\partial^2 Q}{\partial \Theta^2} = K_1 + K_2 \Delta_0 L \sin \Theta + K_2 L^2 \cos 2\Theta - PL \cos \Theta. \tag{16}$$
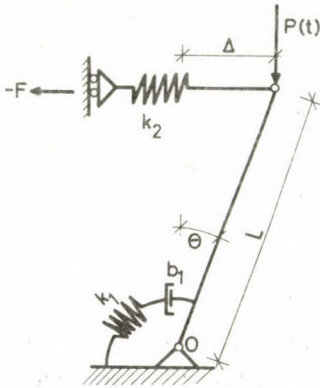
Fig. 2.
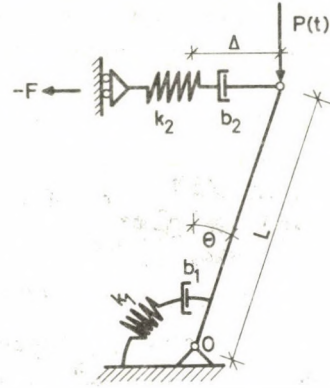
Fig. 3.

This expression is exactly the same as the denominator of Eq. (13). Consequently, if $\partial^2 Q/\partial\Theta^2$ is equal to zero, then $\dot\Theta$ is infinite. If we want to obtain the critical time, we have to solve (13) for $\Theta(t)$. Then we have to introduce the solution into condition $\partial^2 Q/\partial\Theta^2 = 0$ [This is Eq. (16)]. If it has a solution for t, then it is the critical time.

Let us define the change of the potential energy of the structure in Fig. 3. as

$$Q = \frac{1}{2} K_1 (\Theta - \Theta_d - \Theta_0)^2 + \frac{1}{2} K_2 (\Delta - \Delta_d - \Delta_0)^2 - PL(\cos \Theta_0 - \cos \Theta). \qquad 17)$$

Here Δ_d is the displacement of the piston in the b_2 dashpot. Differentiating (17) again twice with respect to Θ, we obtain

$$\frac{\partial^2 Q}{\partial\Theta^2} = K_1 + K_2 L \sin \Theta (\Delta_d + \Delta_0) + K_2 L^2 \cos 2\Theta - PL \cos \Theta . \qquad (18)$$

Comparing (18) to (9), we can see that in the case of elastic structures the Hesse matrix depends on the initial imperfection, while in the case of viscoelastic structures it generally depends on creep (internal parameters) and the loading too. That is why the critical time of a viscoelastic structure can not be defined usually from the critical deformation of the equivalent elastic structure. (The structure in Fig. 1 is the equivalent elastic structure of the structures in Figs 2 and 3). The analysis of circular cylindrical and spherical shells in the papers of Obrecht [8] and Xirouchakis and Jones [9], [10] also shows this fact.

Hayman has shown that in the case of statically determinate structures the Hesse matrix of a viscoelastic structure and that of the equivalent structure become singular at the same deformation. In some cases the Hesse matrix of statically indeterminate structures with finite degree of freedom formally can be independent of the internal parameters if the independent variables are chosen skilfully. In the case of the structure in Fig. 2, if Δ is chosen as an independent parameter instead of Θ, and (18) is differentiated with respect to it, instead of (16) we obtain an expression which depends on Θ_d.

References

1. Freudenthal, A. M.: The Inelastic Behaviour of Engineering Materials and Structures, John Wiley and Sons., Inc., New York, 1950 p. 518
2. Hayman, B.: Aspects of Creep Bucking, Proceeding R. Soc. London. A *364* (1978), p. 393
3. Hayman, B.: Creep Bucking—A General View of the Phenomenon, IUTAM Symposium Leicester /UK 1980 in Creep of Structures Ed. A.R.S. Ponter, D. R. Hayhurst. Springer Verlag, p. 289
4. Karman, T.—Biot, M. A.: Mathematical Methods in Engineering, McGraw-Hill, New York, London 1940
5. D. Laugharne Thornton, M. A.: Mechanics Applied to Vibrations and Balancing, Chapman and Hall, London, 1939
6. Biot, M. A.: Theory of Stress-Strain Relations in Anisotropic Viscoelasticity and Relaxation Phenomena. Journal of Applied Physics Vol. 25, No. 11, Nov. 1954, p. 1385
7. Hoff, N. J.: A Survey of the Theories of Creep Buckling, Proc. of the Third U.S. National Congress of Applied Mechanics Held at Brown University Providence, Rhode Island June 11—14, 1958. Pergamon Press, p. 29
8. Obrecht, H.: Creep Buckling and Postbuckling of Circular Cylindrical Shells under Axial Compression, International Journal of Solids and Structures *13* (1977), p. 337
9. Xirouchakis, P. C.—Jones, N.: Axysimmetric and Bifurcation Creep Buckling of Externally Pressured Spherical Shells, International Journal of Solids and Structures *16*, (1980), p. 131
10. Jones, N.,—Xirouchakis, P. C.: The Creep Buckling of Shells. IUTAM Symposium Leicester /UK 1980 in Creep of Structures, Ed. A.R.S. Ponter D. R. Hayhusrt, Springer Verlag, p. 308

ELASTIC STRESSES IN CRACKED PRESTRESSED PRETENSIONED CONCRETE COMPOSITE BEAMS WITH BONDED TENDONS

L. JANKÓ*

Computation methods have long been known for the design of precast, prestressed beams with bonded tendons, interacting with monolithic r.c. slabs, either under service conditions (no tensile stress) or in ultimate condition. This time, the beam stress state *after cracking* will be analyzed. The presented method yields extreme fibre stresses of the cracked composite beam (slab + beam), the steel stress increment, the crack width, and the elastic limit load.

Symbols

Roman letters

A_{Ib}, A_{Isl}	ideal cross-sectional areas of uncracked beam and slab, resp. $(\varphi = 0)$;
A_{ps}	tendon cross-sectional area (area of prestressed reinforcement);
$a = a_{sl} + a_b$	distance between ideal centroids $(\varphi = 0)$ of uncracked slab S_{Isl} and uncracked beam S_{Ib};
b_u, b_l	upper and lower flange widths, respectively;
b	web thickness;
d_u, d_l	upper and lower flange thicknesses, respectively;
d	distance measured from extreme compressed fiber of beam to centroid of tendons (effective depth of beam section);
d_{sl}	monolithic (in-situ) slab thickness:
D_1, D_2, D_3	dead load components (D_1: dead load of beam, D_2: one of slab, D_3: one of waterproofing, paving (finishing) etc.);
$E_{c.sl}, E_{c.b}$	initial moduli of the elasticity of slab and beam concrete, resp. $(\varphi = 0)$;
E_s	tendon modulus of elasticity (Young's, modulus);
e	distance between compressive force N and centroid S_{Ib} of uncracked beam;
e_{xII}	distance of compressive force N from neutral axis x_{II} of a cracked beam;
e_{ps}	prestressing force eccentricity referred to S_{Ib};
h	overall thickness of beam (without slab),
I_{ps}	tendon moment of inertia about their centroid;
I_{cu}	so-called "curvature moment of inertia" of beam;
I_{Ib}, I_{Isl}	moment of inertia about centroid (S_{Ib} or S_{Isl}) of uncracked beam or slab $(\varphi = 0)$;
I_{xII}	so-called "stress moment of inertia" about neutral axis x_{II} of cracked beam;

* Dr. L. Jankó, Lajos u. 142, H-1036 Budapest, Hungary

$M(\ldots,\ldots)$

external moment (with load subscripts in parentheses);

$\Delta M_{c,b}^{\varphi}, \Delta N_{c,b}^{\varphi}$
$\Delta M_{c,sl}^{\varphi}, \Delta N_{c,sl}^{\varphi}$
$\Delta M_{ps}^{\varphi}, \Delta N_{ps}^{\varphi}$

resultants of stresses from accessory effects (subscript c, b: neat concrete cross-section of the beam, deducing tendon cross-sections; sl: slab cross-section; ps: tendon); accessory effects: creep and shrinkage;

$M_b' = M(1, 2, s_0)$

moment acting at S_{1b} from dead loads of beam D_1 and of slab D_2, as well as from initial prestressing tendon force P_{so},

$M_{ex} = M_b' + M(3, p) + \Delta N_{ps}^{\varphi} e_{ps}$

external moment sum of total load (dead loads, prestressing force, live load, accessory stresses) acting at S_{1b} (neglecting ΔM_{ps}^{φ});

M_{sl}

share of moment from total load on cracked slab;

N

share of compressive force from total load on cracked beam (resultant of beam concrete stresses and of tension increment ΔT due to external load);

N_{sl}

as for M_{sl} but normal force;

$N_{ex} = N + N_{sl}$

external compressive force on the total composite cross-section after cracking (effective initial prestressing force deducing losses: $N_{ex} = P_{so} - \Delta N_{ps}^{\varphi}$);

$n_c = \dfrac{E_{c,sl}}{E_{c,b}}$

ratio of initial moduli of elasticity of slab to beam concrete ($\varphi = 0$);

$n = \dfrac{E_s}{E_{c,b}}$

ratio of moduli elasticity of tendons to beam concrete ($\varphi = 0$);

$P_{so} = P_s - \Delta P_s(rel., \Delta t)$

initial prestressing force deducing effects of steel relaxation and of temperature difference at beam prefabrication (so-called *effective* initial prestressing force);

p

live load;

S_{1b}, S_{1sl}

centroids of ideal cross-sectional areas ($\varphi = 0$) of uncracked beam and slab, respectively;

ΔT

resultant tension increment (due to external loads) in tendons,

x_{cb}

distance of the overall beam concrete cross-section centroid S_{cb} (including tendon cross-sections) from the compressed extreme fibre;

x_{1b}

distance between the ideal cross-sectional centroid S_{1b} and the compressed extreme fibre of the uncracked beam ($\varphi = 0$);

x_{11}

depth to the neutral axis of the beam section (effective depth of the cracked beam section);

Greek letters

$\alpha = \dfrac{d_u}{d}$

geometry constant;

$\beta = \dfrac{b_u}{b}$

geometry constant;

$\varepsilon_{sh,b}^{\chi}, \varepsilon_{sh,sl}^{\chi}$

final values of shrinkage coefficients of beam and slab, respectively;

$\varepsilon_{c,b}^{u}$

compressive strain of the beam top (compressed) fibre (subscripts I and II refer to uncracked and cracked state, respectively, load subscripts are in parentheses; without subscript c it comprises inherent compression due to creep and shrinkage);

$\varepsilon_{c,b}^{t}$

specific strain of the extreme tensile fibre of the beam;

$\varepsilon^l_{c,sl}, \varepsilon^u_{c,sl}$ — specific compressions of bottom and top fibres of the slab (see comments on $\varepsilon^u_{c,b}$);

$\zeta = \dfrac{b_l}{b}$ — geometry constant;

$\eta = \dfrac{x}{\zeta}$ — curvature parameter;

$\vartheta = \rho - \omega$ — eccentricity parameter;

$\kappa = \dfrac{h - d_l}{d}$ — geometry constant;

$\kappa_{bI}, \kappa_{bII}$ — curvatures of uncracked and cracked beam, respectively (the uncracked beam is only subject to permanent loads—dead load + prestressing force + accessory effects);

$\kappa_{slI}, \kappa_{slII}$ — the same as before but for the slab;

$\mu = \dfrac{A_{ps}}{bd}$ — ratio of prestressed reinforcement (tendons);

$\xi = \dfrac{x_{II}}{d}$ — relative effective depth of the cracked beam under eccentric axial load;

$\rho = \dfrac{x_{Ib}}{d}$ — constant for the centroid position S_{Ib} of the beam in uncracked state;

$\sigma^u_{c,b}$ — stress in the beam top fibre (with load subscripts in parentheses);

$\sigma^l_{c,sl}, \sigma^u_{c,sl}$ — stresses in bottom and top fibres of the slab (with load subscripts in parentheses);

$\Delta\sigma_{ps}$ — tendon stress variation (compared to prestress deducing losses, $\Delta T = \Delta\sigma_{ps} A_{ps}$)

$\Delta\sigma^{u,\varphi}_{c,b}$ — stress due to creep and shrinkage in the beam top fibre;

$\Delta\sigma^{l,\varphi}_{c,sl}$ — the same for the slab bottom fibre;

$\tau = \dfrac{I_{ps}}{bd^3} n$ — parameter;

$\varphi'_b, \varphi'_{sl}$ — final values of creep coefficients of beam and slab, respectively;

$\chi = \dfrac{x_{cb}}{d}$ — constant for the centroid position S_{cb} of the complete beam concrete cross-section (comprising tendon cross-sectional areas);

$\psi = \dfrac{h}{d}$ — geometry constant;

$\omega = \dfrac{e}{d}$ — relative eccentricity referred to centroid S_{Ib};

Subscripts, superscripts

I	uncracked;
II	cracked;
φ	superscript for accessory stresses due to creep and shrinkage;
b	beam (without slab);
c	concrete;
com	composite beam (beam + slab);
l	lower (bottom) fiber;
ex	external (moment, force, load);
ps	prestressed (prestressed reinforcement (tendons));
sl	slab;
u	upper (top) fiber;
1, 2, 3	parts of dead load;
0, 1, ∞	subscripts for times t_0 (prestress), t_1 (casting the monolithic slab and waterproofing, paving (finishing), etc.) and t_∞ (final state: completion of accessory effects).

1. Introduction

Bridge construction practice prefers gridwork made of a monolithic slab and precast, prestressed beams. Single beams may be qualified according to methods, relying on the *service* condition and the *ultimate* condition at failure. The Hungarian Building Code for Road Bridges requires exemptness from tensile stresses for the so-called *service moment* calculated from the dead load and a given percentage of the full live load (about 35% of the full live load "A"*).

Analysis of stress pattern in the primary *beam without monolithic slab* (precast beams) after cracking may follow research work by Tassi and Klatsmányi [1], [6], [7] indicating both the exact solution of the problem, and an approximate method describing essentials of the involved phenomena by simple, easy means for the structural engineering practice.

In engineering practice, the beam is considered to cope with the *nominal load* (dead load + full live load) if the stress in the top fibre of the beam cross-section, considered to be *uncracked*, is lower than permissible (and if the steel stress increment can be absorbed by the reserve in the tendon or by the ordinary reinforcement). In the positive case the quoted approximate method predicts closure of beam cracks after removal of loads in excess of the service load.

Exemptness from excessive *residual deformations* is safeguarded in certain building codes by imposing the quoted stress limit.

Demonstrating criteria of exemptness from tensions and of limited residual deformations on a beam assumed *to be uncracked*, the approximate method is seen to be correct only for beams without a slab [6], [7]. Correctness of the approximate

* Symbol in the Code.

method as a function of various parameters can be shown [1], [6], [7] to depend on the prestress rate: the error to the detriment of safety in extreme fibre stresses of an *uncracked* beam does not exceed 20% if the mean concrete stress arising from prestress considered as centric is not less than half the basic concrete strength value.

Further analyses concerning *composite beams* will be presented below.

It is attempted to develop a method for determining stress conditions in the *cracked* beam, the tendon stress increment, *crack opening*, and the *ultimate elastic load*.

Chapter 2 will be concerned with the stress and strain condition of cracked I-beams, relying on references.

Recapitulating particulars, Chapter 3 gives an account of the devised method, numerically illustrated in Chapter 4, deducing practical conclusions from numerical results.

2. Cross-sectional characteristics of cracked beams under eccentric compression

Most of what in stated below is known from references [1], [2], [4], [7] but the discussion in Chapter 3 is more easily followed by referring to Chapter 2 than to the special literature.

First, let us consider the geometry conditions of a beam *without* monolithic slab vs. *eccentricity e*.

In any cross-section of a *cracked* r.c. beam under eccentric compression the following equilibrium conditions have to be met [9] (compressive force being affected by a positive, and compressive stress by a negative sign):

$$N = \frac{-\sigma_{c,b}^u}{x_{\text{II}}} \int z \, dA = \frac{-\sigma_{c,b}^u}{x_{\text{II}}} S_{x_{\text{II}}}, \tag{2.1}$$

$$Ne_{x_{\text{II}}} = \frac{-\sigma_{c,b}^u}{x_{\text{II}}} \int z^2 \, dA = \frac{-\sigma_{c,b}^u}{x_{\text{II}}} I_{x_{\text{II}}}. \tag{2.2}$$

Hence:

$$e_{x_{\text{II}}} = \frac{I_{x_{\text{II}}}}{S_{x_{\text{II}}}}, \tag{2.3}$$

$$\sigma_{c,b}^u = -\frac{N x_{\text{II}}}{S_{x_{\text{II}}}} = -\frac{N x_{\text{II}}}{I_{x_{\text{II}}}} e_{x_{\text{II}}}. \tag{2.4}$$

In conformity with Fig. 1, relative effective depth (ξ), curvature $\kappa_{b\text{II}}$, specific strains of extreme fibres $(\varepsilon_{c,b}^u, \varepsilon_{c,b}^l)$ and stress in the top fibre $\sigma_{c,b}^u$ are related by:

$$\eta = \frac{\chi}{\xi}, \tag{2.5}$$

$$\tan \gamma_b = \kappa_{b\text{II}} = \frac{-\varepsilon_{c,b}^u + \varepsilon_{c,b}^l}{h} = -\eta \frac{\psi}{\chi} \frac{\sigma_{c,b}^u}{E_{c,b} h}, \tag{2.6—7}$$

5*

Fig. 1. Basic data, notations. Curvature moment of inertia I_{cu} of the cracked cross-section

$$\eta = - \frac{-\varepsilon_{c,b}^u + \varepsilon_{c,b}^l}{\psi} \chi \frac{E_{c,b}}{\sigma_{c,b}^u}. \tag{2.8}$$

Further on, moment of inertia about neutral axis x_{II}—to be called *"stress" moment of intertia*—will be needed (involved in (2.4) for the stress in the compressed extreme fibre):

$$I_{x_{II}} = \frac{bx_{II}^3}{3} + nA_{ps}(d-x_{II})^2 + (b_u-b)\left[d_u\left(x_{II} - \frac{d_u}{2}\right)^2 + \frac{d_u^3}{12}\right] +$$

$$+ \frac{(b_l-b)}{3}[x_{II}-(h-d_l)]^3 + nI_{ps}, \tag{2.9}$$

$$I_{x_{II}} = \frac{bd^3}{12} \left\{ 4\xi^3 + 12\eta\mu(1-\xi)^2 + (\beta-1)\left[12\alpha\left(\xi - \frac{\alpha}{2}\right)^2 + \alpha^3 \right] + \right.$$

$$\left. + 4(\zeta-1)(\xi-\kappa)^3 + 12\tau \right\}. \tag{2.10}$$

The corresponding static moment is:

$$S_{x_{II}} = \frac{bx^2}{2} - nA_{ps}(d-x_{II}) + (b_u - b)\cdot\left(x_{II} - \frac{d_u}{2}\right)d_u + (b_l - b)\frac{[x_{II}-(h-d_l)]^2}{2}, \tag{2.11}$$

$$S_{x_{II}} = bd^2 \left\{ \frac{\xi^2}{2} - n\mu(1-\xi) + (\beta-1)\left(\alpha\xi - \frac{\alpha^2}{2}\right) + \frac{1}{2}(\zeta-1)(\xi-\kappa)^2 \right\}. \tag{2.12}$$

Introducing notations

$$e_{x_{II}} = x_{II} - (x_{lb} - e) = [\xi - (\rho - \omega)]d = (\xi - \vartheta)d \tag{2.13}$$

Eqs (2.3), (2.10), (2.12) yield — knowing the eccentricity e — a *characteristic* equation for relative effective depth ξ:

$$a_3\xi^3 + a_2\xi^2 + a_1\xi + a_0 = 0. \tag{2.14}$$

For a neutral axis intersecting the lower flange, coefficients become $(d > x_{II} \geq (h-d_l) \rightarrow \zeta \neq 1)$:

$$a_3 = \zeta,$$

$$a_2 = -3\zeta\vartheta,$$

$$a_1 = 6n\mu(1-\vartheta) + 3\alpha(\beta-1)(\alpha-2\vartheta) - 3\kappa(\zeta-1)(\kappa-2\vartheta),$$

$$a_0 = -6n\mu(1-\vartheta) - \alpha^2(\beta-1)(2\alpha-3\vartheta) + \kappa^2(\zeta-1)(2\kappa-3\vartheta) - 6\tau, \tag{2.15a-d}$$

For a neutral axis intersecting the web $(x_{II} \leq (h-d_l))$ substitution $\zeta = 1$ may yield the corresponding coefficients.

For a neutral axis intersecting the upper flange $(x_{II} \leq d_u)$ substitution $\zeta = \beta = 1$ (rectangle) is imposed.

The above yield cross-sectional stresses and compressions (strains) for any eccentricity e.

Let us now consider the *curvature conditions*.

Eccentricity e of the normal force N acting on the cracked beam is referred to the centroidal axis of the uncracked ideal cross-section (S_{Ib}) yielding for the curvature in general (Fig. 1):

$$\tan \gamma_b = \kappa_{bII} = \frac{M}{E_{c,b}I_{cu}}, \tag{2.16}$$

$$M = Ne. \tag{2.17}$$

To determine the "curvature" moment of inertia I_{cu}, let us express the curvature according to the strain diagram (Fig. 1):

$$\kappa_{bII} = \frac{-\varepsilon^u_{c,b}}{x_{II}} = \frac{-\sigma^u_{c,b}}{E_{c,b}x_{II}} = \frac{Ne_{x_{II}}}{E_{c,b}I_{x_{II}}}. \tag{2.18}$$

Eqs (2.16) to (2.18) yield for I_{cu}:

$$I_{cu} = \frac{e}{e_{x_{II}}} I_{x_{II}} \equiv \frac{\omega}{\xi - \vartheta} I_{x_{II}}. \tag{2.19}$$

It should be noted that for an eccentricity e_c of force N referred to centroid S_{cb} of the uncracked complete concrete cross-section, Eq. (2.18) is replaced by

$$\kappa_{b_{II}} = \frac{Ne_c}{E_{c,b}I_{cu,c}} \tag{2.20}$$

$(I_{cu,c} \neq I_{cu})$.

The concept of "curvature moment of inertia" *has been introduced by Dulácska* [2] in his stability analyses. At present, this cross-sectional characteristic will facilitate writing *of conditions of compatibility* between the monolithic slab and the precast beam. Further analyses will rely on

$$A_1 = \zeta\xi^3 - 6n\mu(1 - \xi) + (\beta - 1)\alpha^2(3\xi - 2\alpha) - (\zeta - 1)\kappa^2(3\xi - 2\kappa) - 6\tau, \tag{2.21}$$

$$A_2 = +3\zeta\xi^2 - 6n\mu(1 - \xi) - (\beta - 1)3\alpha(\alpha - 2\xi) + (\zeta - 1)3\kappa(\kappa - 2\xi), \tag{2.22}$$

$$\vartheta = \rho - \omega = \frac{A_1}{A_2}. \tag{2.23}$$

(according to Eqs (2.13) to (2.15)), permitting to determine eccentricity e for a given effective depth x_{II}.

These geometry characteristics for a precast beam have been illustrated in Fig. 2.

The real form of the beam cross-section is not exactly I;
the listed dimensions b_u, b_l, d_u, d_l belong to a I-section with uncracked characteristics x_{Ib}, A_{Ib}, I_{Ib} identical to those of the real beam. Moments of inertia I_{cu}, $I_{x_{II}}$ are equal if neutral axis x_{II} of the cracked cross-section in eccentric compression is coincident with the ideal centroidal axis x_{Ib} of the uncracked cross-section. Of course, equality also subsists for $e \to \infty$ (pure bending, cracked state). It is interesting to see *how fast* the "curvature moment of inertia" for a given structure *decreases* after cracking (e_{cr} = cracking eccentricity; e_k = kernel radius for the bottom fibre). Accordingly, also the "curvature moment of inertia" *markedly increases with eccentricity.*

Occurrence of a compressive force causes the curvature to increase less abruptly than in pure bending $\left(I_{IIb} \approx \frac{1}{4} I_{Ib} \right)$.

After cracking, none of functions κ_{bII} and $\sigma^u_{c,b}$ in Fig. 2 is linearly dependent on eccentricity e (while in the tested range they are nearly rectilinear). For $e \to \infty$ both
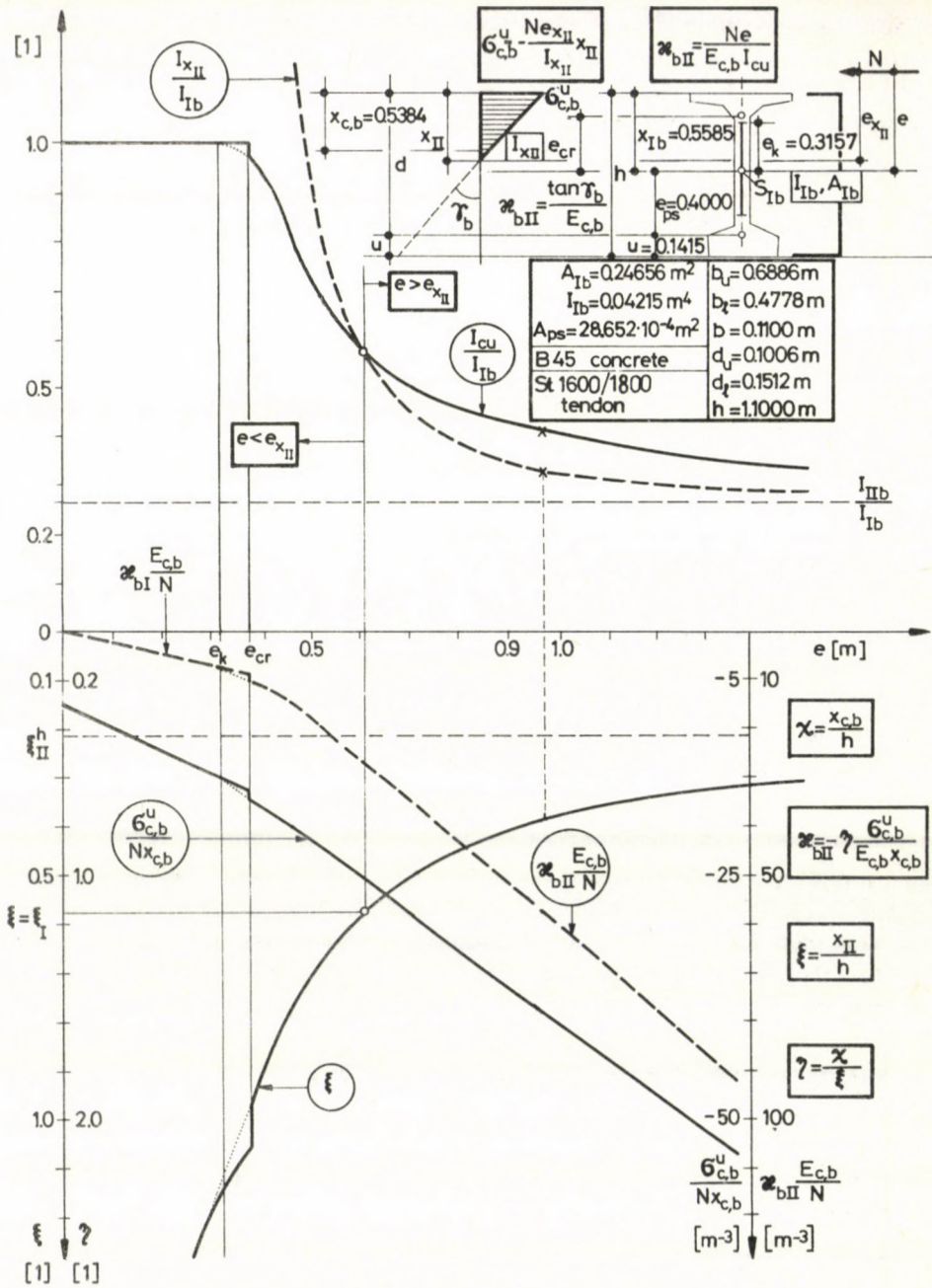
Fig. 2. Cross-sectional characteristics of cracked beams under eccentric compression

functions tend to infinity (the N value being fixed). For $e \to \infty$ and $Ne \to$ const. both functions have a limit value (uncracked stress state, pure bending). For a given e, of course, extreme fibre stresses and curvature are *linear* functions of external compression N. The elastic linearity is valid in this form.

3. Analysis of the beam in interaction with a monolithic r.c. slab

3.1 Basic assumptions, approximations, neglects

1. Tendons and concrete are of a linear-elastic material.
2. Cross-sections are assumed to remain in plane (Bernoulli-Navier hypothesis).
3. The effect of ordinary beam reinforcement is neglected.
4. The beam is either a priori made with *bonded* tendon or grouted.
5. The effect of the cracked tensile concrete zone to reduce the tendon strain (the stiffness increase due to "growth" of modulus E_s) is not directly reckoned with. It can be approximated e.g. by standard methods, where E_s is understood to be the increased modulus.
6. Internal equilibrium stresses due to *creep and shrinkage* are reckoned with as *in the uncracked beam*. This equilibrium stress system alters the eccentricity of forces *on cracked beam elements*, hence also "curvature" moment of inertia I_{cu}. Accordingly, accessory effects cannot be simply superposed.
7. *Steel relaxation* is complete soon after prestressing.
8. A monolithic r.c. slab is rectangular and of symmetric reinforcement.
9. Moment of inertia of the cracked beam involves the moments of inertia I_{ps} of tendons *about their centroid* but the share ΔM_{ps}^{φ} on tendons due to creep and shrinkage—by orders less than the others—is omitted from equilibrium equations.

Also there are load effects to be reckoned with (dead load, working (live) load, prestress, creep, shrinkage) will be discussed below, not directly involving the external moments from accessory effects in hyperstatic beams, but the latter may be comprised among dead load moments to that sense.

Internal equilibrium inherent stresses due to creep and shrinkage in the cross-sections need to be predetermined by some convenient method for applying the presented method (accordingly, ideal cross-sectional characteristics have to be calculated with $\varphi = 0$). In the numerical example in Chapter 4, Frey's method relying on Trost's material model has been applied [3].

3.2 Description of the method

In the *uncracked* beam, stress resultants M_b', N_b' (Fig. 3) arise from a beam dead load D_1, slab weight D_2 and initial prestressing force P_{s_0}.

Moment $M(3, p)$ in the composite cross-section of a beam, assumed to remain uncracked under further loads, could be decomposed according to e.g. [1] to moments and forces M_{bl}'', N_{bl}'' and M_{sll}, N_{sll} in the beam and in the slab, respectively. Accessory stresses due to creep and shrinkage in slab and beam may be superposed on the former ones.
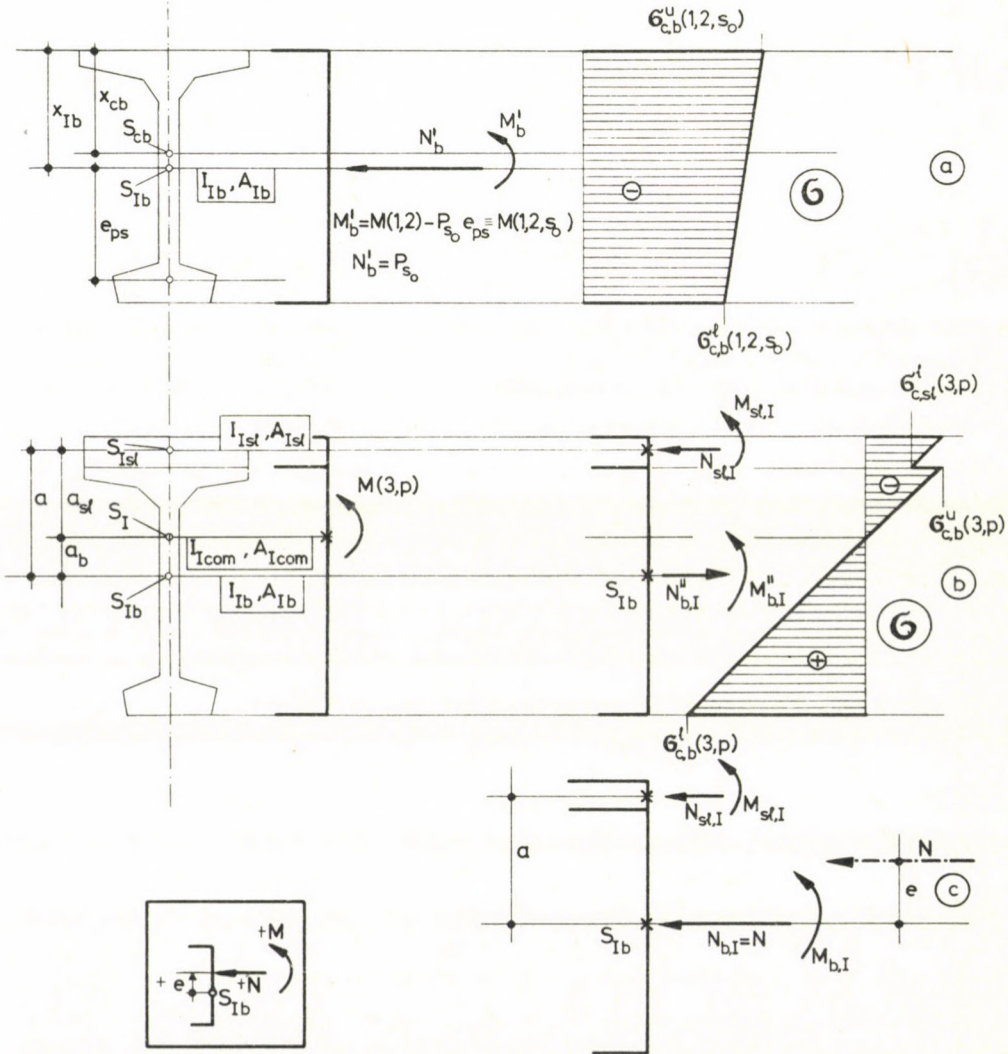

Fig. 3. Well-known stress components in crack-free state

For a *cracked* beam, the starting condition will be that where all constant loads are already acting, and also stress excesses $\Delta\sigma^\varphi(\infty, 0)$ from accessory effects (shrinkage, creep, [3], time $t = t_\infty$) subsist. Initial prestressing force has been considered as that *reduced* by the effects of steel relaxation and temperature difference Δt^0 (Hoyer prestressing system):

$$P_{s_0} = P_s - \Delta P_s(\text{rel.}, \Delta t^0) . \tag{3.1}$$

After cracking, the slab is subject to M_{pl}, N_{sl}, and the beam to compressive force N of eccentricity e. According to Fig. 4c, resultants of slab and beam accessory stresses are ΔM_{sl}^φ, ΔN_{sl}^φ and $\Delta M_{c,b}^\varphi$, $\Delta N_{c,b}^\varphi$ respectively, forces balanced in uncracked condition by steel moments and forces ΔM_{ps}^φ, ΔN_{ps}^φ seen in dashed lines in Fig. 4c. Since accessory effects alter the eccentricity of forces on structures (beam, slab)—affecting in turn, the beam "curvature moment of inertia" (Fig. 2)—accessory stresses *cannot be superposed* on final stresses due to loads. After accessory stresses have developed, prestressing force P_{s_0} decreases by ΔN_{ps}^φ but the decrease in this form cannot be taken otherwise into consideration than in the equilibrium equations. Compatibility equations have to involve compressions (strains) and curvatures due to moments and forces ΔM_{sl}^φ, ΔN_{sl}^φ, $\Delta M_{c,b}^\varphi$, $\Delta N_{c,b}^\varphi$ in Fig. 4c, permitting exact determination of the stress jump along the joint line between slab and beam, and curvature of the structural members, in compliance with the impossibility to exactly account for accessory stresses by simply reducing the prestress. With external stress resultants N_{ex} and M_{ex} arising after accessory effects, equilibrium equations for the cracked condition (Fig. 4) become (neglecting ΔM_{ps}^φ):

$$N_{ex} = P_{s_0} - \Delta\tilde{N}_{ps}^\varphi , \tag{3.2}$$

$$N_{ex} = N + N_{sl} , \tag{3.3}$$

$$M_{ex} = M(1, 2, 3, s_0, p) + \Delta\tilde{N}_{ps}^\varphi e_{ps} , \tag{3.4}$$

$$M_{ex} = Ne + M_{sl} + N_{sl}a . \tag{3.5}$$

Here $\Delta\tilde{N}_{ps}^\varphi$ gets an overdash, it being somewhat different from ΔN_{ps}^φ:

$$\Delta\tilde{N}_{ps}^\varphi = \Delta N_{ps}^\varphi + nA_{ps}\Delta\sigma_{c,b,t}^\varphi$$

where $\Delta\sigma_{c,b,t}^\varphi$ is concrete stress in tendons centroid due to accessory effects (upper, framed part in Fig. 5).

Namely, ΔN_{ps}^φ belongs to the condition following cross-sectional deformations due to accessory stresses ($\Delta\sigma^\varphi$). Thus, according to the present mode of discussion, this **force has to be increased as mentioned above to result in the force** $(P_{s_0} - \Delta\tilde{N}_{ps}^\varphi)$—considered to be external—belonging to the undeformed cross-section. By the way, this method involves the effect of prestressing force variation ΔT due to external loads (negative, i.e. tensile force, indicated in Fig. 4a) and resultant compression N_b of beam concrete stresses sum up to force N.

Diagram of strain due to total permanent load is seen in the right side part of Fig. 4c. Compatibility of this system means the identity between the increments of compression along the hardened slab joint line i.e. the curvature, and of the curvature of the beam top fibre. Shaded area shows compressions *arising from stresses* $\sigma(1, 2, 3, s_0, \varphi)$, the rest being composed of shrinkage and of compressions proportional to creep.

Unshaded compressions are, in detail (where $\bar{\rho} = 0.8$, concrete ageing coefficient [3], and φ^∞ = creep coefficients belonging to loads applied at prestress (t_0) and after slab concreting (t_1), respectively):

$$K_{\varepsilon, sl}^l = \frac{\sigma_{c, sl}^{l(3)} \varphi_{sl}^\infty + \Delta\sigma_{c, sl}^{l, \varphi}[\infty, 1] \cdot \bar{\rho}\varphi_{sl}^\infty}{E_{c, sl}} + \varepsilon_{sh, sl}^\infty, \tag{3.6}$$

$$K_{\varepsilon, b}^u = \frac{\sigma_{c, b}^u(1, s_0)\varphi_b^\infty + \Delta\sigma_{c, b}^{u, \varphi}[1, 0]\bar{\rho}\varphi_b^\infty + \sigma_{c, b}^u(2, 3)\tilde{\varphi}_b^\infty + \Delta\sigma_{c, b}^{u, \varphi}[\infty, 1]\bar{\rho}\tilde{\varphi}_b^\infty}{E_{c, b}} + \varepsilon_{sh, b}^\infty. \tag{3.7}$$

Accessory stresses are joined by subscripts of time t_0, t_1, t_∞ in brackets. Subsequently, these terms in brackets will be omitted, any accessory stress corresponds to complete increment during interval $t_0 - t_\infty$. Compressions $K_{\varepsilon, sl}^l$ and $K_{\varepsilon, b}^u$ are considered invariable after cracking, not to be detailed further. The quoted system of inherent deformations will be omitted in the analyses, they can be used only in determining external displacements. The respective curvatures, involving $K_{\varepsilon, sl}^u$ and $K_{\varepsilon, b}^l$ written by analogy to the former, become:

$$\kappa_{sl}^\varphi = \frac{K_{\varepsilon, sl}^l - K_{\varepsilon, sl}^u}{d_{sl}}, \tag{3.8}$$

$$\kappa_b^\varphi = \frac{K_{\varepsilon, b}^l - K_{\varepsilon, b}^u}{h}. \tag{3.9}$$

The total dead load combined with the prestress to produce the total accessory stress system $(\Delta M_{c, b}^\varphi, \Delta N_{c, b}^\varphi, \Delta M_{sl}^\varphi, \Delta N_{sl}^\varphi, \Delta M_{ps}^\varphi, \Delta N_{ps}^\varphi)$—to be called starting condition—causes a strain in the bottom fibre of the slab. The live load causes the beam to be cracked, changing the $\varepsilon_{sl, I}^l$ value to $\varepsilon_{sl, II}^l$:

$$\varepsilon_{sl, I}^l = \varepsilon_{c, sl, I}^l + K_{\varepsilon, sl}^l = \frac{\sigma_{c, sl}^{l(3)} + \Delta\sigma_{c, sl}^{l, \varphi}}{E_{c, sl}} + K_{\varepsilon, sl}^l, \tag{3.10}$$

$$\varepsilon_{sl, II}^l = \varepsilon_{c, sl, II}^l + K_{\varepsilon, sl}^l = -\frac{N_{sl}}{E_{c, sl} A_{lsl}} + \frac{M_{sl}}{2 E_{c, sl} I_{lsl}} d_{sl} + K_{\varepsilon, sl}^l. \tag{3.11}$$

The compression increment (in a slab of symmetric reinforcement):

$$\Delta\varepsilon_{sl}^l = \varepsilon_{sl, II}^l - \varepsilon_{sl, I}^l = \frac{1}{E_{c, sl}} \left[-\frac{N_{sl}}{A_{lsl}} + \frac{M_{sl}}{2 I_{lsl}} d_{sl} - \sigma_{c, sl}^{l(3)} - \Delta\sigma_{c, sl}^{l, \varphi} \right]. \tag{3.12}$$

Fig. 4. Equilibrium of internal stresses in cracked composite cross sections

Elements of deformation (strains and curvatures)

Beam top fibre compression in the starting condition and after cracking, respectively (2.4):

$$\varepsilon_{bi}^u = \varepsilon_{c,b,1}^u + K_{\varepsilon,b}^u = \frac{\sigma_{c,b}^u(1, 2, 3, s_0) + \Delta\sigma_{c,b}^{u;\varphi}}{E_{c,b}} + K_{\varepsilon,b}^u,$$ (3.13)

$$\varepsilon_{bII}^u = \varepsilon_{c,b,II}^u + K_{\varepsilon,b}^u = -\frac{N e_{x_{II}} x_{II}}{E_{c,b} I_{x_{II}}} + K_{\varepsilon,b}^u.$$ (3.14)

Compression increment:

$$\Delta\varepsilon_b^u = \varepsilon_{bII}^u - \varepsilon_{bi}^u = \frac{1}{E_{c,b}}\left[-\frac{N e_{x_{II}} x_{II}}{I_{x_{II}}} - \sigma_{c,b}^u(1, 2, 3, s_0) - \Delta\sigma_{c,b}^{u;\varphi} \right].$$ (3.15)

Expressing M_{sl} and N_{sl} from equilibrium equations (3.2) to (3.5) and substituting into (3.12), *compatibility* condition

$$\Delta\varepsilon_{sl}^l = \Delta\varepsilon_b^u$$ (3.16)

yields for force N acting on the beam:

$$N^* = \frac{A}{B(\xi)}.$$ (3.17)

Notations mean $(\varepsilon_{c,b}^u(3) = \varepsilon_{c,sl}^l(3))$:

$$\sigma^* = \sigma_{c,b}^u(1, 2, s_0) + \Delta\sigma_{c,b}^{u;\varphi} - \Delta\sigma_{c,sl}^{l;\varphi}\frac{1}{n_c},$$ (3.18)

$$n_c = \frac{E_{c,sl}}{E_{c,b}},$$ (3.19)

$$A = -\sigma^* + \left(\frac{N_{ex}}{A_{lsl}} - \frac{M_{ex} - N_{ex}a}{2I_{lsl}}\right)\frac{1}{n_c},$$ (3.20)

$$B(\xi) = \frac{e_{x_{II}} x_{II}}{I_{x_{II}}} + \left(\frac{a-e}{2I_{lsl}} + \frac{1}{A_{lsl}}\right)\frac{1}{n_c}.$$ (3.21)

Force N obtained from (3.17) is other than the true one N^*, the curvature compatibility being still missing.

In the starting condition, and after beam cracking, the respective slab curvatures are (tan γ_{sll}, tan γ_{slll} in Fig. 4).

$$\kappa_{sll} = \frac{M(3)}{E_{c,b} I_{1\,com}} + \frac{\Delta M_{sl}^\varphi}{E_{c,sl} I_{lsl}} + \kappa_{sl}^\varphi,$$ (3.22)

$$\kappa_{slll} = \frac{M_{sl}}{E_{c,b} I_{1\,com}} + \kappa_{sl}^\varphi.$$ (3.23)

Curvature increment:

$$\Delta\kappa_{sl} = \kappa_{sl\,II} - \kappa_{sll} = \frac{M_{sl} - \Delta M_{sl}^{\varphi}}{E_{c,sl}I_{lsl}} - \frac{M(3)}{E_{c,b}I_{1\,com}}. \tag{3.24}$$

Beam curvature in starting condition, and after cracking, resp. ($\tan\gamma_{bl}$, $\tan\gamma_{bll}$ in Fig. 4):

$$\kappa_{bl} = \frac{M_b'}{E_{c,b}I_{1b}} + \frac{M(3)}{E_{c,b}I_{1\,com}} + \frac{\Delta M_{c,b}^{\varphi}}{E_{c,b}I_{c,b}} + \kappa_{bl}^{\varphi}, \tag{3.25}$$

$$\kappa_{bll} = \frac{Ne_{x_{II}}}{E_{c,b}I_{x_{II}}} + \kappa_{bl}^{\varphi}. \tag{3.26}$$

Curvature increment:

$$\Delta\kappa_b = \kappa_{bll} - \kappa_{bl} = \frac{1}{E_{c,b}}\left[\frac{Ne_{x_{II}}}{I_{x_{II}}} - \frac{M_b'}{I_{1b}} - \frac{M(3)}{I_{1\,com}} - \frac{\Delta M_{cb}^{\varphi}}{I_{c,b}}\right]. \tag{3.27}$$

Expressing moment M_{sl} from equilibrium equations (3.2) to (3.5) and substituting into (3.24), *compatibility condition*

$$\Delta\kappa_{sl} = \Delta\kappa_b \tag{3.28}$$

yields for N:

$$N^{**} = \frac{C}{D(\xi)}. \tag{3.29}$$

Notations mean:

$$C = \frac{M_{ex} - N_{ex}a - \Delta M_{sl}^{\varphi}}{I_{lsl}n_c} + \frac{M_b'}{I_{1b}} + \frac{\Delta M_{c,b}^{\varphi}}{I_{c,b}}, \tag{3.30}$$

$$D(\xi) = \frac{e_{x_{II}}}{I_{x_{II}}} + \frac{e - a}{I_{1,sl}n_c} \tag{3.31}$$

Under actual conditions, in addition to the equilibrium conditions, both compatibility conditions are satisfied:

$$N^* = N^{**} = N.$$

Rather than by further reductions, the solution is advisably found by computer iteration. Assuming a convenient starting ξ value, eccentricity $e(\omega, \vartheta)$ results from (2.21) to (2.23). Depth $e_{x_{II}}$ below force N is obtained from (2.13). Now, substituting ξ into (2.10) yields "stress" moment of inertia $I_{x_{II}}$.

Available parameters are applied to calculate N^* from (3.17) and N^{**} from (3.29). For $N^* \neq N^{**}$, the procedure is iterated, increasing or decreasing the ξ value until equality $N^* = N^{**} = N$ (within a specified error limit).

N being known, equilibrium equations (3.2) to (3.5) yield moment and force M_{sl}, N_{sl}, resp. acting on the slab. Steel stress increment ($\Delta\sigma_{ps}$) needed for determining the crack width is obtained from Fig. 1 as usual.

4. Compressed flange stresses as a function of the load process

Top fibre stresses $\sigma^u_{c,b}$, $\sigma^u_{c,sl}$ of precast beam and monolithic slab with cross-sectional characteristics according to Fig. 2 are seen in Fig. 5. The beam meets the fundamental requirement of the introductorily outlined approximate method: the stress in the top fibre of the beam due to combined dead and full live loads (the so-called *nominal* load $M_{nom} = M(1, 2, 3, p)$—assuming no crack—is lower than the permissible $(f^{pe}_{c,b} = 18$ MNm$^{-2})$.

The Hungarian Code of Road Bridges requires exemptness from tensile stresses of the bottom fibre under so-called *service moment* (M_{ser}).

The service moment is composed from the dead load moment $M(1, 2, 3)$ and the reduced (α_r) fundamental (unfactored) values of the full live traffic moment: $M_{ser} = M(1, 2, 3) + \alpha_r \bar{M}(p)$. The full live load of the bridge consists of concentrated loads ($4 \times 0.18 = 0.72$ MN) and an uniform load of 0.004 MNm^{-2} intensity.

$M_{ser} = 1.4637 + 0.35 \times 1.2562 = 1.9069$ MNm in the case of Fig. 5.

M_{cr} in the diagram is the cracking moment.

Accessory stresses (creep, shrinkage) have been determined according to [3].

The obtained results successively pass into those to be calculated, assuming uncrackedness achieved at moment M_0 for stress $\sigma^l_{c,b} = 0$ (e_K in Fig. 2), where also tangents coincide and stress functions of both extreme fibres are ascending, but later the beam function will be concave from below. The functions are nonlinear, namely both force N and eccentricity e vary continuously. While beam stresses differ little from those for an assumed uncrackedness, those *for the slab are much poorer*. The slab behaves elastically up to about 90% of the nominal load: $M^{el}_{lim} \cong 0.9 M_{nom} = 2.460$ MNm. Permissible stress: $f^{pe}_{c,sl} = 11$ MNm^{-2}. Plastic behaviour starts at about 79% of the total live moment $\bar{M}(p)$ ($\bar{M}(p) = 1.2562$ MNm).

Transition to the ultimate condition at failure is seen in a dash-dot line. The ultimate condition arises from the so-called *maximum external moment* (design value of the external moment) according to the code applying divided *safety* factors: $M_{max} = \gamma_g M(1, 2, 3) + \gamma_q \bar{M}(p) = 2.9711$ MNm (where $\gamma_g = 1$ and $\gamma_q = 1.2$ is a safety factor for the live load). Numbers at horizontal tangents to $\sigma - \varepsilon$ diagrams framed in the right-hand-side margin of Fig. 5 are ultimate (failure) stresses involving safety factor for concrete $\gamma_c = 1.5$ (-21 and -13 MNm^{-2}).

The extremal value of moment M_{max} being in excess of the nominal moment M_{nom} by as little as about 9%, the results agree with our observation: such a high nominal moment cannot be the beam in the elastic range. Stress distributions due to nominal load in an uncracked (dash line) and a cracked (full line) beam are seen in the upper right hand corner of the figure. *Plastic behaviour* upon M_{max} moment is seen in the dash-dot line. Confrontation of these two diagrams points to the fitness of the presented method to correctly describe stress conditions after cracking.

Approximate *crack width* analysis specified in the Building Code for Road Bridges showed the crack width at the beginning of the plastic range to be correct. It is
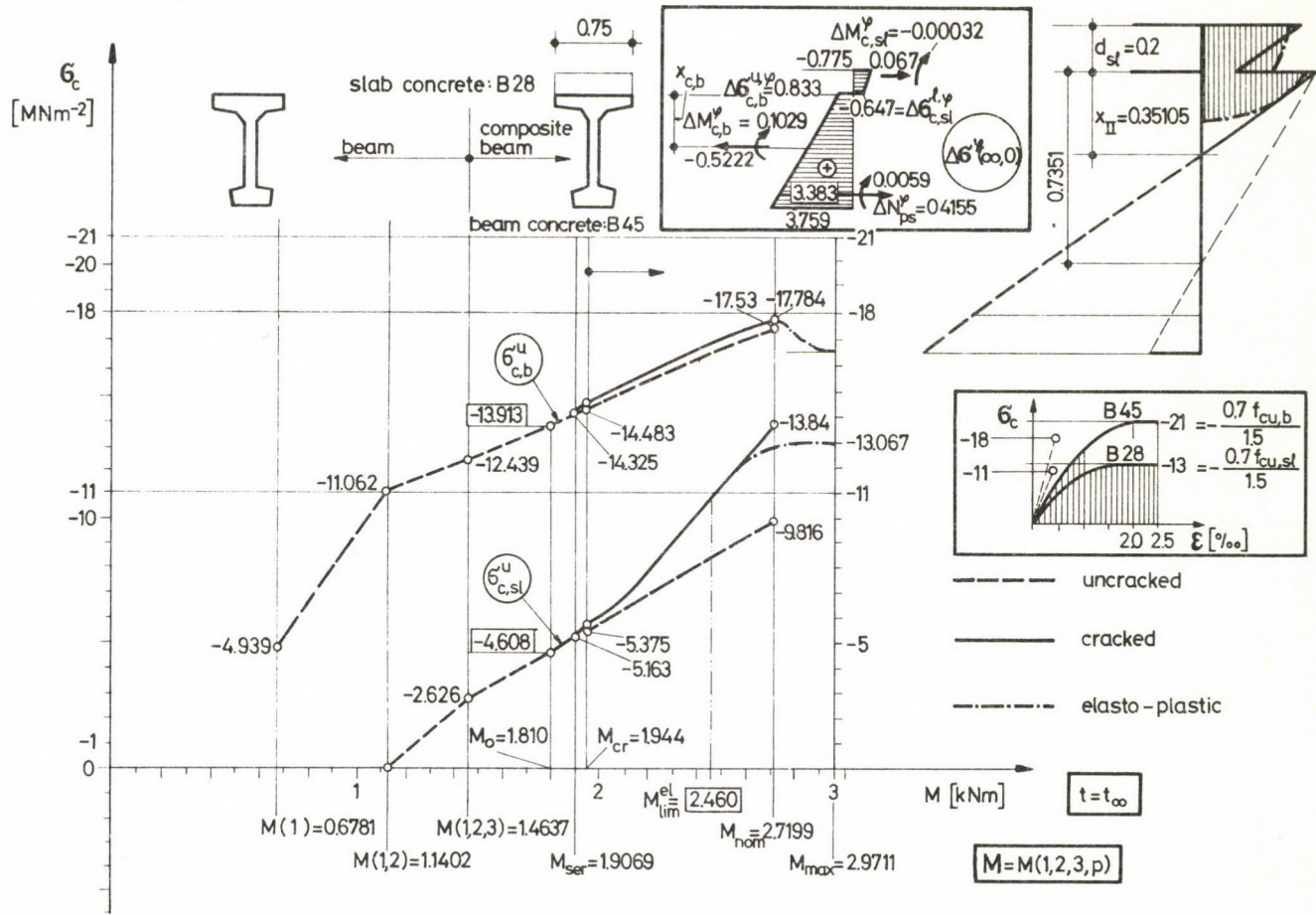
Fig. 5. Compressive stresses in top fibres of beam and slab assuming cracked and uncracked cross sections

interesting to observe the agreement between beam top fibre stresses obtained with the introductorily outlined approximate method, and those presented in this paper. Top fibre of the beam designed according to the approximate method develops elastic stresses under the full nominal load, but the *slab* gets into the plastic range at about 90% of the nominal load, *limit of the elastic load capacity* M_{lim}^{el} of the tested beam. Moments in excess shift the neutral axis upwards, widening the cracks. A higher than ultimate elastic moment causes *plastic deformations* in the beam, unloading would not entrain recovery.

Summary

A method has been developed for the stress-strain analysis of cracked precast *composite* beams, i.e. those interacting with monolithic r.c. slabs.

First, eccentricity-dependent variations of the cracked beam cross-sectional characteristics, in particular, "*stress*" and "*curvature*" moments of inertia have been determined. Before cracking, the "curvature" moment of inertia is identical to the moment of inertia of the ideal cross-section in an uncracked state, while after cracking, with increasing eccentricity, it gradually passes into pure bending moment of inertia in a cracked state. Considering the prestressing force as an external force were written out as the *equilibrium* equations.

With the aid of the mentioned moments of inertia the *compatibility* equations were deduced regarding both the *identical changes of strains* (along the joint line between the slab and the beam) and the *identical change of curvatures*.

The method is suited for determining the full elastic behaviour and the *ultimate elastic load* of the cracked composite beam.

The presented exact treatment may yield the tendon stress increment in the cracked beam, permitting to predict *crack width*.

It was numerical investigation the stresses of a composite beam dimensioned for the nominal load on the basis of an uncrackedness approach. Calculating beam stresses from prestressing up to the application of the nominal load (dead load + full live load) showed the beam *to behave elastically* up to about 90% of the nominal load, hence 79% of the full live load.

Crack widths remain permissible until the ultimate elastic load.

Thereafter the slab *starts plastic behaviour* (elastic stress peaks flatten), with increasing crack widths that only partly close after unloading (plastic remaining own strains).

References

1. Bölcskei, F.—Dulácska, E.: Statikusok könyve* (Manual of Structural Engineers). Műszaki Könyvkiadó, Budapest 1974
2. Dulácska, E.: A rugalmas vasbeton rúd kihajlása* (Buckling of Elastic Reinforced Concrete Beams.) Építés—Építészettudomány (1978), 1—2, 45—65
3. Frey, J.: Zur Berechnung von vorgespannten Beton-Verbundträgern im Gebrauchzustand. Beton- und Stahlbetonbau, (1980), 11, 257—262
4. Hampe, E.: Spannbeton. 2. Aufl. VEB Verlag für Bauwesen, Berlin 1980, 153
5. Herberg, W.: Spannbetonbau I. B. G. Teubner Verlagsgesellschaft, Leipzig 1956
6. Klatsmányi, T.—Tassi, G.: Contribution to the Analysis of Stresses in Prestressed Concrete Beams. Periodica Polytechnica (1970), 14, 311—325
7. Tassi, G.: Feszített vasbeton tartók számítása, repedéskorlátozásra és a repedés tágasságra ható paraméterek* (Design of Prestressed Concrete Beams for Crack Width Limitation, and Parameters Affecting the Crack Width.) Mélyépítéstudományi Szemle No. 9, (1972), 438—448
8. Tassi, G.: Limit Analysis of Prestressed Concrete Beams. Periodica Polytechnica (1969), 13, 83—92
9. Palotás, L.: A vasbeton elmélete* (The Theory of Reinforced Concrete.) Akadémiai Kiadó, Budapest 1973

* In Hungarian.

SOME RECENT EXPERIMENTS
ON SOIL STABILIZATION
IN AGRICULTURAL ROAD CONSTRUCTION

Á. Kézdi and E. Biczók*

The aim of this experimental work was to decide which stabilization method could be applied most successfully and most economically in some areas that could be taken as typical in Hungary. Two regions were chosen: a loess area and a clay area in the mountains. In these areas we tried cement, fly ash and chemical stabilizations were tried applying different technologies: local materials mixed in situ, transported materials mixed in situ and premixed materials. In the present study the experiences obtained in planning and in construction are presented.

1. Introduction

The question of transport rentability in the Hungarian agriculture is coming even more into prominence since large-scale farming and increased mechanization has generally become spread. Further progress necessitates the improvement of agricultural road network. In order to work properly at all times, the surface of roads must have a correct bearing capacity and their material must be stable. These tasks can only be accomplished by soil stabilization. Although these requirements can undoubtedly be better satisfied by Macadam roads or by high-quality asphalt or concrete roads, the limit in supply of available raw materials, namely in stone, cement and bitumen and the high costs of the traditional building methods make impossible the construction of roads this way. Therefore, the question is never raised whether we construct Macadam or a stabilized earth road, but, whether we are able to construct stabilized roads or nothing.

Recognizing all this, the Ministry of Agriculture and Food took the case of stabilization of main agricultural roads into the technical development programme. Co-ordination of the some five year research work was made by the Plant Protection and Agrochemical Centre of the Ministry of Agriculture and Food. The research programme, the laboratory investigations and the experimental technologies were elaborated by the Geotechnical Department of the Budapest Technical University.

The Road Research Institute and the Energy Economy Institute also co-operated, as consultants.

* Dr. E. Biczók, Research engineer, Dept. for Geotechnique, Technical University of Budapest, Hungary

Investigation of this problem has long traditions in our department. Yet in the thirties Prof. József Jáky urged the introduction of that method, but the condition in agriculture at that time did not make it possible. In the fifties, an intensive development directed by the senior author of this article, started, when, the most important physical and technological problems of the soil stabilization were made clear by large scale laboratory investigations and by building test roads. The experiences of this work were presented in the book "Stabilized earth-roads" (Kézdi, 1967.).

2. The aim of the research work

The direct aim of the research work was to decide which stabilization method could be applied most successfully and most economically in some areas that could be taken as typical in Hungary. Two regions were chosen: a loess area close to Szekszárd (Zomba) and a clay area in the mountains (Nógrád County, Szécsény).

In these two areas three kinds of stabilization methods were applied:

— cement

— fly ash and lime

— chemical stabilization, the latter one was made with the chemical agents trademark RRP and CBV.

All the technologies available in Hungary were tested:

— in the case if the soil in the crown of the road was suitable for stabilization, the technology of in-situ mixing was applied,

— if the soil in the crown of the road was not stabilizable, material from a neighbouring gravel or stone pit was transported onto the crown of the road and stabilized by using the technology of in-situ mixing.

— the pre-mixed technology was also tested. Ready made mixture from a neighbouring mixing plant of a Directorate of Public Roads was transported onto the prepared surface.

The length of the test sections varied between 150—500 metres. On the same test site these sections were subjected to equal traffic, to equal loads, to equal weather conditions, therefore the methods are comparable and this made the choice of the right procedure possible.

3. Experimental soil stabilization at Zomba

For experimental purposes one of the main inner roads of the co-operative farm "Egyesült Erővel" was chosen. The earthwork of the road was made by the co-operative farm. In the crown of the road two kinds of soil could be found: yellow loess and yellow-brown lean clay. Physical characteristics of these soils are given in *Table 1*.

Table 1. Physical characteristics of soils at Zomba

Soil	$w_L\%$	$w_P\%$	$I_P\%$	ρ_d^{max} g/cm³	pH	CaCO₃
y e l l o w						
loess	30.2	18.3	11.9	1.71	7.7	12.4
brown clay	34.2	19.2	15.0	1.65	7.3	2.2

3.1. Planning the stabilization

The purpose of planning was to determine the required quantity of each stabilizing material. For that purpose cylindrical specimens were prepared which consisted of a mixture of soil and different quantities of stabilizing material. The samples were stored in wet surroundings, then strength, durability and freezing resistance tests were performed. The samples of proper composition had to meet the relations of the Standard "Road 5-72" of the Ministry of Traffic and Posts.

Stabilization with cement means to mix the soil and the cement at the proper rate and to moisten and compact them. Yet in the laboratory experiments we took into consideration that fly ash-portland cement would be used in the construction. Setting of this kind of cement is slow, and therefore the unconfined compression strength values were determined after 14, 28 and 56 days, the durability tests were started after the 14th day and the freezing tests after the 28th day were started (see *Figure 1*). The
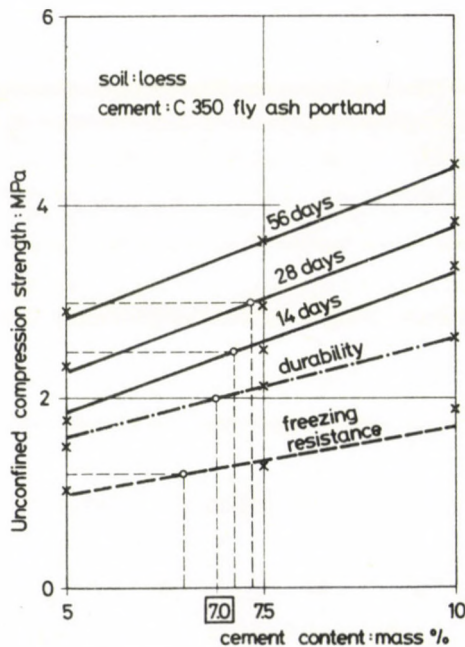
Fig. 1. Compression strength of soil cement cylinders

strength requirements of the standard were applied to these dates. The necessary cement quantity was increased by about 10 per cent because of the uncertainties of the in-situ mixing. Both values are presented in *Table 2*.

In the case of *stabilization with fly ash and lime* the hydraulic binder was lime and fly ash from Pécs mixed at the rate 1:4. Because of the very slow binding process of lime—and fly ash—additive stabilization compression tests were performed after 30, 60 and 90 days, and the durability and freezing tests were started after 60 days. As an example the results of the investigations performed in loess is presented in *Figure 2*.

With fly ash and lime many fine grains are added to the soil so the compacting characteristics will be changed. *Figure 3* shows an example compacting curves of loess and fly ash—lime mixtures at different rates are presented. Prescriptions for the construction are shown in *Table 3*.

Table 2. Characteristics of soil cement road construction

Soil	$c\%$	c_1 kg/m^2	c_1' kg/m^2	$\rho_d^{95\%}$ g/cm^3	$w_{on\ site}\%$
loess	7	18	20	1.76	9 – 13
clay	10	25	25	1.67	10 – 14
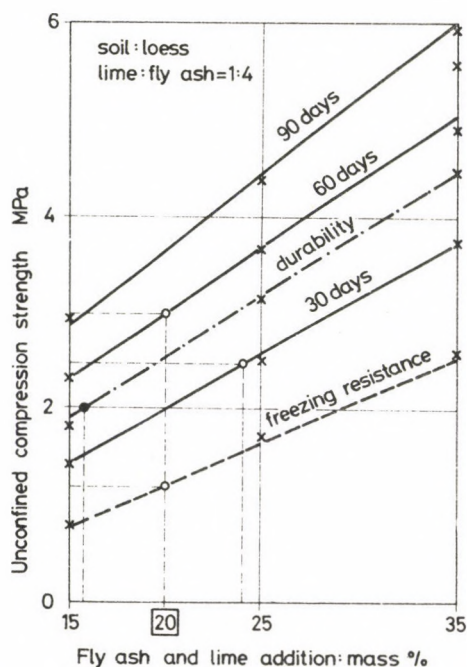
Fig. 2. Compression strength of fly ash and lime stabilized cylinders
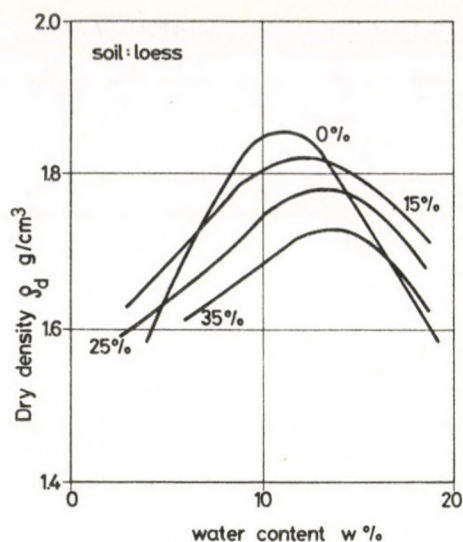
Fig. 3. Compaction test of soil and fly ash and lime

Table 3. Characteristics of soil fly ash road construction

Soil	Lime + fly ash addition		Lime kg/m²	Fly ash kg/m²	$\rho_d^{95\%}$ g/cm^3	$w_{on\ site}$ %
	$p\%$	p' kg/m²				
loess	20	45	9	36	1.71	9
clay	25	55	11	44	1.65	11

In the case of *chemical stabilization* we did not performed the tests mentioned above, because we did not want the treated soils to behave as a pavement, therefore in the following we do not speak of stabilization but of chemical treatment.

The most important purpose of this method is to change the soil-water interaction in a favourable direction by surface reactions. For this reason the method is mostly applicable in case of cohesive soils. In the experiments two chemicals were used:

Reynolds Road Packer 235 (RRP) and Chemische Bodenverbesserung (CBV). As to recommendations of the manufacturers "on the treated soils much higher bearing capacity can be reached than on non-treated ones". It was particularly investigated how the chemicals changed the physical characteristics of soils: the plasticity index of soils decreased and both the values of the optimal water content and the maximum density in the compaction test increased by only a little, using each chemical. As a control we made the manufacturer investigated the soils, according to their statement the soil was *conditionally suitable* to chemical stabilization. Addition of chemicals was in each case 6 litres per 100 square metres.

3.2. Construction works

The construction was made from May to July 1981.

The *cement and the fly ash -lime stabilization* means performing much the same operations. Thickness of stabilized layer was 15 centimetres.

Before the operations the compactness of the soil in the crown was checked in order to determine the necessary cutting depth. After loosening the surface by ploughing the next stage was the pulverization to a prescribed depth. The aim of the operation is to disintegrate the clods to the degree demanded by stabilization. This was not easy at all in cohesive soils. *Figure 4* illustrates how the quantity of clods bigger than 5 millimetres changed after each run of the pulverizer-mixer. It can be seen in the requirement, that the quantity of clods bigger than 5 millimetres should not exceed 10 per cent, was not reached.

The next task was to spread the stabilizer and to admix it with the soil. The dry mixing was performed by a rotary scraper again. Then, *water was added* to the mixture to reach the optimum water content for compaction. The last operation was the *compaction*. *Figure 5* illustrates the connection between the number of runs and compactness in the stabilization of lean clay with fly ash and lime. It can be seen that the values of compactness determined by isotope measurements are somewhat less than that of the direct sampling. Probably this resulted from that, that the radiometric method did not take the grains of lime and fly ash into account.

Chemical stabilization began by loosening the soil, too, then pulverisation was made by a rotary scraper. Addition of the chemicals was performed in several runs,
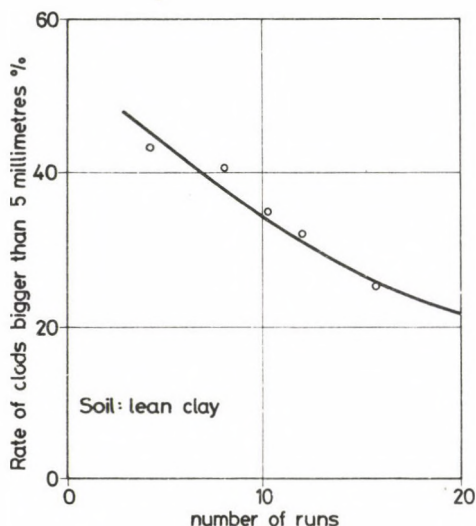
Fig. 4. Connection between pulverizing and number of runs
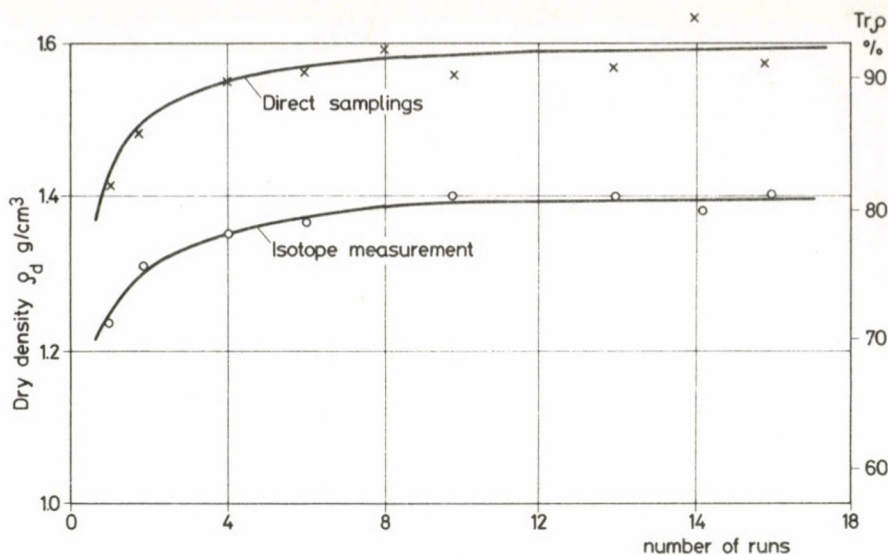
Fig. 5. Connection between number of runs and compactness

diluted as prescribed. Hereupon came the period of rest, sprinkling at intervals and three weeks later the surface of the road was compacted.

Each stabilized section got a coating surface definitely necessary to prevent freezing in winter.

3.3. Evaluation of the experiment

Completion of the road construction was followed by a one year long period of observations. The traffic on the road was continuously recorded. On the basis of analysing the traffic data the planning traffic value is 12 500 pieces of 100 kN unit axles in a year i.e., the road falls within the very light (A) load category, thus the value of the admissible deflection is 1.5 millimeter. Bearing capacity of the road was measured by deflection measurements and by plate loading tests three times: two months after finishing, after the spring period and at the end of the one year observation.

The results of the measurements are to be seen on *Figure 6*. Besides, the damage of the road surface were visually observed. Based upon all these we can say that, though the *cement stabilized* sections had a deflection exceeding by little the prescribed value of 1.5 millimeter, the experiment proved to be successful. The method can be offered for stabilization of loess and silt in a thickness of 20 centimetres.

The *fly ash and lime stabilization* was definitely successful, because deflections were less than 1.5 millimeter, thus the method can be applied in loess and silt to a thickness of 15 centimetres, in lean clay $(I_p < 20\%)$ to a thickness of 20 centimetres.
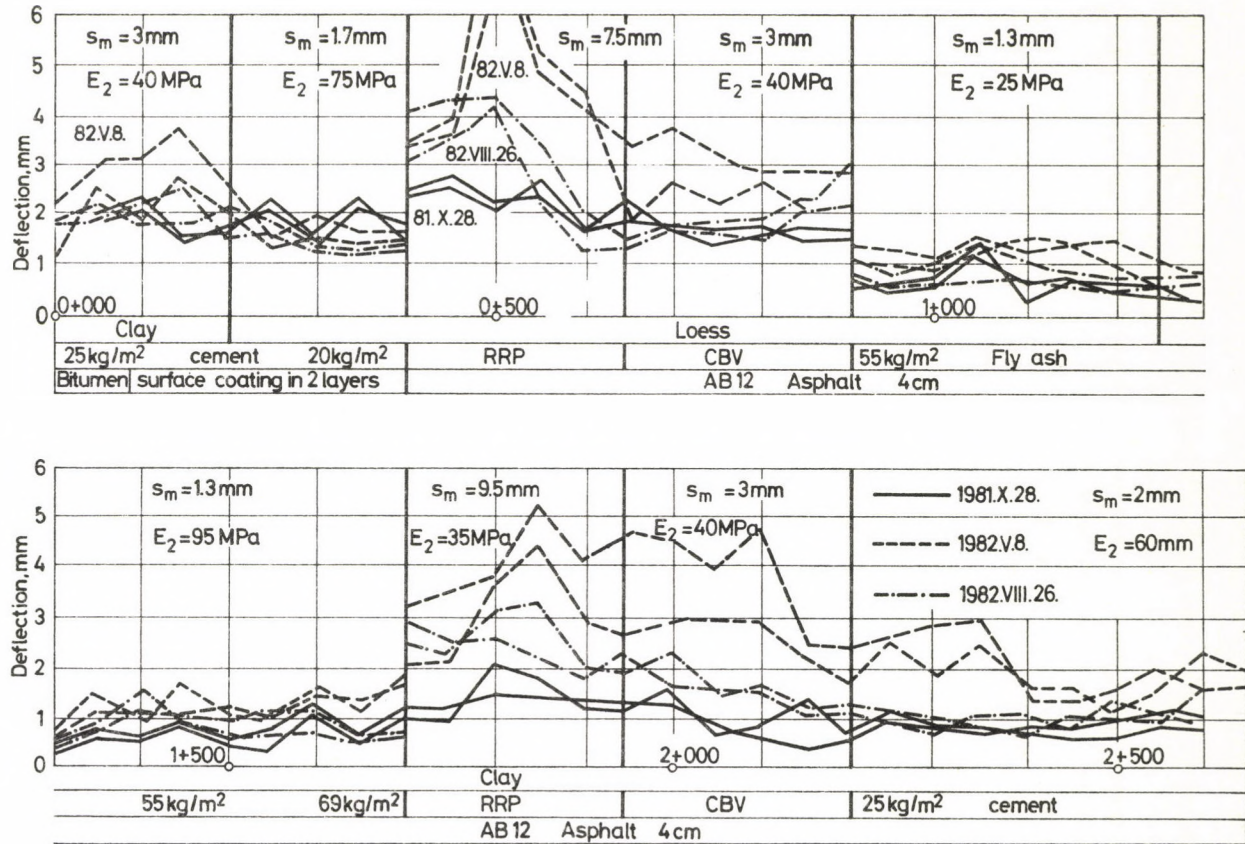
Fig. 6. Measured deflections and bearing capacity of test road at Zomba

The *chemical treatment* had no success. The chemical RRP gave an especially bad result. The pavement laid upon loess and lean clay treated with RRP crumbled entirely already some months later. The deflections of the section treated with the chemical CBV are somewhat less, but in loess the pavement totally crumbled and in lean clay the first signs of damage could be observed.

Figure 7 allows some interesting comparisons, analysing the per unit costs. The costs of materials, transportation and machine operations are separately shown. Dotted line shows the extrapolated costs of stabilizations certainly reaching the required technical characteristics, proved by experiments.

4. Experimental soil stabilization at Szécsény

For experimental purposes one of the main road of the co-operative farm "II. Rákóczi Ferenc" was chosen. In the crown of the road there were medium and highly cohesive clay soils. Therefore, it was intended to stabilize by transported spoil from a neighbouring gravel pit by cement, by fly ash and lime, respectively, and great hopes were attached to the chemical treatment, too.

4.1. Planning the stabilizations

To reach the purposes mentioned above, detailed laboratory investigations were made. In case of *cement stabilization* we determined the quantity of cement necessary for the successful stabilization of the spoil from the gravel pit, later the technology was elaborated based upon these.

The *fly ash stabilization* was planned to perform with the spoil from the gravel pit and with the mixture of lime and fly ash from Kazincbarcika.

For *chemical treatment* the chemical agents trade mark RRP and CBV were used here, too. The essential physical characteristics of the soils are illustrated in *Table 4*.

According to the laboratory investigations the chemicals decreased the values of the plasticity index and improved the compactibility of soils a little. The manufacturer of the chemicals also investigated the soils: the brown clay was not, but the red brown and the yellow clay was suitable for chemical stabilization. The quantity of chemical to be used was given: for both soils 6 litres per 100 square metres.

4.2. Construction works

The construction began in 1980. *Chemical treatment* in the three soils were performed according to the technology reported above. It did not fulfil expectations. The rains in the autumn, but even more in the winter and in the spring almost totally

M: material
T: transport
L: labor
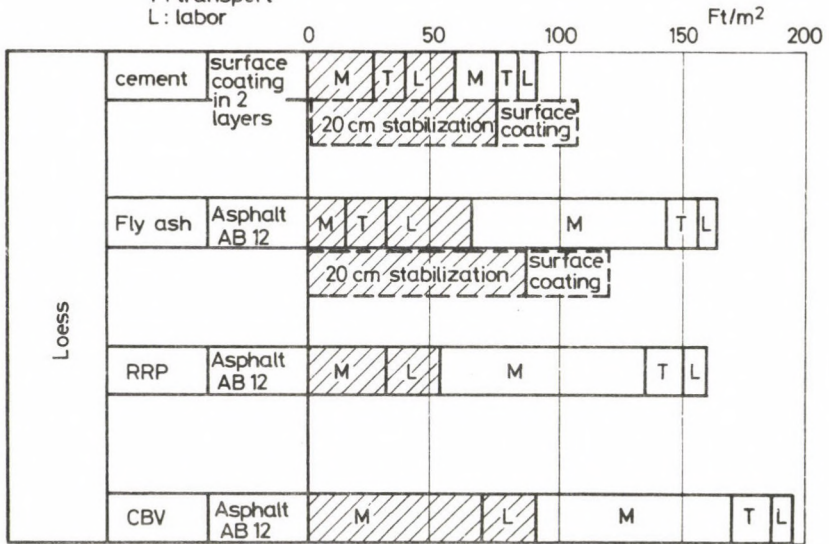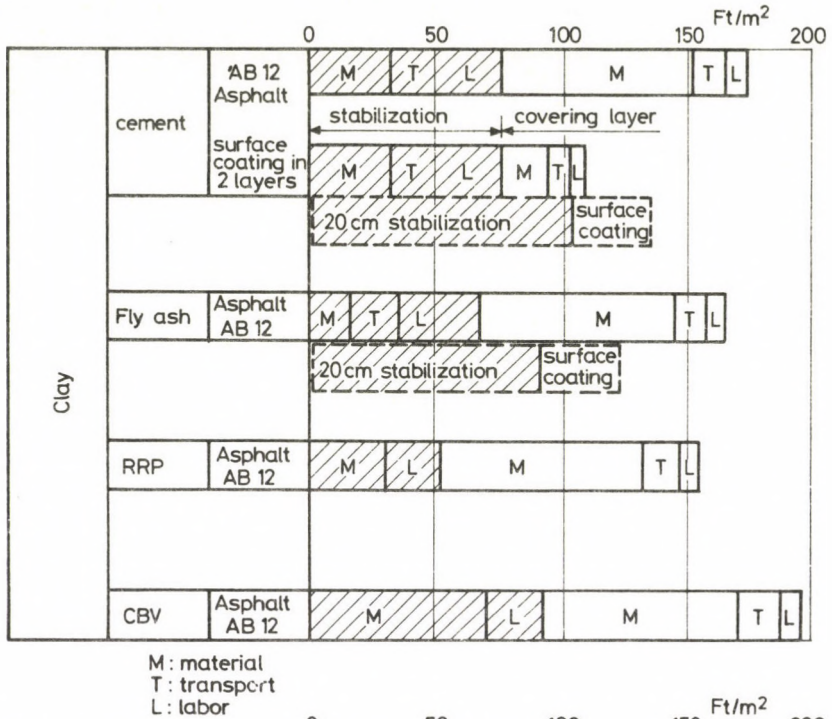
Fig. 7. Distribution of costs of construction at Zomba

Table 4. Physical characteristics of soils at Szécsény

Soil	$w_L\%$	$w_P\%$	$I_P\%$	$CaCO_3$	Organic cont.%
brown clay	38.8	17.1	21.7	0.4	4.8
brown clay	51.0	19.5	31.5	0.4	5.3
yellow clay	46.1	16.6	29.5	0.3	4.8

damaged the road, except of a short section. In the springtime the road was in a worse condition than other roads of the co-operative farm not treated by chemicals. Then it was decided to stop further experiments, except the section holding out some hope mentioned before.

Cement stabilization was performed on a section of about 400 metres long, but in a very bad quality. For this reason and for several other problems the construction firm had to be exempted from further operation.

The further construction was performed by the Salgótarján Directorate of Public Roads from May to July 1981.

The *fly ash stabilization* was made applying several methods, the local possibilities maximally taken into consideration. The fly ash was in every case wet fly ash from the nearby thermal power station of Visonta, transported on plateau trucks. As activating material in addition to the calcium hydrate, the byproduct of calcium hydrate from Dorog was used, too. The raw material was the spoil from the gravel pit of the co-operative farm, transported to the road crown, in other cases it was the soil of a neighbouring gravel pit. In these two cases stabilization was made by in-situ mixing. On a third section pre-mixed stabilization was made. In this case the mixture of soil— calcium hydrate—fly ash made at the mixing plant of the Directorate of Public Roads was ready made and transported by plateau trucks to the road crown and after spreading, was compacted.

4.3. Evaluation of the experiment

After finishing the road came a year long observation period, while traffic was permanently recorded. The analysis showed the value of the planning traffic was 10 000 pieces of 100 kN unit axles, i.e. the road fell is within the very light (A) load category, thus the value of the admissible deflection was 1.5 millimeter. Bearing capacity of the road was also checked three times: after finishing the road, after wintertime and at the end of the observation period. Deflection measurements and plate loading tests were performed. The results of the tests are shown in *Figure 8*.

The *cement stabilization* of the gravel and sand did not succeeded here, but it was due to the bad quality of construction, the method is further recommended.

All of the *fly ash stabilizations* gave good results. Taking into consideration the technical parameters, the best was the pre-mixed soil of a stone pit with fly ash, the next
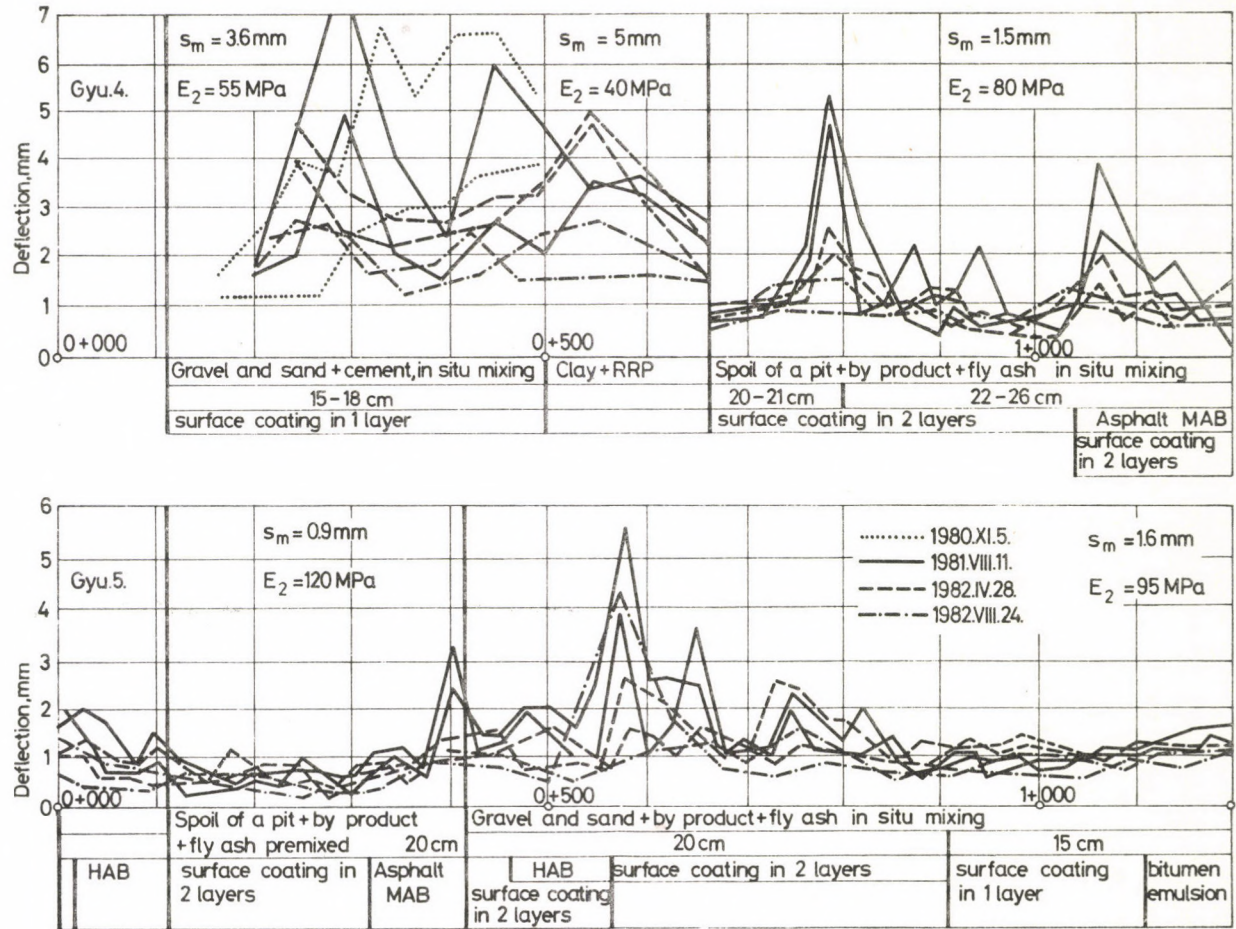
Fig. 8. Measured deflections and bearing capacity of road Szécsény

one is the in-situ mixing of the spoil of a stone pit and the last one is the in-situ mixing of the gravel spoil.

The *chemical treatment* did not fulfil the expectations here either. As was mentioned, after the first winter the road sections treated with chemicals were in worse condition than the other roads of the co-operative farm that were untreated. The some 150 metres long section made with RRP that needed a continuous maintenance and because of the repeated puddling would slowly take on the character of a mechanical stabilization. The chemicals remained were spreed on another area of Szécsény, on another clay. The section treated with RRP is already completely damaged, the part treated with CBV is still in good condition.

Figure 9 illustrates the per unit costs of the stabilizations. Dotted lines show the extrapolated costs of stabilizations fulfilling the technical requirements. Attention should be paid to the fact that the costs of the cement stabilization should not be compared to the cost of other stabilizations, because it was performed by another construction firm a year earlier.

Summary

In our experiments, on the one hand, well-known stabilization methods were investigated in order to expand their field of application, on the other hand new materials and methods were tested.

Summarizing the experiences the following conclusion can be drawn:

Application field of the *cement stabilization* is found in regulations. The thickness of stabilizations made from loess and silty soils shall be 20 centimetres.

The *fly ash stabilization* may be economical near to thermal power stations within a distance of 100 km. Instead of calcium hydrate which is difficult to obtain, the by-product of calcium hydrate also suits as activating material. In the absence of local materials (spoil of gravel or stone pit) premixed stabilization can also be applied, if a mixing plant can be found within 100 kilometres.

In connection with the *chemical treatments* we gained bad experiences. The chemical RRP did not prove to be fit on any experimental section, and the treatment with the CBV also proved unsuccessful, except in one case.

Finishing the experimental period we express our hope that the stabilization methods, which proved succesful would soon be used to a great extent and would help to solve the transport problems in agriculture.

Finally we wish to express our thanks to associate professor Mr. István Lazányi, who elaborated the basic conception of this experimental programme.
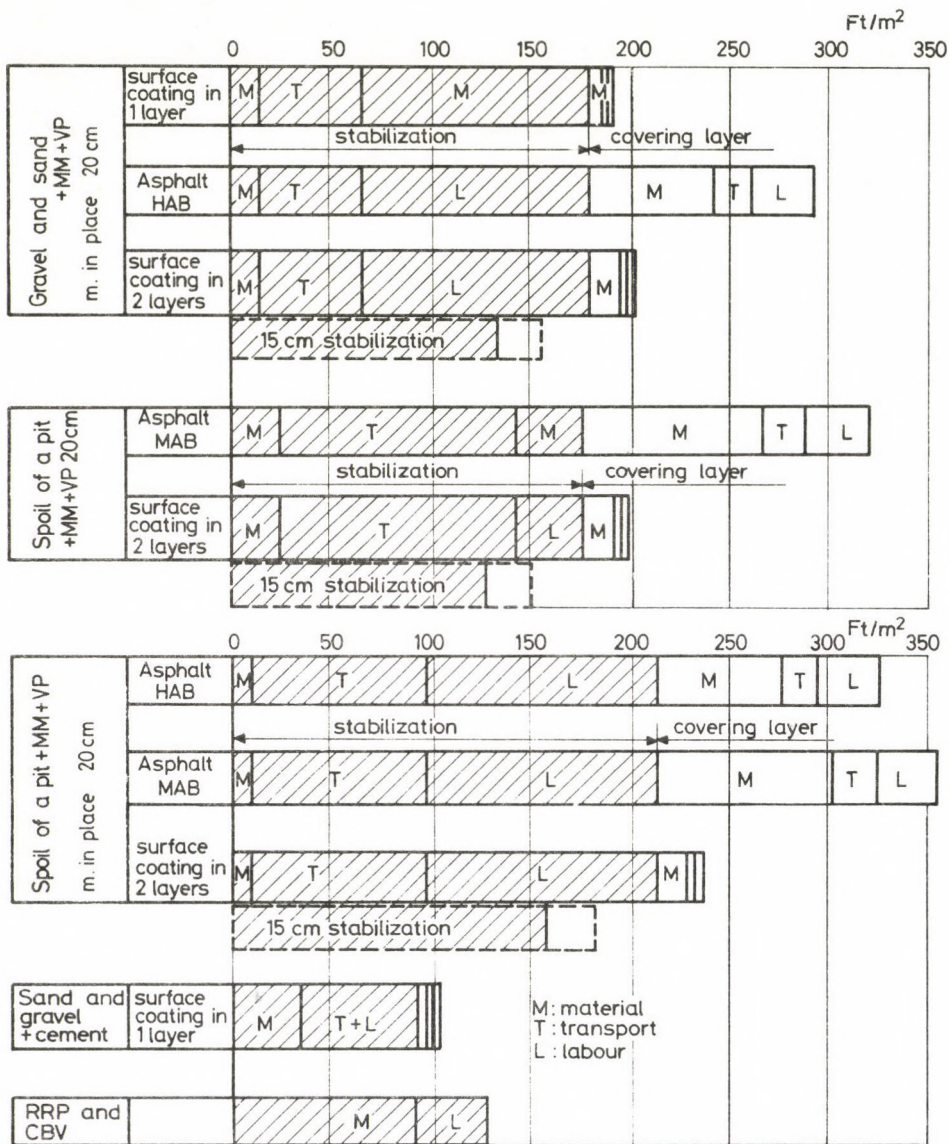
Fig. 9. Distribution of costs of building at Szécsény

References

1. Kézdi, Á.: Stabilized Earth Roads. Publishing House of the Hungarian Academy of Sciences, Budapest 1969*
2. Gáspár, L.: Some Recent Experiences on Soil Stabilization. Publication No. 61 of the Research Institute for Roads, Budapest 1973*
3. Lackner, L.: Some Recent Construction Experiences of a Dry Fly Ash Stabilization under Traffic. Scientific Review of Civil Engineering, 1977/8*
4. Some Recent Issues for Utilization of Fly Ash in Road Construction. Publication of the Ministry of Traffic and Posts, Directorate of Public Roads at Tatabánya, 1980*
5. Dimensioning Instructions for Agricultural Roads. Publication of Enterprise for Agricultural Investments, 1977*
6. Planning of Stabilized Road Bases. No. 5—79 Instruction of the Ministry of Traffic and Posts.*
7. Controlling and Qualifying Investigations for Construction of Stabilized Basis Layers of Road Pavements. No. 7—75 Technical Directives of the Ministry of Traffic and Posts*
8. Requirements for Pavement Bases without Binder and with Hydraulic Binder. Hungarian Standard No. 07-3209-81*
9. Stabilization of Sands with Fly ash or Granulated Dross. No. 61—82/1977 Provisional Technical Directives of the Department for Public Roads of the Ministry of Traffic and Posts*
10. Stabilized Pavements. Cement Stabilization. TGL 28374/01. Lime Stabilization TGL 28374/02. (Standards of the German Democratic Republic)

* in Hungarian

LATERAL BUCKLING OF ARCHES WITH FORK-LIKE SUPPORTS, ELASTICALLY RESTRAINED ALONG THEIR ENTIRE LENGTHS AGAINST LATERAL DISPLACEMENT AND ROTATION

L. KOLLÁR*–I. BÓDI**

The arches of a tent structure are supported against lateral buckling, on the one hand, by the tensile stiffness, on the other hand, by the shear rigidity of the fabric. The tensile stiffness acts as a row of springs, and the shear rigidity acts in the form of distributed elastic bending moments on the arch. The paper takes these two effects into account, and determines the critical compressive force of the arch with "fork-like" supports.

1. Introduction

Lateral-torsional buckling of centrally compressed arches, elastically supported against lateral displacement, is dealt with in [2]. This lateral restraint is in most cases provided by the fabric roofing stretched onto the arches. Detailed investigations of the static properties of the fabric [3] showed that it exerts, besides hindering lateral displacement, also another restraint: the shear rigidity of the fabric hinders the rotation in lateral direction of the arch as well. This elastic restraint comes about in the form of distributed horizontal forces, which act, as a rule, at a point G different from the shear centre T of the arch, so that they also exert twisting moments on the arch [3].

In this paper we shall consider this restraining effect, in addition to that against lateral displacement treated in [2]. The assumptions and approximations to be used are identical with those of [2].

2. Notations

The notations showed in Fig. 3 of [2] are to be supplemented by the following (see also Fig. 1):

G — point of application of the lateral shear restraint;
v_G — y-directed displacement of point G;
t_g — distance between shear centre T and G;

* L. Kollár, Karap u. 9. H-1122, Budapest, Hungary
** I. Bódi, Budapesti Müszaki Egyetem, Vasbetontanszék, Müegyetem rkp. 3, H-1111 Budapest, Hungary

Fig. 1. The cross-section of the arch supported by the fabric

g — modulus of shear restraint $[N]$ (referred to unit arc length), with whose aid the horizontal force $\bar{q}_{yg}$ can be computed by the formula

$$\bar{q}_{yg} = gv''_G, \tag{1}$$

see in [3]. Here prime denotes differentiation with respect to the arc length.

3. Differential equations of lateral buckling

According to [4] the differential equation system of an arch in the state of bifurcation of equilibrium is:

$$M'_z + \frac{M_x}{R} + \bar{m}_z = 0. \tag{2a}$$

$$T'_y + \bar{q}_y = 0, \tag{2b}$$

$$M'_x + \frac{M_z}{R} - T_y + \bar{m}_x = 0, \tag{2c}$$

where M and T are the internal forces developing during buckling, and $\bar{m}$ and $\bar{q}_y$ denote the loading terms which come about due to buckling, referred to unit arc length.

Due to the shear rigidity of the fabric, these loading terms have to be completed, with respect to those defined by Eqs (6a) and (6b) in [2], by the following terms marked by the subscript g:

$$\bar{q}_{yg} = gv''_G = g(v''_T - t_g\varphi''), \tag{3a}$$

$$\bar{m}_{zg} = -g(t_g - e)v''_G = -g(t_g - e)(v''_T - t_g\varphi''). \tag{3b}$$

Hence, we finally obtain for the loading terms:

$$\bar{q}_y = -Nv''_T + Ne\varphi'' - c(v_T - t_c\varphi) + g(v''_T - t_g\varphi''), \tag{4a}$$

$$\bar{m}_z = N\left[\frac{t-e}{R}\varphi - (i_x^2 + i_y^2)\varphi'' - \frac{i_x^2}{R^2}\varphi\right] + c(t_c - e)(v_T - t_c\varphi) -$$

$$- g(t_g - e)(v''_T - t_g\varphi''), \tag{4b}$$

$$\bar{m}_x = 0. \tag{4c}$$

Expressing the internal forces by the displacements of the shear centre T, we obtain the following expressions:

$$N = qR = \text{const.,} \tag{5a}$$

$$T_y = N(v_T' - e\varphi') + c \int\limits_{(s)} (v_T - t_c\varphi)\, ds - g(v_T' - t_g\varphi'), \tag{5b}$$

$$M_x = EI_x\left(\frac{\varphi}{R} - v_T''\right), \tag{5c}$$

$$M_z = GI_T\left(\varphi' + \frac{v_T'}{R}\right) - EI_\omega\left(\varphi''' + \frac{v_T'''}{R}\right) + eT_y. \tag{5d}$$

After performing the necessary derivations, we introduce the expressions (5) into Eqs (2a) and (2c). Eq. (2a) thus becomes:

$$GI_T\left(\varphi'' + \frac{v_T''}{R}\right) - EI_\omega\left(\varphi'''' + \frac{v_T''''}{R}\right) + eN(v_T'' - e\varphi'') - \frac{EI_x}{R}\left(\frac{\varphi}{R} - v_T''\right) +$$

$$+ N\left(\frac{t - e}{R} - \frac{i_x^2}{R^2}\right)\varphi -$$

$$- (i_x^2 + i_y^2)N\varphi'' + ct_c(v_T - t_c\varphi) - gt_g(v_T'' - t_g\varphi'') = 0. \tag{I}$$

If we differentiate Eq. (2c) once with respect to s, and substitute for T_y' according to (2b), we arrive at the second differential equation:

$$EI_x\left(\frac{\varphi''}{R} - v_T''''\right) + \frac{GI_T}{R}\left(\varphi'' + \frac{v_T''}{R}\right) - \frac{EI_\omega}{R}\left(\varphi'''' + \frac{v_T''''}{R}\right) +$$

$$+ N(e\varphi'' - v_T'') - c(v_T - t_c\varphi) + g(v_T'' - t_g\varphi'') = 0. \tag{II}$$

Eqs (I) and (II), containing the unknown displacement functions v_T and φ, constitute the differential equation system of lateral buckling of the arch investigated. The critical compressive force N_{cr}, causing buckling, can always be computed from these equations, taking into account the boundary conditions corresponding to the supports of the arch.

It should be kept in mind that Eqs (I) and (II) have been developed with the assumption that R and N are constant all along the arc length. The equations are thus valid, strictly speaking, for circular arches acted upon by a constant radial load q only. For arches of other shapes, however, the result can be used as an approximation.

4. Solution for "fork-like" supports

In the case of "fork-like" supports, when the end cross-sections of the arch are prevented from displacing laterally, but can freely rotate, and they cannot turn about the arch axis, but can freely warp, the following boundary conditions hold:

$$\left. \begin{array}{l} s=0: \\ s=l: \end{array} \right\} \qquad v_T = 0; \tag{6a}$$

$$\frac{\varphi}{R} - v_T'' = 0; \tag{6b}$$

$$\varphi = 0; \tag{6c}$$

$$\varphi'' + \frac{1}{R} v_T'' = 0. \tag{6d}$$

This special kind of support allows to assume the unknown displacement functions in the form:

$$\varphi = \sum_{k=1, 2, 3 \ldots} \varphi_k \sin(\lambda_k s), \tag{7a}$$

$$v_T = \sum_{k=1, 2, 3 \ldots} v_k \sin(\lambda_k s), \tag{7b}$$

where $\lambda_k = k \dfrac{\pi}{l}$, and φ_k and v_k are constant coefficients.

Since every term satisfies the boundary conditions (6a) to (6d) and the differential equation system (I) and (II), the linear equation system for the coefficients decomposes and can be written in the form:

$$\begin{bmatrix} a_{11} & a_{12} \\ a_{21} & a_{22} \end{bmatrix} \begin{bmatrix} \varphi_k \\ v_k \end{bmatrix} = \begin{bmatrix} 0 \\ 0 \end{bmatrix}. \tag{8}$$

The coefficient matrix is symmetric $(a_{12} = a_{21})$, and its elements are the following:

$$a_{11} = -\lambda_k^2 [GI_T + \lambda_k^2 EI_\omega - N(e^2 + i_x^2 + i_y^2) + gt_g^2] + \frac{1}{R} \left[N \left(t - e - \frac{i_x^2}{R} \right) - \frac{EI_x}{R} \right] - \\ - ct_c^2, \tag{9a}$$

$$a_{12} = a_{21} = -\lambda_k^2 \left[Ne + (GI_T + \lambda_k^2 EI_\omega + EI_x) \frac{1}{R} - gt_g \right] + ct_c, \tag{9b}$$

$$a_{22} = \lambda_k^2 \left[N - (GI_T + \lambda_k^2 EI_\omega) \frac{1}{R^2} - \lambda_k^2 EI_x - g \right] - c. \tag{9c}$$

The value of the critical compressive force $N = N_{cr}$ can be obtained from the condition

$$\det \mathbf{A} = a_{11} a_{22} - a_{12}^2 = 0,$$

which yields an equation of the second degree for N_{cr}:

$$K_2 N_{cr}^2 + K_1 N_{cr} + K_0 = 0. \tag{10}$$

Performing the multiplications and dividing by λ_k^2, we arrive at the following expressions for the coefficients:

$$K_2 = (i_x^2 + i_y^2)\lambda_k^2 + \frac{t-e}{R} - \frac{i_x^2}{R^2}; \tag{11a}$$

$$K_1 = -EI_x \left[\frac{1}{R^2} + \lambda_k^4(e^2 + i_x^2 + i_y^2) + \lambda_k^2 \left(\frac{t+e}{R} - \frac{i_x^2}{R^2} \right) \right] -$$

$$- (GI_T + \lambda_k^2 EI_\omega) \left[\lambda_k^2 + \frac{1}{R^2} \left(\frac{t-e}{R} - \frac{i_x^2}{R^2} \right) + \frac{\lambda_k^2}{R^2} i_x^2 \right] -$$

$$- c \left[(e - t_c)^2 + i_x^2 + i_y^2 + \frac{1}{\lambda_k^2} \left(\frac{t-e}{R} - \frac{i_x^2}{R^2} \right) \right] -$$

$$- g \left[\lambda_k^2(e - t_g)^2 + \lambda_k^2(i_x^2 + i_y^2) + \frac{t-e}{R} - \frac{i_x^2}{R^2} \right]; \tag{11b}$$

$$K_0 = EI_x(GI_T + \lambda_k^2 EI_\omega)\left(\lambda_k^2 - \frac{1}{R^2} \right)^2 +$$

$$+ c \left[EI_x \left(\lambda_k t_c + \frac{1}{\lambda_k R} \right)^2 + GI_T + \lambda_k^2 EI_\omega \right] +$$

$$+ g \left[EI_x \left(\lambda_k^2 t_g + \frac{1}{R} \right)^2 + \lambda_k^2(GI_T + \lambda_k^2 EI_\omega) \right] + cg(t_g - t_c)^2. \tag{11c}$$

Hence we obtained a closed formula for the critical compressive force of the arch with fork-like support.

5. Numerical example

Let us determine the critical compressive force of the timber arch shown in Fig. 2, supported against lateral displacement and rotation. It corresponds to one of the arches of the tent structure investigated in Sect. 6.2 of [3].

The geometric data of the structure not given in Fig. 2 are as follows:

$$l = 2\alpha R = 2 \frac{75.41°}{180°} \pi(9.30) = 24.48 \text{ m},$$

$$\lambda_k = k\frac{\pi}{l} = 0.1283k \ (k = 1, 2, 3, \ldots),$$

$$E = 10^7 \text{ kN/m}^2,$$

$$G \approx 0.4E = 4(10^6) \text{ kN/m}^2,$$
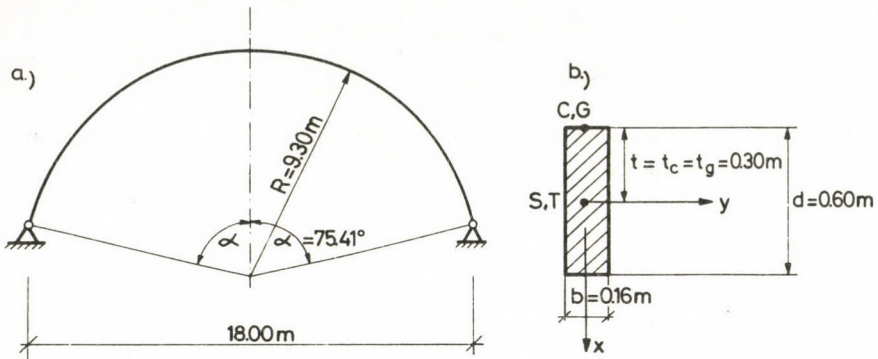
Fig. 2. The timber arch investigated numerically. a — elevation; b — cross-section

$$EI_x = 10^7 \frac{0.60(0.16)^3}{12} = 2048 \text{ kNm}^2,$$

$$GI_t = 4(10^6) \frac{0.60(0.16)^3}{3.6055} = 2726.5 \text{ kNm}^2,$$

$$EI_\omega \approx 0,$$

$e = 0$ (since S and T coincide),

$t = t_c = t_q = 0.30$ m

$i_x^2 \approx 0,$

$$i_y^2 = \frac{0.60^2}{12} = 0.030 \text{ m}^2$$

The characteristics of the elastic support are (see in [3]):

$c_{\text{eff}} = 4.54 \text{ kN/m}^2,$
$g = 216 \text{ kN}.$

Introducing the above data into Eqs (11a, b, c), the quadratic equation (10) for N_{cr} assumes the following form:

$$N_{kr}^2 \left(i_y^2 \lambda_k^2 + \frac{t}{R} \right) + N_{kr} \left\{ -EI_x \left[\frac{1}{R^2} + \lambda_k^4 i_y^2 + \lambda_k^2 \frac{t}{R} \right] - \right.$$

$$- GI_T \left[\lambda_k^2 + \frac{t}{R^3} \right] - c \left[t_c^2 + i_y^2 + \frac{1}{\lambda_k^2} \frac{t}{R} \right] - g \left[\lambda_k^2 (t_g^2 + i_y^2) + \frac{t}{R} \right] \right\} +$$

$$+ EI_x GI_T \left(\lambda_k^2 - \frac{1}{R^2} \right)^2 + c \left[EI_x \left(\lambda_k t_c + \frac{1}{\lambda_k R} \right)^2 + GI_T \right] +$$

$$+ g \left[EI_x \left(\lambda_k^2 t_g + \frac{1}{R} \right)^2 + \lambda_k^2 GI_T \right] + cg(t_g - t_c)^2 = 0. \tag{12}$$

Let us solve Eq. (12), assuming half wave numbers $k = 1, 2, 3, 4, 5$, for four different cases: taking both tensile and shear stiffnesses of the fabric into account, neglecting the shear stiffness, neglecting the tensile stiffness, and for the case of the unsupported arch.

The values of N_{cr} (in kN) are compiled in Table 1:

Table 1

	$c = 4.54 \, \text{kN/m}^2$ $g = 216 \, \text{kN}$	$c = 4.54 \, \text{kN/m}^2$ $g = 0$	$c = 0$ $g = 216 \, \text{kN}$	$c = 0$ $g = 0$
$k = 1$	488.5	276.4	217.4	1.9
$k = 2$	371.3	150.7	301.2	79.9
$k = 3$	496.7	273.7	465.3	241.9
$k = 4$	717.3	493.3	699.6	475.3
$k = 5$	1013.5	789.0	1002.1	777.4

The values of the table show that if elastic support is present, buckling in more than one half waves is the most onerous.

According to the reasoning given in [3], the stiffness c of the elastic support of the fabric should be taken equal to zero in the cases $k \geq 2$. Thus, for $k = 1$, $N_{cr} = 488.5$ kN, computed with $c = 4.54 \, \text{kN/m}^2$ and $g = 216$ kN, is valid, while for $k \geq 2$ the critical forces computed with $c = 0$ and $g = 216$ kN have to be considered. These values have been printed in italics in the table. Among them, the value 301.2 kN, corresponding to $k = 2$, is the smallest, so that it represents the critical compressive force of the arch supported by the fabric. This is 158 times the critical force 1.9 kN of the unsupported arch. (It should be remarked that this exceptionally low value of the critical force of the unsupported arch can be explained by the fact that the central angle $2\alpha = 150.82°$ of our arch is quite close to $2\alpha = 180°$, in which case $N_{cr} = 0$, since the arch will tilt laterally like a rigid body, due to the assumed fork-like support.)

The results of Table 1 show the following interesting feature. If we denote the critical compressive force of the unsupported arch with N_{cr}^{unsupp}, the critical force N_{cr} of the elastically supported arch can approximately be given by the following formula:

$$N_{cr} \approx N_{cr}^{unsupp} + c \frac{l^2}{\pi^2 k^2} + g. \tag{13}$$

This relation can be rendered likely in the following way. In [5] we find Eq. (2–37) which shows that the critical force of a bar on an elastic foundation can be obtained by summing up the critical force of the unsupported bar and the expression $cl^2/(\pi^2 k^2)$; and [1] proves that the critical force of a bar elastically restrained against rotation along its entire length is also given by the sum of the critical force of the unsupported bar and of the modulus of elastic restraint g. In our case the phenomenon is somewhat more complicated because of the possibility of twisting deformation and of the varying position of the point of attachement C (and G) of the fabric. This is the reason why we put an "approximately equal" sign in Eq. (13). In the cases $k \geq 2$ the term containing c has to be omitted from Eq. (13).

References

1. Csonka, P.: Buckling of Bars Elastically Built-in along their Entire Length. Acta Techn. Hung. **32** (1961), 423—427
2. **Kollár, L.—Gyurkó, J.: Lateral Buckling of Elastically Supported Arches. Acta Techn. Hung., 94 (1982), 37—45**
3. Kollár, L.: The Supporting Effect of the Fabric of Tent Structures Stretched onto an Arch Row on the Lateral Buckling of the Arches. Acta Techn. Hung. **94** (1982), 197—214
4. Love, A. E. H.: A Treatise on the Mathematical Theory of Elasticity. Dover Publ., New York 1944
5. Timoshenko, S. P.—Gere, J. M.: Theory of Elastic Stability. McGraw-Hill, New York/Toronto/London 1961

BEITRAG ZU DEN METHODEN DER ÄQUIVALENTEN LINEARISIERUNG FÜR SCHWINGUNGSSYSTEME TEIL II

GY. PATKÓ*

Im ersten Teil der Arbeit wurde eine Verallgemeinerung der direkten Linearisierungsmethode von Panovko vorgestellt, und es wurde die Methode der Linearisierung über der Phasenkurve eingeführt. Auf Grund der letzten Methode wurde eine Definition des Maßes der Nichtlinearität vorgeschlagen. Im zweiten Teil der Arbeit wird die Bedeutung der Transformation der unabhängigen Variablen bei der Linearisierung über der Phasenkurve untersucht. Es wird gezeigt, daß mehrere zur Untersuchung der nichtlinearen Schwingungssysteme angewandten Methoden eine anschauliche geometrische Deutung haben.

5. Der Einfluß der Transformation der unabhängigen Variablen bei der Linearisierung über der Phasenkurve

5.1. Vor der Annäherung der Kennfläche $f(x, \dot{x})$ wurde die dimensionlose Zeit

$$\tau = \Omega t, \qquad \text{bzw.} \qquad \tau = \alpha t \qquad (5.1)$$

in den Punkten 4.1. und 4.2. eingeführt. Dadurch kann das Bogenelement auf der Phasenebene interpretiert werden. Mit der Transformation (5.1) wird die Phasenkurve auf der Phasenebene $x - x'$ ein Kreis, womit die Rechnungen bedeutend vereinfacht werden. Die Wahl der Transformationen ist aber willkürlich. Man könnte auch andere Transformationen benutzen.

5.2. In den Bewegungsgleichungen (3.1) und (3.2) wird die dimensionlose Zeit

$$\tau = vt$$

eingeführt, wobei v eine vorläufig unbekannte Konstante ist. So können die Gleichungen (3.1) und (3.2) in der Form

$$mv^2 x'' + f(x, vx') = F \cos \frac{\Omega}{v} \tau, \qquad (5.2)$$

$$mv^2 x'' + bvx' + cx + d = F \cos \frac{\Omega}{v} \tau \qquad (5.3)$$

geschrieben werden. Mit Strich ist wieder die Ableitung nach τ bezeichnet. Die

* Patkó Gyula, Középszer u. 60. IV/3. H-3529 Miskolc, Ungarn

stationären Schwingungen von (5.3) werden durch

$$x = a_0 + a_1 \cos\left(\frac{\Omega}{v}\tau - \vartheta_1\right) \tag{5.4}$$

beschrieben, wobei die Konstanten a_0, a_1, ϑ_1 bei Kenntnis von b, c und d aus den Formeln (3.4)—(3.6) berechnet werden können. Aus (5.4) ergibt sich

$$x' = -a_1 \frac{\Omega}{v} \sin\left(\frac{\Omega}{v}\tau - \vartheta_1\right). \tag{5.5}$$

Die zu (5.4) und (5.5) gehörende Phasenkurve auf der Phasenebene $x - x'$ ist eine Ellipse der Form

$$\left(\frac{x - a_0}{a_1}\right)^2 + \left(\frac{vx'}{\Omega a_1}\right)^2 = 1.$$

Der auf der Phasenkurve stehende elliptische Zylinder schneidet die Kennfläche $f(x, vx')$ in einer Raumkurve und die Ebene $bvx' + cx + d$ in einer Ellipse. Die Größen b, c und d werden jetzt so bestimmt, daß die zwischen den zwei Kurven liegende Fläche des Mantels des elliptischen Zylinders minimal wird. Deshalb wird vorgeschrieben, daß das Quadratintegral

$$J_2 = \oint_{(s)} [f(x, vx') - (bvx' + cx + d)]^2 \, ds \tag{5.6}$$

minimal sei. Es wird die Bezeichnung

$$\psi = \frac{\Omega}{v}\tau - \vartheta_1$$

eingeführt, mit der das Bogenelement der Phasenkurve nach (5.4) und (5.5) in der Form

$$ds = a_1 \frac{\Omega}{v} \sqrt{1 - \frac{\Omega^2 - v^2}{\Omega^2} \sin^2\psi} \, d\psi \tag{5.7}$$

geschrieben werden kann. Weil man bei der Minimierung des Integrals (5.6) zu elliptischen Integralen gelangt, ist es zweckmäßig, die Fälle $v < \Omega$ und $v > \Omega$ zu trennen. Mit den Bezeichnungen

$$k^2 = 1 - \left(\frac{v}{\Omega}\right)^2, \qquad p^2 = \left(\frac{v}{\Omega}\right)^2 - 1 \tag{5.8}$$

kann (5.7) in der Form

$$ds = a_1 \frac{\Omega}{v} \sqrt{1 - k^2 \sin^2\psi} \, d\psi, \qquad \text{bei} \qquad v < \Omega$$

oder

$$ds = a_1 \frac{\Omega}{v} \sqrt{1 + p^2 \sin^2 \psi}\, d\psi, \qquad \text{bei} \qquad v > \Omega$$

geschrieben werden. Auf Grund der Bedingungen

$$\frac{\partial J_2}{\partial b} = 0, \qquad \frac{\partial J_2}{\partial c} = 0, \qquad \frac{\partial J_2}{\partial d} = 0 \tag{5.9}$$

erhält man bei $v < \Omega$ die Formeln

$$b = -\frac{3}{4\Omega a_1} \frac{k^2}{(1-k^2)F(k) - (1-2k^2)E(k)} \cdot$$

$$\cdot \int_0^{2\pi} f(a_0 + a_1 \cos \psi, -a_1 \Omega \sin \psi) \sqrt{1 - k^2 \sin^2 \psi}\, \sin \psi\, d\psi, \tag{5.10}$$

$$c = \frac{3}{4a_1} \frac{k^2}{(1+k^2)E(k) - (1-k^2)F(k)} \cdot$$

$$\cdot \int_0^{2\pi} f(a_0 + a_1 \cos \psi, -a_1 \Omega \sin \psi) \sqrt{1 - k^2 \sin^2 \psi}\, \cos \psi\, d\psi, \tag{5.11}$$

$$d = -ca_0, \tag{5.12}$$

und weiterhin zwischen a_0 und a_1 die Beziehung

$$\int_0^{2\pi} f(a_0 + a_1 \cos \psi, -a_1 \Omega \sin \psi) \sqrt{1 - k^2 \sin^2 \psi}\, d\psi = 0. \tag{5.13}$$

Mit $F(k)$ und $E(k)$ sind die vollständigen elliptischen Integrale erster und zweiter Gattung vom Modul k bezeichnet.

Bei $v > \Omega$ ergeben sich aus den Bedingungen (5.9) die Formeln

$$b = -\frac{3}{4a_1\Omega} \frac{p^2}{\sqrt{1+p^2}\left[(1+2p^2)E\left(\frac{p}{\sqrt{1+p^2}}\right) - F\left(\frac{p}{\sqrt{1+p^2}}\right)\right]} \cdot$$

$$\cdot \int_0^{2\pi} f(a_0 + a_1 \cos \psi, -a_1 \Omega \sin \psi) \sqrt{1 + p^2 \sin^2 \psi}\, \sin \psi\, d\psi, \tag{5.14}$$

$$c = \frac{3}{4a_1} \frac{p^2}{\sqrt{1+p^2}\left[F\left(\frac{p}{\sqrt{1+p^2}}\right) - (1-p^2)E\left(\frac{p}{\sqrt{1+p^2}}\right)\right]} \cdot$$

$$\cdot \int_0^{2\pi} f(a_0 + a_1 \cos \psi, -a_1 \Omega \sin \psi) \sqrt{1 + p^2 \sin^2 \psi}\, \cos \psi\, d\psi, \tag{5.15}$$

$$d = -ca_0, \tag{5.16}$$

und zwischen a_0 und a_1 die Beziehung

$$\int_0^{2\pi} f(a_0 + a_1 \cos \psi, \; -a_1 \, \Omega \sin \psi) \, \sqrt{1 + p^2 \sin^2 \psi} \; d\psi = 0 \,. \tag{5.17}$$

Bei gegebenem Wert von v können die Funktionen $a_0 = a_0(a_1, \Omega)$, $b = b(a_1, \Omega)$, $c = c(a_1, \Omega)$ aus (5.10)—(5.17) berechnet werden, mit deren Hilfe die Annäherung des Amplitude-Frequenzganges und des Phasen-Frequenzganges des nichtlinearen Systems erfolgen kann.

Bei autonomen Systemen steht α anstatt Ω in den obigen Beziehungen. Stabile Grenzzykel können ähnlich zu den im Punkt 4.2. beschriebenen gesucht werden.

5.3. Der Wert von v wurde in den obigen Rechnungen als ein freier Parameter angesehen. Für ihn können weitere Vorschriften gemacht werden. Mit der Veränderung von v bei festen a_1 und Ω verändern sich der linearisierte Dämpfungswert $b(a_1, \Omega)$, Federwert $c(a_1, \Omega)$ und die Funktion $a_0 = a_0(a, \Omega)$. Wenn der Wert von v richtig gewählt wird, können die obigen Ergebnisse genauer als die des Punktes 4. sein (vgl.: Punkt 5.4.). Damit ist der Einfluß von v zu dem der in Punkt 2. und 3. erwähnten Gewichtsfunktionen ähnlich.

Die obigen Ergebnisse können offensichtlich auch durch Gewichtsfunktionen modifiziert werden. In diesem Falle werden die gewichteten Abweichungen über der Phasenkurve s minimiert, das heißt die Größen b, c und d werden aus der Bedingung

$$J = \oint_{(s)} \{[f(x, vx') - (bvx' + cx + d)] \kappa(x, x')\}^2 \, ds \overset{!}{=} \text{Minimum}$$

berechnet.

Die Ergebnisse des Punktes 5.2. können dem Gedankengang des Punktes 4.1. folgend erhalten werden, wenn dort die mit der Gewichtsfunktion

$$\kappa(x, x') = \sqrt[4]{\left[\frac{\Omega}{v}(x - a_0)\right]^2 + x'^2} \tag{5.18}$$

gewichteten Abweichungen über dem Kreis mit dem Radius a_1 und dem Mittelpunkt $(a_0, 0)$ minimiert werden. Zur Frage, wie der Wert von v richtig gewählt werden muß, geben die obigen Darlegungen keine Antwort. Die im Punkt 4. gewählten Werte $v = \Omega$ und $v = \alpha$ haben die Rechnungen bedeutend vereinfacht. Diese einfache Durchführbarkeit der Rechnungen kann einer der Gesichtspunkte sein.

5.4. Als Beispiel wird die Lösung der Bewegungsgleichung

$$\ddot{x} + \alpha_0^2 x + \varepsilon x^3 = 0 \tag{5.19}$$

durch die der linearen Differentialgleichung mit konstanten Koeffizienten

$$\ddot{x} + b\dot{x} + cx + d = 0 \tag{5.20}$$

angenähert.

Hier ist $f(x, \dot{x}) = \alpha_0^2 x + \varepsilon x^3$, das heißt sie hängt von $\dot{x}$ nicht ab. $a_0 = 0$ ist eine Lösung von (5.13) und (5.17), und das bedeutet, daß die maximalen Auslenkungen zum Koordinatenursprung symmetrisch sind und $d = 0$.

Im Falle $b = 0$ ist die allgemeine Lösung von (5.20)

$$x = a_1 \cos(\alpha t - \vartheta_1) \qquad (5.21)$$

wobei $\alpha = \sqrt{c}$ ist und a_1, ϑ_1 die von den Anfangsbedingungen abhängigen Konstanten sind. Es wird die dimensionslose Zeit $\tau = vt$ eingeführt und die Ableitung nach τ wieder mit Strich bezeichnet. So können die Differentialgleichungen in der Form

$$v^2 x'' + \alpha_0^2 x + \varepsilon x^3 = 0, \qquad (5.22)$$

$$v^2 x'' + bvx' + cx = 0 \qquad (5.23)$$

geschrieben werden. (5.21) hat die Form

$$x = a_1 \cos\left(\frac{\alpha}{v}\tau - \vartheta_1\right), \qquad (5.24)$$

aus der man

$$x' = -a_1 \frac{\alpha}{v} \sin\left(\frac{\alpha}{v}\tau - \vartheta_1\right) \qquad (5.25)$$

erhält. Es werden wiederum die Abkürzungen

$$\psi = \frac{\alpha}{v}\tau - \vartheta_1, \qquad k^2 = 1 - \left(\frac{v}{\alpha}\right)^2, \qquad p^2 = \left(\frac{v}{\alpha}\right)^2 - 1 \qquad (5.26)$$

eingeführt. Weil hier autonome Systeme untersucht werden, tritt in (5.10)—(5.17) α an die Stelle von Ω und die Phasenkurve s ist durch (5.24), (5.25) bestimmt. Nach (5.10) und (5.14) erhält man $b \equiv 0$, was ein offensichtliches Ergebnis ist, weil durch (5.19) ein konservatives System beschrieben wird. Man erhält nach [19] bei $v < \alpha$ aus (5.11)

$$c = \alpha_0^2 + \varepsilon a_1^2 \frac{2(1-k^2)(1-3k^2)F(k) + (3k^4 + 7k^2 - 2)E(k)}{5k^2[(1+k^2)E(k) - (1-k^2)F(k)]} \qquad (5.27)$$

und bei $v > \alpha$ aus (5.15)

$$c = \alpha_0^2 + \varepsilon a_1^2 \frac{2(1+3p^2)F\left(\dfrac{p}{\sqrt{1+p^2}}\right) + (3p^4 - 7p^2 - 2)E\left(\dfrac{p}{\sqrt{1+p^2}}\right)}{5p^2\left[F\left(\dfrac{p}{\sqrt{1+p^2}}\right) - (1-p^2)E\left(\dfrac{p}{\sqrt{1+p^2}}\right)\right]}. \qquad (5.28)$$

Wenn man letzte Formeln zusammenfaßt, dann kann

$$\alpha^2 = \alpha_0^2 + \varepsilon a_1^2 H\left(\frac{v}{\alpha}\right) \qquad (5.29)$$

für die Näherung des Quadrates der Eigenkreisfrequenz α geschrieben werden. Die Bedeutung von $H(v/\alpha)$ is aus (5.26)—(5.29) ersichtlich. Die Funktion $H(v/\alpha)$ ist im Bild 7. dargestellt. Weil der Wert von v nicht festgelegt wurde, kann man für ihn weitere Vorschriften machen. Er kann beispielsweise so gewählt werden, daß die beste Annäherung für die Eigenkreisfrequenz α durch (5.29) erhalten wird.

Zum Beispiel ergibt sich

$$\alpha^2 = 0,75 \ \varepsilon a_1^2$$

aus (5.29) im Falle $\alpha_0^2 = 0$ und bei der Wahl $v/\alpha = 1$. Die Bewegungsgleichung (5.19) kann auch exakt gelöst werden, wobei man **bei $\alpha_0 = 0$, den Wert**

$$\alpha^2 = 0,7178 \ \varepsilon a_1^2 \tag{5.30}$$

erhält (vgl.: [2], S. 85.). Falls die obige Näherung angewandt wird, so ergibt sich das Ergebnis (5.30) bei der Wahl $(v/\alpha) = 1,5629$.

Es ist ersichtlich, daß die Rechnungen durch die Transformationen (5.1) der unabhängigen Variable wesentlich vereinfacht werden. Auf Grund von Punkt 5.2. kann man mit erhöhtem Aufwand genauere Ergebnisse erhalten, aber zur richtigen **Wahl von v** ist entsprechende Erfahrung nötig.

5.5. Die in Punkt 5.4. behandelte Aufgabe kann auch mit Hilfe der Gewichtsfunktion

$$\kappa(x, x') = \sqrt{\left[\frac{\alpha}{v}(x - a_0)\right]^2 + x'^2} \ ,$$
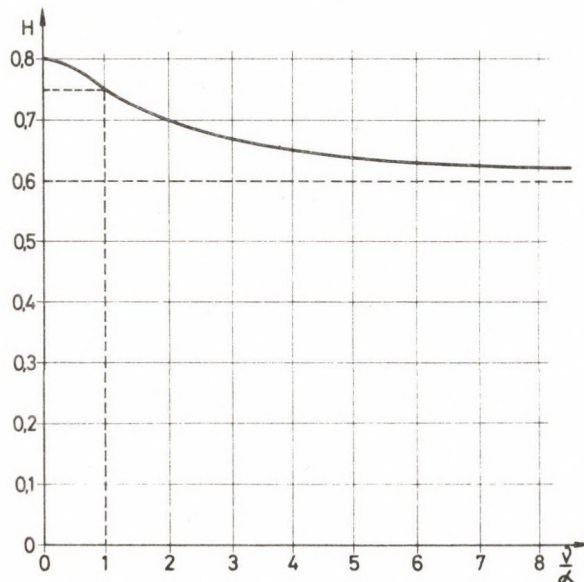

Bild 7

die einfacher als (5.18) ist, dem Gedankengang von 4.2. folgend, gelöst werden. So erhält man nach einfachen Rechnungen

$$\alpha^2 = \alpha_0^2 + \varepsilon a_1^2 \frac{5 + \dfrac{v^2}{\alpha^2}}{2\left(3 + \dfrac{v^2}{\alpha^2}\right)}.$$

Die Beziehung (5.30), die für $\alpha_0 = 0$ als genau angenommen werden kann, ergibt sich hier bei der Wahl $v/\alpha = 1,2619$.

6. Vergleich der Linearisierung über der Phasenkurve mit anderen Methoden

6.1. Im Laufe der Zeit wurden qualitative Methoden entwickelt, die — oder deren Varianten — im Wesentlichen gleichwertige Ergebnisse liefern. Sie können in zwei Gruppen aufgeteilt werden.

Zu einer dieser Gruppen gehören die Methoden, die von einer dierekten Linearisierung ausgehen. Der Zweck ist, die nichtlineare Differentialgleichung irgendwie durch eine lineare zu ersetzten. Solche Methoden sind die direkte Linearisierungsmethode von Panovko [15], die Methode der harmonischen Linearisierung [18], die äquivalente bzw. optimale Linearisierung [4—6] usw. Zu dieser Gruppe gehört auch die Methode der Linearisierung über der Phasenkurve.

Die zu der anderen Gruppe gehörenden analytischen Methoden haben zum Ziel, Näherungen höherer Ordnung herzustellen. Solche Methoden sind die Methode von Bubnow—Galerkin, die Methode der harmonischen Balance [16], die Methode der Störungsrechnung von Poincaré [11], die asymptotische Methode von Krylow—Bogoljubow [20] usw. Der erste Schritt dieser Methoden kann — wie es in der Literatur üblich ist — so konstruiert werden, daß die durch sie erhaltenen Ergebnisse mit den der zur ersten Gruppe gehörenden Methoden identisch oder näherungsweise gleich sind. Die Operationen dieser ersten Schritte sind, wie es von Fall zu Fall überprüft werden kann (vgl.: Punkt 6.4.), mit einer Linearisierung äquivalent.

Auf Grund des obigen besteht die Bedeutung der Linearisierung über der Phasenkurve darin, daß

— sie mehreren zur ersten Gruppe der obigen Einteilung gehörenden Methoden eine anschauliche geometrische Deutung gibt,

— durch sie eine anschauliche geometrische Deutung für den ersten Schritt der zur zweiten Gruppe gehörenden Methoden gegeben werden kann.

In den Punkten 6.2. und 6.4. wird beispielsweise je eine Methode beider Gruppen der obigen Einteilung mit der Linearisierung über der Phasenkurve gegenübergestellt.

6.2. Die Methode der harmonischen Linearisierung wird zur Lösung von zahlreichen Aufgaben mit Erfolg angewandt (vgl.: z. B. [18]). Sie ist ein Sonderfall der

Methode der harmonischen Balance, und daraus kann sie folgenderweise abgeleitet werden.

Durch die harmonische Balance wird die periodische Lösung z. B. der Bewegungsgleichung

$$m\ddot{x} + f(x, \dot{x}) = F \cos \Omega t \tag{6.1}$$

in der Form

$$x = A_0 + \sum_{n=1}^{\infty} (A_n \cos n\Omega t + B_n \sin n\Omega t) \tag{6.2}$$

gesucht. Die Beziehung (6.2) wird in (6.1) eingesetzt. Die Funktion $f(x, \dot{x})$ wird in eine Fourier-Reihe entwickelt, und in (6.1) wird die Gleichheit der Koeffizienten der einzelnen harmonischen Glieder vorgeschrieben. So erhält man zur Bestimmung der Koeffizienten A_0, A_n, B_n ($n = 1, 2, \ldots$) ein nichtlineares algebraisches Gleichungssystem, dessen Lösung bei unendlich vielen Unbekannten unmöglich ist. In der Praxis wird deswegen nur ein Abschnitt der Reihe (6.2) angewandt.

Eine Näherung der Lösung von (6.1) wird in der Form

$$x = A_0 + A_1 \cos \Omega t + B_1 \sin \Omega t \tag{6.3}$$

gesucht. Es ist zweckmäßig (6.3) in die Form

$$x = a_0 + a_1 \cos \psi \tag{6.4}$$

zu schreiben, wobei die trigonometrischen Funktionen zu einer Schwingung umgeformt wurden und die früher angewandte Abkürzung $\psi = \Omega t - \vartheta_1$ und $a_0 = A_0$ eingeführt ist. Die Näherung (6.4) wird in (6.1) eingesetzt und die Funktion $f(x, \dot{x})$ in die Fourier-Reihe

$$f(a_0 + a_1 \cos \psi, -a_1 \Omega \sin \psi) = c_0 + c_1 \cos \psi + b_1 \sin \psi + \ldots \tag{6.5}$$

entwickelt, deren Koeffizienten aus den Formeln

$$c_0 = \frac{1}{2\pi} \int_0^{2\pi} f(a_0 + a_1 \cos \psi, -a_1 \Omega \sin \psi) \, d\psi \,, \tag{6.6}$$

$$c_1 = \frac{1}{\pi} \int_0^{2\pi} f(a_0 + a_1 \cos \psi, -a_1 \Omega \sin \psi) \cos \psi \, d\psi \,, \tag{6.7}$$

$$b_1 = \frac{1}{\pi} \int_0^{2\pi} f(a_0 + a_1 \cos \psi, -a_1 \Omega \sin \psi) \sin \psi \, d\psi \,, \tag{6.8}$$

berechnet werden können. Analog zu (6.3) bzw. (6.4) werden hier nur Glieder bis zur zweiten Harmonischen der Fourier-Reihe mitgenommen. So ergibt sich aus (6.1)

$$-m\Omega^2 a_1 \cos \psi + c_0 + c_1 \cos \psi + b_1 \sin \psi = F \cos (\psi + \vartheta_1) \,. \tag{6.9}$$

Die Größen a_0, a_1, ϑ_1 können aus (6.9) auf Grund der Gleichheit der einzelnen Harmonischen berechnet werden. Mit den Bezeichnungen

$$b = -\frac{b_1}{a_1 \Omega}, \qquad c = \frac{c_1}{a_1}, \qquad d = c_0 - c a_0 \qquad (6.10)$$

hat (6.9) die Form

$$-m\Omega^2 a_1 \cos \psi + c(a_0 + a_1 \cos \psi) - b a_1 \Omega \sin \psi + d = F \cos (\psi + \vartheta_1), \qquad (6.11)$$

aus der sich die Formeln (3.4)—(3.6) für die Größen a_0, a_1, ϑ_1 ergeben. Es ist leicht einzusehen, daß man auch dann zur Gleichung (6.11) gelangt, falls die periodische Lösung der Form (6.4) der linearen Differentialgleichung

$$m\ddot{x} + b\dot{x} + cx + d = F \cos \Omega t \qquad (6.12)$$

anstatt der von (6.1) gesucht wird, wobei die Größen b, c, d in (6.12) durch (6.10) und (6.6)—(6.8) definiert sind.

Jeder nichtlinearen Differentialgleichung der Form von (6.1) kann eine lineare Differentialgleichung der Form von (6.12) so zugeordnet werden, daß ihre in der Form (6.4) gesuchten Lösungen übereinstimmen. (6.12) wird als die zu (6.1) gehörende harmonisch linearisierte Differentialgleichung bezeichnet. Die Methode, mit Hilfe deren man von (6.1) ausgehend zu (6.12) gelangt, heißt die Methode der harmonischen Linearisierung.

Die durch die Beziehungen (6.10) und (6.6)—(6.8) definierten Größen b, c und d stimmen mit den Ergebnissen (4.5)—(4.7) überein. Die durch die obige harmonische Linearisierung erhaltenen Ergebnisse sind mit denen durch Linearisierung über die Phasenkurve in Punkt 4.1. erhaltenen identisch. Im Zusammenhang mit dem in Punkt 6.1. gesagten kann also diese Variante der Methode der Linearisierung über der Phasenkurve, die im Punkt 4.1. beschrieben ist, auch als eine geometrische Deutung der oben beschriebenen Methode der harmonischen Linearisierung aufgefaßt werden.

6.3. Auf ähnliche Weise kann gezeigt werden, daß die Methoden der optimalen Linearisierung [4], bzw. der äquivalenten Linearisierung [5], [6] auch anschauliche geometrische Deutungen haben.

6.4. Im folgenden wird die erste Näherung der asymptotischen Methode von Krylow—Bogoljubow [20] untersucht.

6.4.1. Bei dieser Methode wird angenommen, daß die Funktion $f(x, \dot{x})$ schwach nichtlinear ist, das heißt sie in der Form

$$f(x, \dot{x}) = kx + \varepsilon g(x, \dot{x}) \qquad (6.13)$$

geschrieben werden kann, wobei $k > 0$ und ε ein kleiner Parameter ist. Im autonomen Falle kann also

$$m\ddot{x} + kx + \varepsilon g(x, \dot{x}) = 0 \qquad (6.14)$$

anstatt (4.9) geschrieben werden. Mit den Bezeichnungen

$$\frac{k}{m} = \omega^2 \quad \text{und} \quad \frac{g(x, \dot{x})}{m} = f_1(x, \dot{x}) \tag{6.15}$$

hat (6.14) die Form

$$\ddot{x} + \omega^2 x + \varepsilon f_1(x, \dot{x}) = 0 . \tag{6.16}$$

Aus (6.16) ist ersichtlich, daß ω die Eigenkreisfrequenz des bei $\varepsilon = 0$ erhaltenen linearen Systems ist.

In erster Näherung wird die Lösung von (6.16) in der Form

$$x = a \cos \psi$$

gesucht, wobei a und ψ aus den Differentialgleichungen

$$\frac{da}{dt} = \frac{\varepsilon}{2\pi\omega} \int_0^{2\pi} f_1(a \cos \psi, -a\omega \sin \psi) \sin \psi \, d\psi ,$$

$$\frac{d\psi}{dt} = \omega + \frac{\varepsilon}{2\pi a\omega} \int_0^{2\pi} f_1(a \cos \psi, -a\omega \sin \psi) \cos \psi \, d\psi$$

berechnet werden können (vgl.: [20], S. 51.).

Im weiteren werden nur die stationären Schwingungen untersucht. Dabei bestehen die Gleichungen $da/dt = 0$ bzw. $d\psi/dt = \alpha$ und es können die Schwingungsamplitude aus

$$0 = \int_0^{2\pi} f_1(a \cos \psi, -a\omega \sin \psi) \sin \psi \, d\psi \tag{6.17}$$

sowie die Eigenkreisfrequenz der Schwingungen aus

$$\alpha = \omega + \frac{\varepsilon}{2\pi a\omega} \int_0^{2\pi} f_1(a \cos \psi, -a\omega \sin \psi) \cos \psi \, d\psi \tag{6.18}$$

berechnet werden. Mit Vernachlässigung von ε^2 ergibt sich aus (6.18)

$$\alpha^2 = \omega^2 + \frac{\varepsilon}{\pi a} \int_0^{2\pi} f_1(a \cos \psi, -a\omega \sin \psi) \cos \psi \, d\psi . \tag{6.19}$$

Mit Rücksicht auf (6.13) und (6.15) können (6.17) und (6.19) in der Form

$$0 = \int_0^{2\pi} f(a \cos \psi, -a\omega \sin \psi) \sin \psi \, d\psi , \tag{6.20}$$

$$m\alpha^2 = \frac{1}{\pi a} \int_0^{2\pi} f(a \cos \psi, -a\omega \sin \psi) \cos \psi \, d\psi \tag{6.21}$$

geschrieben werden. Die Gleichungen (6.20) und (6.21) sind ähnlich zu den in Punkt 4.2. erhaltenen Ergebnissen. Falls (4.25) für die Funktion $f(x, \dot{x})$ gültig ist, das heißt $a_0 = 0$, dann können (4.24) und (4.23) aus (6.20) und (6.21) so erhalten werden, daß man in den rechten Seiten der letzten Gleichungen a_1 anstatt a und α anstatt ω schreibt.

6.4.2. In [20] (S. 109.) wird gezeigt, daß die Ergebnisse der ersten Näherung auch so erhalten werden können, daß die äquivalente lineare Differentialgleichung

$$m\ddot{x} + \lambda_e(a)\dot{x} + k_e(a)x = 0 \tag{6.22}$$

anstatt (6.14) gelöst wird, wobei die Größen $\lambda_e(a)$ und $k_e(a)$ aus den Formeln

$$\lambda_e(a) = -\frac{\varepsilon}{\pi a \omega} \cdot \int_0^{2\pi} g(a \cos \psi, -a\omega \sin \psi) \sin \psi \, d\psi \,,$$

$$k_e(a) = k + \frac{\varepsilon}{\pi a} \int_0^{2\pi} g(a \cos \psi, -a\omega \sin \psi) \cos \psi \, d\psi$$

berechnet werden können. Letztere können mit (6.13) in der Form

$$\lambda_e(a) = -\frac{1}{\pi a \omega} \int_0^{2\pi} f(a \cos \psi, -a\omega \sin \psi) \sin \psi \, d\psi \tag{6.23}$$

$$k_e(a) = \frac{1}{\pi a} \int_0^{2\pi} f(a \cos \psi, -a\omega \sin \psi) \cos \psi \, d\psi \tag{6.24}$$

geschrieben werden. Bei $a_0 = 0$ unterscheiden sich die linearisierten Feder- und Dämpfungswerte (6.23) und (6.24) von den aus (4.19) und (4.20) berechneten dadurch, daß in den letzten die Eigenkreisfrequenz ω des zu $\varepsilon = 0$ gehörenden linearen Systems anstatt der Eigenkreisfrequenz α des nichtlinearen Systems und a anstatt a_1 stehen.

6.4.3. Die obigen Ergebnisse der asymptotischen Methode können, dem Gedankengang des Punktes 4.2. folgend, auch durch geometrische Überlegungen erhalten werden. In den Differentialgleichungen (6.14) und (6.22) wird die dimensionlose Zeit $\tau = \omega t$ eingeführt, wobei $\omega = \sqrt{k/m}$. So können (6.14) und (6.22) in der Form

$$m\omega^2 x'' + kx + \varepsilon g(x, \omega x') = 0 \,, \tag{6.25}$$

$$m\omega^2 x'' + \lambda_e \omega x' + k_e x = 0 \tag{6.26}$$

geschrieben werden (mit Strich ist wieder die Ableitung nach τ bezeichet). Im Falle $\varepsilon = 0$ hat die Lösung (6.25) die Form

$$x = a \cos(\tau - \vartheta_1) \tag{6.27}$$

wobei a und ϑ_1 die von den Anfangswerten abhängigen Konstanten sind. Aus (6.27) folgt

$$x' = -a \sin(\tau - \vartheta_1). \qquad (6.28)$$

Auf der Phasenebene (x, x') ist die zu (6.27) und (6.28) gehörende Phasenkurve s ein Kreis mit dem Radius a. Der auf der Phasenkurve stehende Kreiszylinder schneidet die Fläche $f(x, \omega x') = kx + \varepsilon g(x, \omega x')$ in einer Raumkurve und die Ebene $\lambda_e \omega x' + k_e x$ in einer Ellipse. Die Größen λ_e und k_e werden so gewählt, daß die zwischen den zwei Kurven liegende Fläche des Mantels des Zylinders klein ist. Auf Grund der Bedingung

$$\oint_{(s)} [f(x, \omega x') - (\lambda_e \omega x' + k_e x)]^2 ds = \text{Minimum}$$

erhält man für die Größen λ_e und k_e die Beziehungen (6.23) und (6.24).

Diese Überlegungen geben der asymptotischen Methode von Krylow— Bogoljubow eine anschauliche geometrische Deutung.

Der Vergleich des obigen mit dem Punkt 4.2. macht klar, daß grundsätzliche Unterschiede zwischen der ersten Näherung der asymptotischen Methode von Krylow—Bogoljubow und der im Punkt 4.2. beschriebenen Methode der Linearisierung über der Phasenkurve (und der Methoden, die damit äquivalente Ergebnisse liefern) bestehen. Sie gründen sich darauf, daß die Transformation von $\tau = \alpha t$ in einem Falle und die von $\tau = \omega t$ im anderen Falle angewandt wird, und dementsprechend die Schwingungen mit der Kreisfrequenz ω in einem Falle und mit der Kreisfrequenz α im anderen Falle zur Bestimmung der äquivalenten Ausgleichsebene zugrunde gelegt werden.

Auch bei den höheren Näherungen der asymptotischen Methode von Krylow— Bogoljubow werden die Werte der nichtlinearen Funktion und ihrer Ableitungen berücksichtigt, die auf einer Phasenkurve der Form von (6.27), (6.28) lokalisiert sind. Diese Phasenkurve ist auch bei den höheren Näherungen ein Kreis mit einem Radius a.

In der Praxis kommt es vor, daß die Funktion $f(x, \dot{x})$ in der Form von (6.13) nicht aufgespalten werden kann, weil der Wert von k nicht eindeutig bestimmbar ist. In diesem Falle schlagen mehrere Verfasser vor (vgl.: z. B. [18], S. 142.), die Grundgedanken der asymptotischen Methoden bei der Wahl $\omega = \alpha$ anzuwenden. Es ist leicht einzusehen, daß die durch die erste Näherung der Methode von Krylow—Bogoljubow erhaltenen Ergebnisse im Falle $a_0 = 0$ mit den Ergebnissen des Punktes 4.2. übereinstimmen.

Hier sei es nur erwähnt, daß die Gegenüberstellung der Ergebnissen des Punktes 4.1. und der Methode von Krylow—Bogoljubow bei harmonisch erregten Schwingungen zu den obigen ähnlichen Schlußfolgerungen führen.

6.5. Es ist noch bemerkenswert, daß die Methode von Poincaré und die Methode der harmonischen Linearisierung (vgl.: [9], S. 102.) sowie die Methode von Poincaré und die Methode von Krylow—Bogoljubow (vgl.: [24]) in speziellen Fällen gleiche Ergebnisse liefern. So kann eine anschauliche geometrische Deutung, ähnlich wie es in

den Punkten 6.2. und 6.4. gemacht wurde, auch für den ersten Schritt der Methode von Poincaré gegeben werden.

6.6. Oben wurde gezeigt, daß verschiedene Näherungsmethoden existieren, die mit der Methode der Linearisierung über der Phasenkurve gleichwertige Ergebnisse liefern. Mann kann erwarten, daß durch diese Näherungen umso bessere Ergebnisse erhalten werden können, je genauer die Raumkurve, die aus der Kennfläche $f(x, \dot{x})$ durch einen Zylinder ausgeschnitten wird, durch eine Ellipse approximiert werden kann (vgl.: Bilder 3 und 5). Üblicherweise wird angenommen, daß diese Bedingung bei kleinem Wert von ε im allgemeinen erfüllt wird. Auf Grund der obigen geometrischen Überlegungen scheint es naheliegend zu sein, daß man sich in Abhängigkeit von der Form der Kennfläche nicht auf kleine Werte von ε beschränken muß. Es kann vorkommen, daß die Methoden, bei denen angenommen wird, daß die nichtlineare Funktion einen kleinen Parameter enthält, in erster Näherung bei großem Wert des kleinen Parameters gute Annäherungen liefern.

7. Schlußfolgerungen

7.1. Der Grundgedanke der direkten Linearisierungsmethode von Panovko kann bei allgemeiner Nichtlinearität von der Form $f(x, \dot{x})$ angewandt werden. Dabei wird die Kennfläche $f(x, \dot{x})$ durch eine Ebene $b\dot{x} + cx + d$ über irgendeinem Gebiet der Phasenebene $(x, \dot{x})$ angenähert. Dieses Gebiet kann auf verschiedene Weise gewählt werden. Bei geeigneter Wahl des Gebietes und der Gewichtsfunktion können die von Panovko gewonnenen Ergebnisse als Spezialfälle erhalten werden.

7.2. Äquivalent lineare Schwingungssysteme können einem anderen Gedankengang folgend, der sich von den bisher angewandten, unterscheidet, erhalten werden. Auch in diesem Falle wird eine lineare Bewegungsgleichung der nichtlinearen zugeordnet. Ihre Koeffizienten werden aber so bestimmt, daß die Abweichungen zwischen der nichtlinearen Funktion und der Näherungsebene über der Phasenkurve der Näherungslösung minimal sind. Die Minimierung der Abweichungen über der Phasenkurve kann auf verschiedene Weise erfolgen. Eine mögliche Variante wird in den Punkten 4. und 5. eingehend dargestellt. Hier wird das Quadratintegral der Abweichungen über der Phasenkurve minimiert. Zur Interpretation des Bogenelements wird eine Transformation in der Phasenebene benötigt. Diese Transformation kann auf verschiedene Weise gewählt werden.

7.3. Nach der Linearisierung über der Phasenkurve kann der relative Fehler des quadratischen Integralmittelwertes berechnet werden. Die Größe des relativen Fehlers ist für das Maß der Nichtlinearität kennzeichnend. Die Definition dieses Maßes der Nichtlinearität (4.30) ist allgemeiner anwendbar als die bisher aus der Literatur bekannten.

7.4. Auf Grund der Linearisierung über der Phasenkurve kann eine anschauliche geometrische Deutung für mehrere in der Untersuchung der nichtlinearen Systeme häufig angewandten Methoden gegeben werden.

Literatur

1. Panovko, Ya. G.: A review of applications of the method of direct linearization, *Appl. Mech. Proc., XI. Int. Congr. Appl. Mech.*, Munich, 1964, 167—171
2. Panovko, Ya. G.: Elements of the applied theory of elastic vibration, Mir, Moscow, 1971
3. Bapat, V. A.—Srinivasan, P.: Effect of static deflection on natural frequency of non-linear spring mass system by direct linearisation method, *Journal of Sound and Vibration*, (1969), **10**, (3), 443—454
4. Blaquière, A.: Une nouvelle méthode de linéarisation locale des opérateurs non-linéaires: approximation optimale. *2-nd Conf. Nonlinear Vibrations* (Warsaw, 1962), Warsaw, 1964
5. Iwan, W.: On defining equivalent systems for certain ordinary nonlinear differential equations, *Int. J. Non-Linear Mechanics*, **4** (1969), 325—334
6. Spanos, P.—Iwan, W.: Harmonic analysis of dynamic systems with non-symmetric nonlinearities, *J. Dynamic Systems, Measurement Control*, **101**, (1979), 31—36
7. Iwan, W.—Patula, E. J.: The merit of different error minimization criteria in approximate analysis, *Journal of Applied Mechanics*, **39** (1972), 257—262
8. Iwan, W.—Patula, E. J.: On the validity of equation difference minimization techniques, *Int. J. Non-Linear Mechanics*, **7**. (1972), 1—17
9. Lurje, A. I.: Einige nichtlineare Probleme aus der Theorie der selbsttätigen Regelung, Akademie Verlag, Berlin 1957
10. Weigand, A.: Einführung in die Berechnung mechanischer Schwingungen, Band I. VEB Verlag Technik, Berlin 1959
11. Andronov, A. A.—Witt, S. E.—Chaikin, S. E.: Theorie der Schwingungen, Teil II. Akademie Verlag, Berlin, 1962
12. Forbat, N.: Analytische Mechanik der Schwingungen, VEB Deutscher Verlag der Wissenschaften, Berlin 1966
13. Sagirow, P.: Zur Frage der Fehlerabschätzung beim Verfahren der Harmonischen Balance, *Zeitschrift für Angewandte Mathematik und Mechanik* **40** (1960), 451—453
14. Urabe, M.: Galerkin's procedure for nonlinear periodic systems, *Archives for Rational Mechanics and Analysis*, **20** (1965), 120—152
15. Пановко, Я. Г.: Способ прямой линеаризации в нелинейных задачах теории упругих колебаний, *Инженерный сборник*, том **XIII.** (1952), 113—122
16. Вибрации в технике, Справочник в 6. томах, том 2.: Блехман, И. И.: Колебания нелинейных механических систем, Машиностроение, Москва 1979
17. Вибрации в технике, Справочник в 6. томах, том. 3.: Диментберг, Ф. М.—Колесников, К. С.: Колебания машин конструкций и их элементов, Машиностроение, Москва 1980
18. Попов, Е. П.—Пальтов, И. П.: Приближенные методы исследования нелинейных автоматических систем, Физматгиз, Москва 1960
19. Градштейн, И. С.—Рыжик, И. М.: Таблицы интегралов, сумм, рядов и произведений, Физматгиз, Москва 1963
20. **Боголюбов, Н. Н. Митропольский, Ю. А.: Асимптотические методы в теории нелинейных колебаний, Наука, Москва 1974**
21. Розенвассер, Е. Н.: Колебания нелинейных систем, Наука, Москва 1969
22. Лойцянский, Л. Г.: Свободные и вынуждённые колебания при наличии квадратического и промежуточного между линейным и квадратичным законов сопротивления, *Инженерный сборник*, том **XVIII.** (1954), 139—148
23. Карабан, В. Н. Дубовицкий, А. Ю.: О способах линеаризации при расчетах свободных колебаний нелинейных систем, В. кн.: *Теория механизмов и машин*, вып. **23**. Харьков, Высшая школа, (1977), 35—39

24. Проскуряков, А. П.: Сравнение периодических решений квазилинейных систем, построенных методом Пуанкаре и методом Крылова—Боголюбова, *Прикладная математика и механика*, **28.** вып. 4. (1964), 765—770

25. Гарбер, Е. Д.: Оценка погрешности метода гармонического баланса, *Автоматика и телемеханика*, Том **XXIV** (1963), 482—492

Contribution to the Construction of the Equivalent Linear Vibrating Systems, Part II. In the first part of the paper a generalization of the Panovko type direct linearization and the introduction of a linearization method above the phase curve were shown. According to the latest a proposal was given to a definition of a measure of non-linearity. In the second part of the paper the character of transformation of the independent variable is analysed in the case of linearization above the phase curve. It is shown, there are several methods for the analysis of non-linear oscillations having clear geometrical meaning.

THE LEANING OF THE PISA TOWER
AND THE GEOHYDROLOGY OF THE AREA

L. RÉTHÁTI*

[Received 29 November, 1982]

The author aimed at finding a correlation between the movement of the tower and the geohydrological characteristics of its environment. He has been trusted with it by the jury for the tender to save the tower, as a relationship of this kind could be supposed to exist.

1. Arrangement of the available data

The calculations were based on time series comprising:

— the inclination of the tower (in s),
— the piezometric level of the deep groundwater,
— the monthly precipitations,

in the years 1967 to 1975 (later to 1977).

The results of the measurements were made available by the "*Commissione per il consolidamento della torre di Pisa*" in diagrammatic form.

First, the data deviating greatly from neighboring values had to be eliminated. These were found to be the following: among the inclination values January 23, 1971 and August 19, 1971; among the piezometric levels August 7 and 20, 1971. This correction was needed because these values would distort the mathematical relationships although they have no technical importance. In the series of the piezometric levels, in addition, twelve missing linear interpolation.

For the purpose of the numerical calculations tables have been worked out which contained the respective values for the days 1., 3., . . ., 29. of the calendar months. The monthly mean values and the monthly precipitation are given in Tables 1–3. (Here and in what follows, the inclination values have the dimension of 0.1 s, the piezometric levels are given in cm, the precipitation in mm.)

The calculated statistical characteristics are presented in the following table.

Denomination	Symbol	Dimension	Mean value	Standard deviation σ
Inclination	α	0.1 s	3705.3	256.6
Piezometric level	W	cm	366.1	142.0
Monthly precipitation	P_m	mm	872	52.6

* Dr. L. RÉTHÁTI, Ráday u. 43., H-1092, Budapest, Hungary

Table 1. Monthly averages of inclination and of piezometric levels. Inclination ($\bar{\alpha}_m$, 0.1 s)

Month	1967	1968	1969	1970	1971	1972	1973	1974	1975	Mean
I.	3376	3440	3500	3556	3604	3715	3803	4015	4130	3682.0
II.	3371	3439	3507	3551	3592	3718	3806	4022	4131	3681.9
III.	3364	3427	3504	3546	3602	3707	3804	4016	4129	3677.7
IV.	3366	3417	3496	3539	3605	3709	3818	4028	4133	3679.1
V.	3372	3438	3500	3545	3614	3722	3831	4049	4131	3689.1
VI.	3386	3449	3513	3556	3638	3734	3854	4058	4148	3703.9
VII.	3389	3465	3510	3566	3632	3741	3884	4066	4146	3710.9
VIII.	3386	3465	3515	3557	3627	3742	3889	4054	4154	3709.7
IX.	3393	3463	3501	3548	3637	3750	3909	4057	4152	3712.1
X.	3384	3454	3478	3541	3629	3746	3945	4094	4153	3713.7
XI.	3404	3482	3522	3574	3663	3773	3967	4112	4173	3741.3
XII.	3424	3492	3547	3589	3694	3796	4001	4123	4191	3761.9
Mean	3385	3452	3508	3556	3628	3738	3876	4058	4146	3705.3

Table 2. Piezometric level ($\bar{W}_m$, cm)

Month	1967	1968	1969	1970	1971	1972	1973	1974	1975	Mean
I.	196	229	203	147	284	447	435	494	346	308.9
II.	174	224	184	189	293	435	443	512	314	307.9
III.	177	231	194	215	282	431	490	505	299	313.7
IV.	195	214	198	223	293	412	513	520	297	318.5
V.	208	231	204	246	310	486	516	507	305	334.9
VI.	219	256	228	264	311	514	559	552	344	360.8
VII.	303	338	280	310	379	549	687	631	415	431.3
VIII.	320	357	309	354	484	569	673	645	431	460.3
IX.	271	305	266	345	505	561	708	608	358	436.2
X.	238	281	225	325	491	535	642	575	327	404.4
XI.	240	260	190	310	470	486	595	520	293	373.7
XII.	240	236	155	291	467	461	526	428	283	343.1
Mean	232	263	220	268	381	491	566	541	334	366.1

Table 3. Precipitation (P_m, mm)

| Month	1967	1968	1969	1970	1971	1972	1973	1974	1975	Mean
I.	33	60	119	193	81	96	45	56	68	83.4
II.	60	221	116	81	60	87	52	85	41	89.2
III.	69	30	110	123	70	63	17	85	105	74.7
IV.	25	56	31	27	44	88	50	79	76	52.9
V.	57	91	61	37	160	38	24	61	67	66.2
VI.	100	38	32	60	76	37	58	25	94	57.8
VII.	0	5	17	25	20	29	15	11	13	15.0
VIII.	26	100	26	100	5	28	46	76	158	62.8
IX.	291	54	104	0	45	74	254	55	70	105.2
X.	68	75	10	27	50	79	127	90	108	70.4
XI.	121	120	251	75	162	73	66	77	160	122.8
XII.	120	86	86	78	38	53	40	18	124	71.4
$\Sigma =$	970	936	963	826	811	745	794	718	1084	872
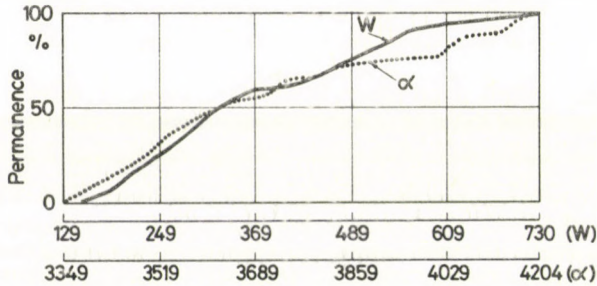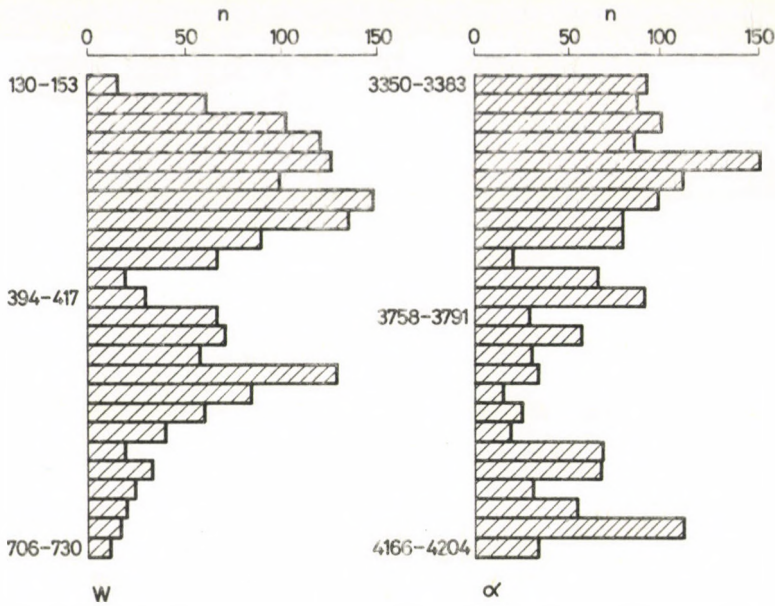
Fig. 1.

The original tables contain each 1620 values of α and W. Hystograms and empirical distribution diagrams, presented on Fig. 1, served to investigate the statistical character of the time series.

2. Analysis of the curves of averages

Figure 2 shows the curves of the yearly averages of W, α and P. The points on the first two diagrams furnish the mean values of the data for January, 1, 3 . . . December 27, 29 for nine years, (1967 to 1975) the third diagram gives the mean monthly precipitations for the same years. The curves can be valued as follows.
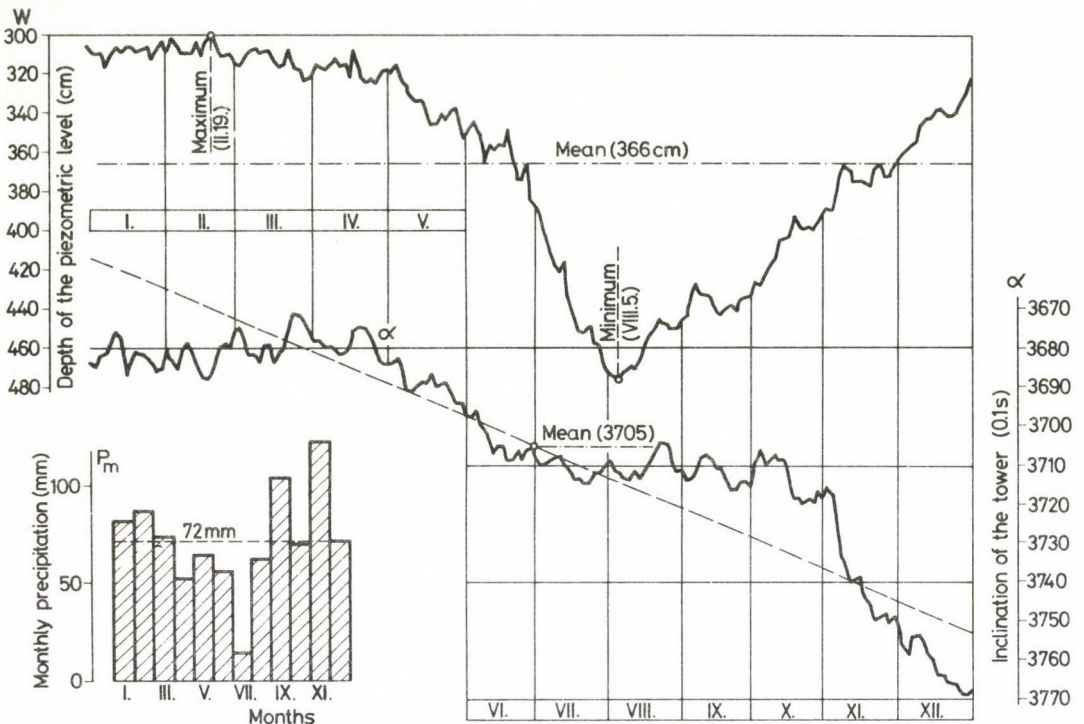
Fig. 2.

The piezometric level reaches on February 19 the highest and on August 5, the lowest level. The difference between them ($\varDelta = 477 - 300 = 177$ cm) is relatively large. The curve is somewhat different from the time series of regular, undisturbed groundwater levels, it practically stagnates in the first three months of the year, the approximately linear section for the preceding five months joins the horizontal section without transition. The curves also reveal that for any construction work beneath the surface, July and August represent the most favourable period.

The curve of the inclinations is much less regular. Its most conspicuous characteristics is that the average values for the end of the year are considerably higher than those for the beginning of the year. The calendar year can be divided into four periods: the rate of inclination stagnates or slightly decreases from January until the end of March (middle of April), then it increases; from the end of July it stagnates again and, from October 11, it starts to increase rapidly.

The distribution of the precipitation is unimodal, having a November maximum and a strikingly low July minimum. This character of the precipitation points toward the effect of the sea.

Using the curves of averages we are able to investigate whether there exists a correlation $v_\alpha = f(\vartheta_w)$ between the rate of inclination (v_α) and the rate of change of the piezometric level (ϑ_w), and, if so, what is the time lag if any in the process.

Fig. 3.

This investigation can be accomplished only, if the abscissa axis of the α-curve is previously modified. This is needed because — in contrast with the W-curve — this curve does not close in itself. The values at the beginning of the year are always higher than those at the end. This increasing inclination of the tower amounts in average to 8.02 0.1 s/month which means that the α-values have to be reduced by 0.2673 0.1 s for every calendar day. The new curve (Fig. 3) gives rise to the following statements.

(a) The modified curve is bimodal: it has two minima, and two maxima.

(b) The W-curve being unimodal (which is usually characterizing groundwater time-curves), curve W and curve α are not conform. So for example, the piezometric level rises rapidly from the beginning of August, however, the inclination which has been "liberated" from the trend increases to half time only and decreases onwards.

In order to prove the non-accidental character of this phenomenon (i.e. it's not being the effect of anomalies in one or two years), the modified α-curves have been constructed for each calendar year. The right procedure will be to determine best fitting straight lines for the α-values of respective year and to plot continuously, according to their signs, the α' ordinate — differences between the measured values and the said line. The α' curves thus obtained are given on Fig. 4. Here, trends for each calendar year and the time series of average α'-values for the years 1967 to 1975 are presented. It can be seen that the character of the curves is for each year identical.

Based on the curves on Figs 3 and 4, it can be stated that the velocity of the inclination is independent of the velocity of the variation of the water level.
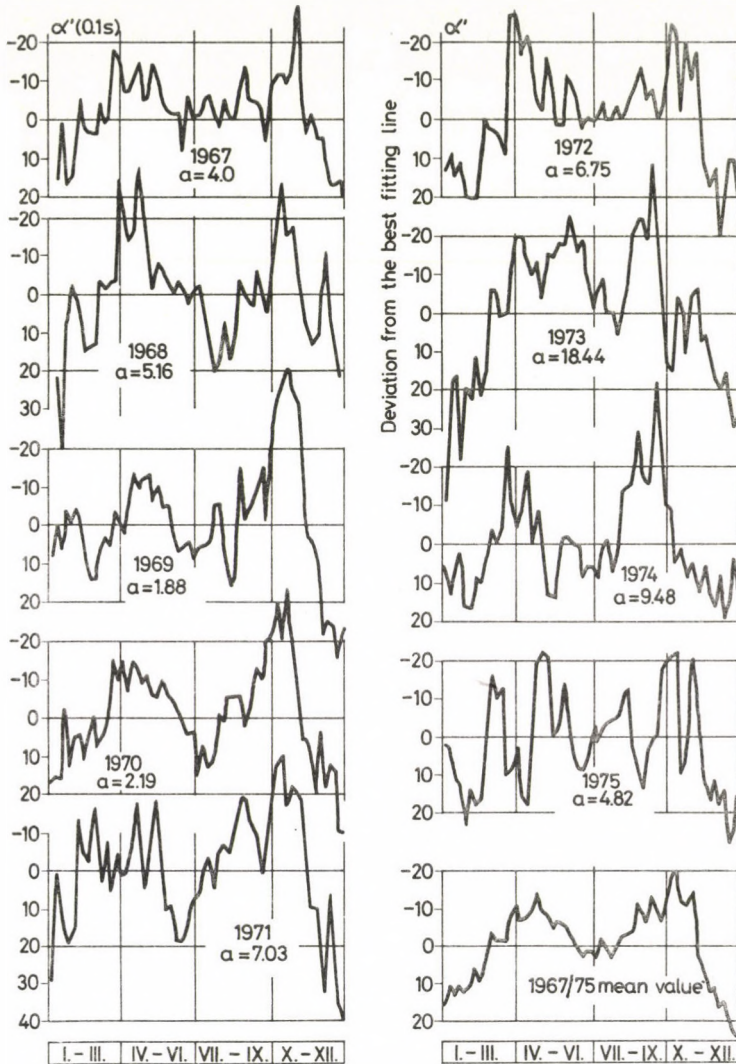
9

Fig. 4.

3. Analysis of curves averaged over many years

3.1 Piezometric level

The curve constructed from the monthly averages for the years 1967 to 1975 is given on Fig. 5. The following statements can be made.

(a) The piezometric level was high between 1967 and 1970 ($\bar{W} = 246$ cm), then it started to fall, reaching in 1973 and 1974 the deepest point ($\bar{W} = 566$, 541 cm,
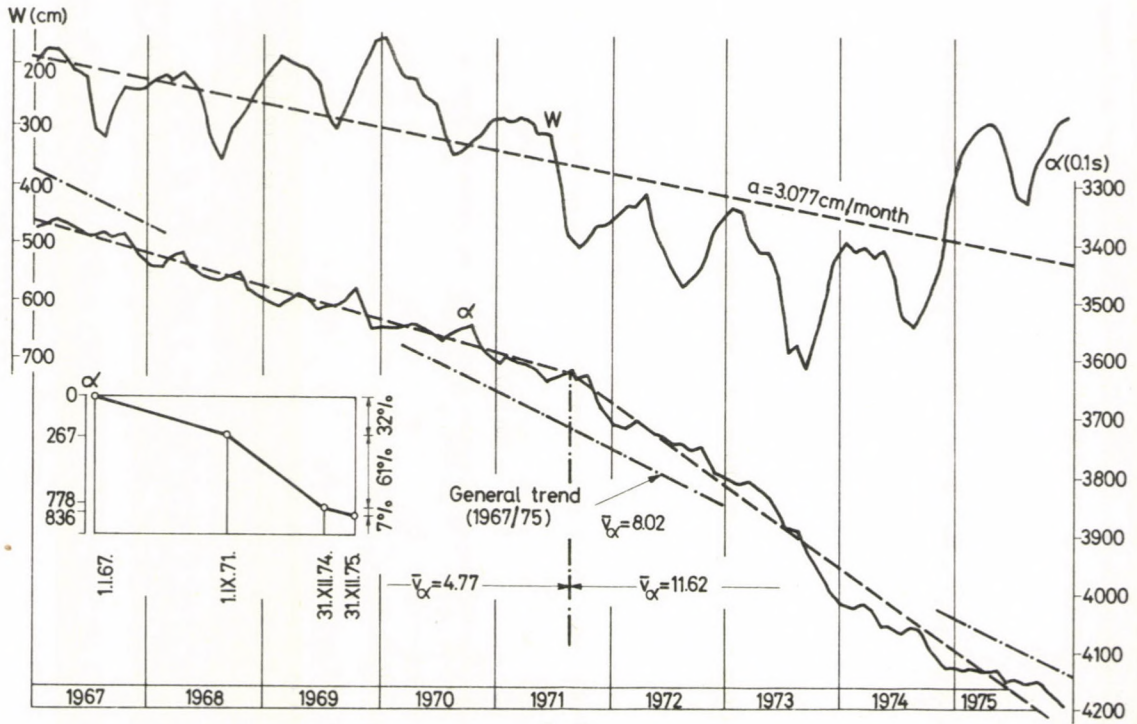
Fig. 5.

respectively). The mean value for 1975 is again near the values measured in 1967 to 1970.

(b) The seasonal fluctuation in each year is clearly visible; the nine curves are rather conform.

(c) The inclination of the best fitting straight line is significant: $a = 3.077$ cm/month which corresponds to 3.32 cm in 9 years. To fit the curve, not a single straight line, but a polygon consisting of three linear sections is suited best.

The influence of the precipitation on the curve of the piezometric levels can be evaluated as follows.

The first question is, whether the difference between two successive maxima or minima of the groundwater levels is determined by the precipitations in this period. The limit values and their differences were the following:

	1967	1968	1969	1970	1971	1972	1973	1974	1975
Maximum	145	200	165	130	260	380	415	480	285
ΔE_M		-55	35	35	-130	-120	-35	-65	195
Minimum	345	390	335	370	515	595	730	685	480
ΔE_m		-45	55	-35	-145	-80	-135	45	205

Correlating the ΔE_M values with the precipitation sum for the months II., III., ..., I., and the ΔE_m values with those for the months VIII., IX., ... VII., the following relationships are obtained:

$$\Delta E_M = 0.3150 \sum_{\text{II.}}^{\text{I.}} P - 321$$

and

$$\Delta E_m = 0.2476 \sum_{\text{VIII.}}^{\text{VII.}} P - 265.$$

The correlation coefficients: 0.677 and 0.588, respectively (the latter is smaller, most likely because the minimum is governed also by temperature which was disregarded here).

In determining the relationship the difference of the data for the years 1974 and 1975 has not been considered.

According to the pairs of point of Fig. 6a and Fig. 6b, the water level in 1975 was 2.80 m higher than would be justified by the amount of precipitation.

The equations may be used also to determine that amount of yearly precipitation which would ensure a dynamic equilibrium:

$$P_{cr} = \frac{321}{0.3150} = 1019, \qquad P_{cr} = \frac{265}{0.2476} = 1070 \text{ mm}.$$
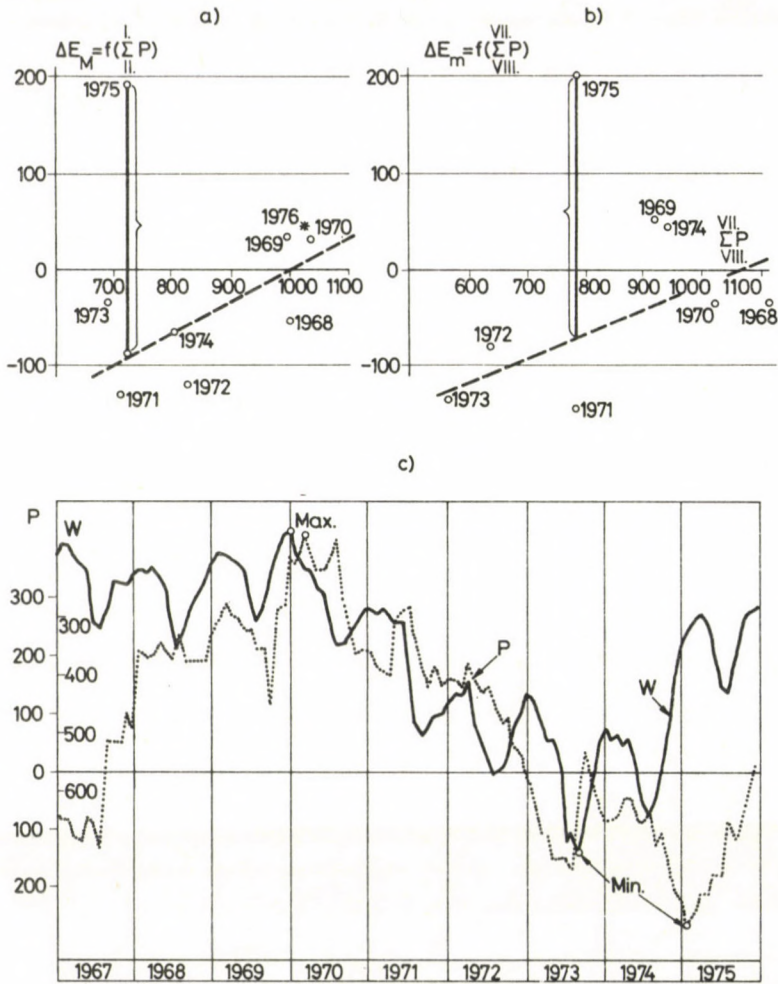
Fig. 6.

Although, the other factors of the water household are not known, it seems that the amount of the critical amount of precipitation is higher than the usual one.

Another check which has to be performed: comparison of the curve of the piezometric levels for many years with the integral curve of the precipitation anomalies. The latter is obtained by forming then summing the differences between the monthly effective precipitation and the calculated average values. Based on Table 3., the measured value in January 1967 was 33 mm, the average of 9 years 83 mm, thus the anomaly $33 - 83 = -50$. For February 1967: $60 - 89 = -29$; the sum: $-50 - 29 = -79$. The final result and the W-curve — copied from Fig. 5 — is given on Fig. 6c. The comparison of these time series leads to the following conclusions:

(a) The curves between 1968 and 1974 run similarly;

(b) Based on the precipitation anomalies in 1967 one would expect a higher ground water level in 1968;

(c) There was a significant shortage of precipitation between November 1973 and February 1975, notwithstanding, the piezometric level kept rising (cf. with the statements in connection with Figs 6a and 6b).

3.2 Inclination of the tower

The time series formed by the monthly averages of the α-values are given on Fig. 5.

The best fitting straight line for all points ($n = 9.12 = 108$) has the equation:

$$\alpha = 8.0192 \cdot n + 3268$$

wherein n is the serial number of the month (January $1967 \equiv 1$); its coefficient has a dimension of 0.1 s/month; the constant 0.1 s.

As can be seen on the figure, this trend line represents a crude approximation only. Based on the relative position of the points, the nine years can be divided into three characteristic periods. These are:

I.: January 1, 1967 to August 31, 1971

II.: September 1, 1971 to December 31, 1974

III.: January 1, 1975 to December 31, 1975.

The constants of the best fitting straight lines for the three periods are (σ_f is the residual standard deviation):

	v_α	r	σ_f
I.	4.769	0.984	13.94
II.	12.768	0.986	24.56
III.	4.822	0.907	7.73

The increment of the inclination is thus made up of three parts (see the diagram in the left corner of Fig. 5): in the first 4.7 years and in the last year occurred 39 per cent of the movement, in the 3.3 years in between 61 per cent. In the period II., the velocity of the movement is 1.7 times greater than in the two others.

3.3 Autoregression investigations

In order to investigate the periodicity which is hidden in the data, autoregression (autocorrelation) functions were prepared. These are given in Fig. 7. There were $9 \times 12 = 108$ data, the width of the interval $i = 1$ month. The p-values which are written on the
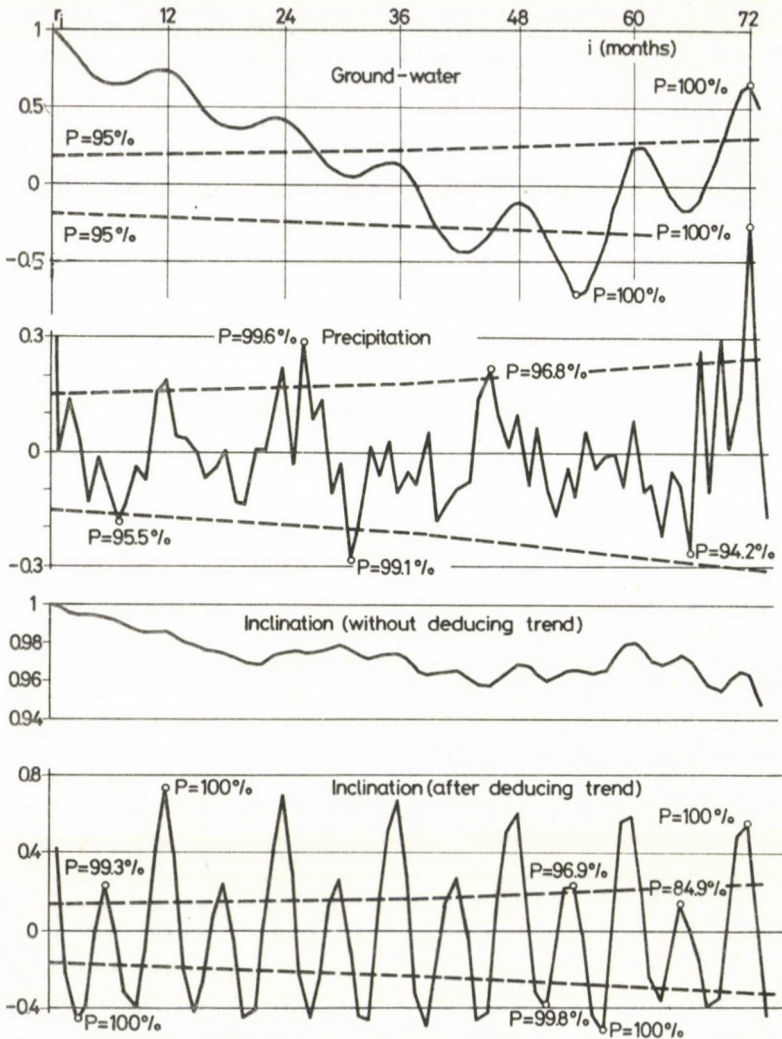
Fig. 7.

curves, were calculated from Anderson's formula:

$$CL = \frac{-1 \pm t_p \sqrt{n+1-i}}{n-i}$$

wherein CL is the critical correlation coefficient, t_p the functional value, calculated from the normal distribution to the probability p, n — the number of data (here $n = 108$), i — the serial number of the month (here 1 to 72). The dashed line connects the CL-values which belong to the probability $p = 95$ per cent ($t_p = 1.645$).

The autocorrelograms can be evaluated as follows.

The autocorrelogram of the groundwater is quite regular, its shape coincides with the regular. The location of the negative minimum points out that the length of the period is 10 years.

The autocorrelation function of the precipitation is much more irregular, the r_i-values are much smaller, consequently, the reliability $p = 95$ per cent is passed in a few months only.

The first diagram related to the inclination values was prepared by making use of the rough α-values (monthly averages); the great trend value in the time series distorts the autocorrelogram. The r_i-values are exceedingly great and the periodicity becomes blurred. This difficulty can be overcome if the best fitting straight line of the α-values is calculated for each calendar year and the deviations from these (α') are taken as a basis of the autoregression investigation. The lowest curve on Fig. 7 proves that thus the periods become distinct: there is a stronger 12 months-period and a weaker 6 months-period. The confidency-levels of the local peaks — with one exception — are all greater than 95 per cent.

The curse of the autocorrelograms in one calendar year can be studied best by calculating the mean of the r_i-values which pertain to $12k + 1, 12k + 2, \ldots, 12(k + 1)$ (Fig. 8).

Although, according to Figs 7 and 8 the autocorrelograms of the groundwater level and of the inclination are both very regular; there are two very substantial differences:

(a) curve W has a single peak in one year, whereas curve α' has two;

(b) the r_i-values of the peaks in the W-curve are functions of i, those pertaining to the peaks of the curve α' are approximately identical. This means that W varies periodically, α' cyclically.

4. Calculation of the critical piezometric level

4.1 Determination of the empirical functions

The empirical distributions of the α and W-values (Fig. 1) and the curves of the averages (Fig. 5) point toward the conclusion that the rate of inclination of the tower depends on the depth of the piezometric level, i.e.

$$v_\alpha = f(\bar{W})$$

wherein $\bar{W}$ is the mean water level of the period concerned.

Now, the year has to be divided into periods, within which the function $f(\bar{W})$ is unequivocal and relatively tight. For this purpose, every month is divided into three parts and the arithmetic mean of α for every decade calculated. Determining now and plotting the mean values for 1967 to 1970 and for 1971 to 1974 respectively, a very interesting picture is obtained which reveals the behaviour of the Tower. (The upper two lines on Fig. 9.)
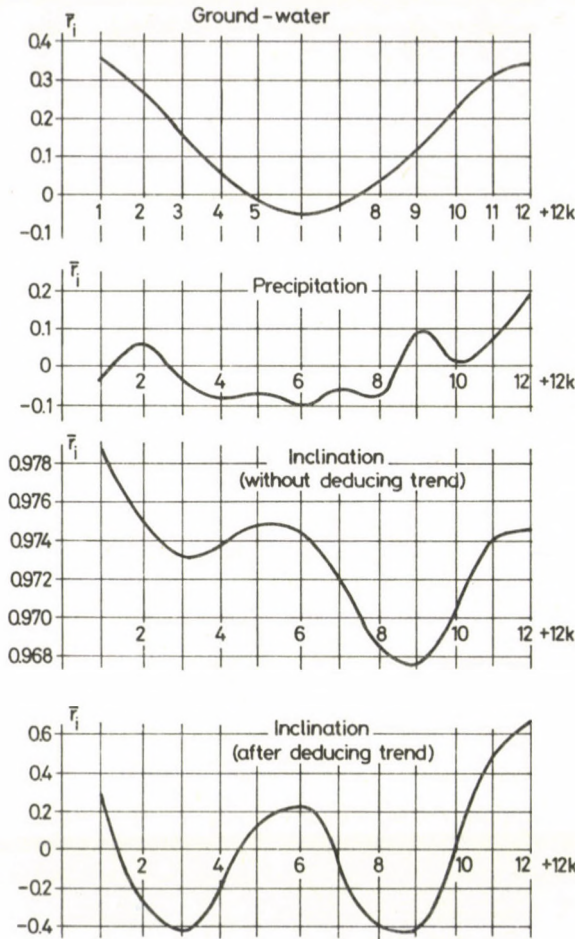
Fig. 8.

(a) In the years with a high water level, the tower is found on October 25 in the same position as it was at the beginning of the year;

(b) in the years with a low water level the successive inclination starts at the beginning of April.

(c) Based on the trend-values exhibited on the first curve, the total calendar year can be divided into four periods (a to d).

The functional relationship will be obtained by calculating for the periods a to d of each calendar year (now including 1975 too) the average trend of the inclination (v_α) and by plotting these vs. the average water level during these periods (Fig. 10). Then, correlating these sets of data the constants a and b in the equation

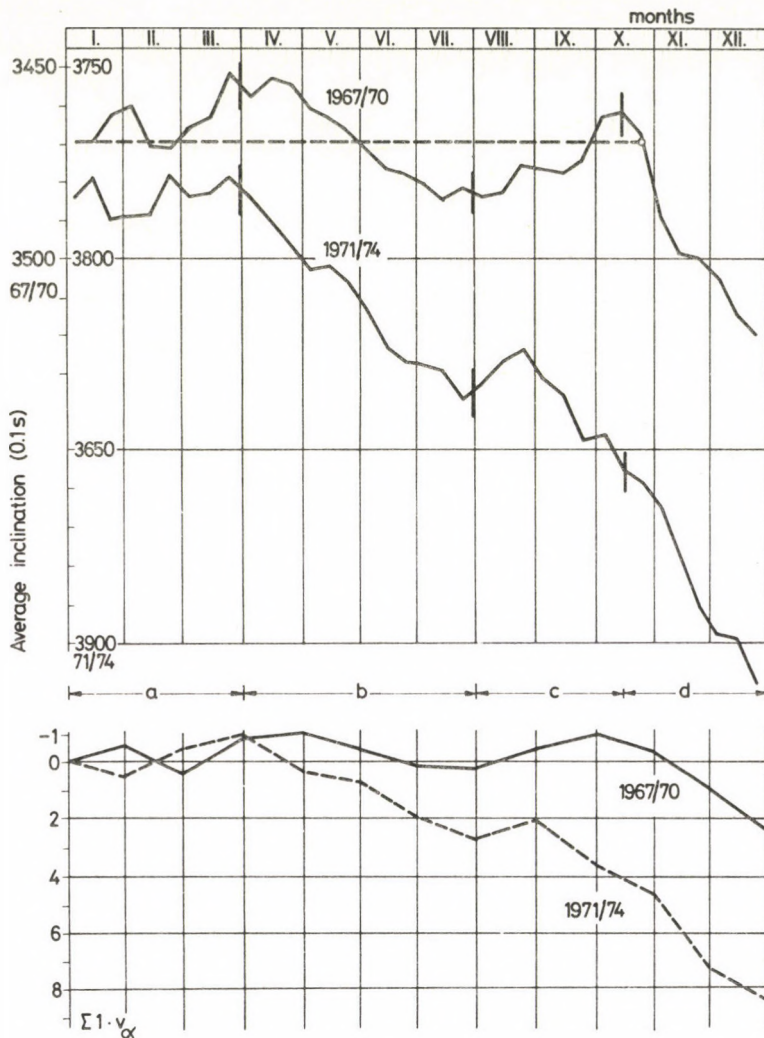$$v_\alpha = a\overline{W} + b$$

can be determined.

Fig. 9.

The results of the calculations are given in Table 4, displaying values of the correlation coefficient r, the standard deviation σ_{v_α} of the v_α-s and the s_f standard deviation around the best fitting straight line. According to this (see also Fig. 10), the interdependence of v_α and $\bar{W}$ in the period d is practically zero, afterwards it increases successively. Between August 1 and October 15 a variation of 1 m in $\bar{W}$ means approximately 1 s/month in the velocity of the inclination. Table 4 shows clearly that the period a can be described with the slightest residual standard deviation ($\sigma_f = 2.70$), period d has a much higher value ($\sigma_f = 7.73$).

Another possibility for the investigation consists in calculating for each calendar months (i.e. for 108 months) the velocity of the inclination and in determining the mean

Table 4. The relationships $v_\alpha = f(\overline{W})$

a) For four periods of the year

Period	a	b	r	$\sigma_{v\alpha}$	σ_f
a	0.010747	−5.55	0.429	2.99	2.70
a	0.022302	3.57	0.656	4.42	3.34
c	0.092463	−41.17	0.908	14.66	6.15
d	−0.002117	25.77	−0.036	7.74	7.73
		Mean:	0.507	7.45	4.98

b) For calendar months

Month	a	b	r	$\sigma_{v\alpha}$	σ_f
I.	4.920	−1.32	0.614	0.95	0.75
II.	−6.712	−1.84	−0.613	1.32	1.04
III.	1.359	−0.93	0.127	1.30	1.29
IV.	7.660	−2.37	0.593	1.60	1.29
V.	−1.721	1.10	−0.383	0.56	0.51
VI.	4.042	−0.69	0.661	0.82	0.61
VII.	4.183	−1.48	0.539	1.12	0.94
VIII.	−0.188	−0.21	−0.023	1.08	1.08
IX.	8.350	−3.37	0.747	1.71	1.14
X.	1.666	0.17	0.309	0.80	0.76
XI.	3.060	0.84	0.337	1.24	1.17
XII.	0.679	0.94	0.087	0.95	0.95
		Mean:	0.419	1.12	0.85

c) For the whole year

a	b	r	$\sigma_{v\alpha}$	σ_f
0.031106	−4.75	0.838	4.74	2.59

values for the months I., II., III., ..., XII., separately for the periods 1967 to 1970 and for 1971 to 1974, respectively. The two curves in the lower part of Fig. 9 show the continuous sums of the so obtained $\bar{v}_\alpha$-values; the difference between the two curves is similar to that of the curves obtained for the periods $a - d$.

In the possession of the monthly trend-values new better differentiated relationships can be found between v_α and $\overline{W}$(including again the year 1975). Results of the regression calculations are summarized in Table 2. It can be concluded that:

(a) excluding three months, the velocity of the inclination increases with increasing depth of the groundwater level, most sensitively in September and January;

(b) the slightest error occurs in the description for the months May and June, the greatest in March and April.

It is possible to determine a correlation between the yearly average values of v_α and $\overline{W}$(see Table 4 and Fig. 10). The approximation of this correlation is a function
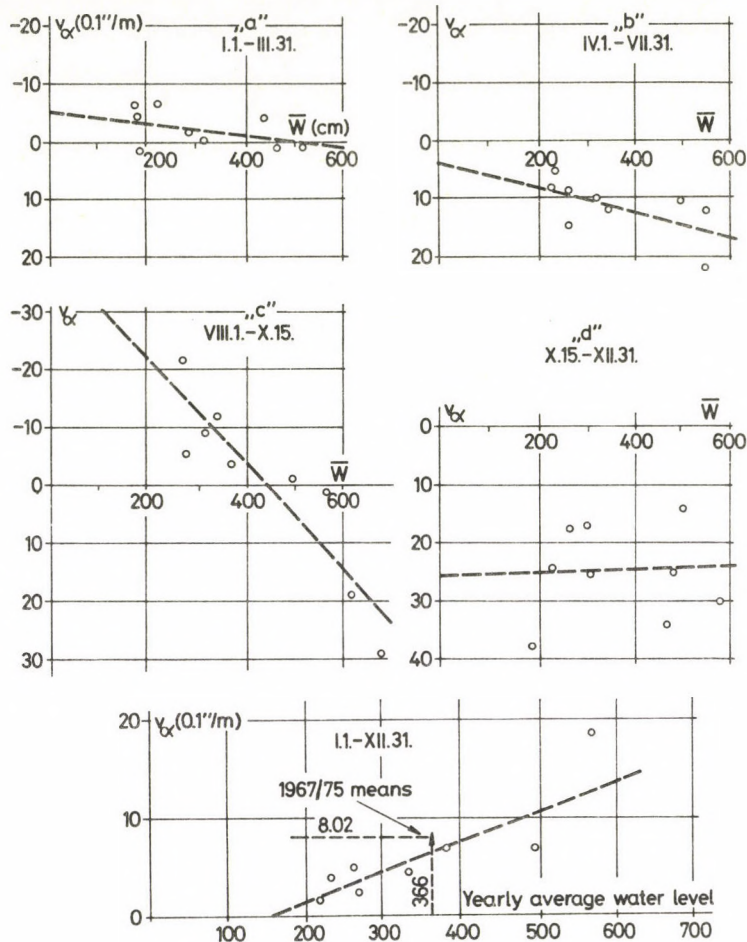
$$v_\alpha = f(W),$$

Fig. 10.

where W is the water level observed on any one day of the year; expediently at the beginning of it. (The search for this correlation is encouraged by the similarity of the yearly water level variations.) The results of the calculations:

Date	a	b	r	σ_f
I. 1.	0.02724	−2.01	0.685	3.45
II. 1.	0.02912	−2.40	0.766	3.04
III. 1.	0.03068	−3.09	0.744	3.16
IV. 1.	0.02834	−2.36	0.801	2.83

With decreasing time scores the tightness of the correlation increases. Starting with the April 1 water level a similar accuracy can be achieved in the prognosis ($\sigma_f = 2.83 \sim 2.59$ 0.1 s/month) which is rather surprising, since the water level on April 1, "does not know" the meteorological data to occur in April to December.

4.2 Checking the empirical functions

The above described empirical relationships are suitable to describe the movement of the Tower based on the knowledge of the piezometric levels.

The increments $\Delta\alpha$, calculated by the equations determined for the periods a to d for the years 1967 to 1975 are given in Table 5. The second column contains the average water level for the period in consideration, the third column its product with the a-

Table 5. Calculation of the polygon describing inclination by using the relationships for the periods a to d

Year	Av. water level	$a \cdot \bar{W}$	Trend	$\Delta\alpha_i$	$\Sigma\Delta\alpha_i$	Values at year's end		
						Measured	Calculated	Difference
67	182	1.956	−3.59	−10.8				
	231	5.152	8.72	34.9				
	284	26.259	−14.91	−37.3				
	240	−0.508	25.26	63.2	50.0	3433	3426	7
68	228	2.450	−3.10	−9.3				
	257	5.732	9.30	37.2				
	319	29.496	−11.67	−29.2				
	256	−0.542	25.23	63.1	61.8	3506	3488	18
69	194	2.085	−3.47	−10.4				
	235	5.241	8.81	35.2				
	276	25.520	−15.65	−39.1				
	182	−0.385	25.38	63.5	49.2	3554	3537	17
70	184	1.977	−3.57	−10.7				
	261	5.821	9.39	37.6				
	345	31.900	−9.27	−23.2				
	304	−0.644	25.13	62.8	66.5	3595	3604	−9
71	286	3.074	−2.48	−7.4				
	323	7.204	10.77	43.1				
	496	45.862	4.69	11.7				
	471	−0.997	24.77	61.9	109.3	3710	3713	−3
72	438	4.707	−0.84	−2.5				
	490	10.928	14.50	58.0				
	563	52.057	10.89	27.2				
	482	−1.020	24.75	61.9	144.6	3810	3857	−47
73	456	4.900	−0.65	−1.9				
	569	12.690	16.26	65.0				
	681	62.967	21.80	54.5				
	576	−1.219	24.55	61.4	179.0	4016	4036	−20
74	504	5.416	−0.13	−0.4				
	553	12.333	15.90	63.6				
	619	57.235	16.06	40.2				
	491	−1.039	24.73	61.8	165.2	4125	4202	−77
75	320	3.439	−2.11	−6.3				
	340	7.583	11.15	44.6				
	384	35.506	−5.66	−14.2				
	292	−0.618	25.15	62.9	87.0	4190	4289	−99
					$\Sigma = 912.6$			

value given in Table 4b. Adding to this the constant b v_α is obtained. Multiplying this with the length of the time intervals a to d (3, 4, 2.5, 2.5 months, respectively), $\Delta\alpha_i$ results. Since the difference between the α values for the date December 31, 1975 and January 1, 1967, amounts to $4190 - 3376 = 814$ 0.1 s, and the calculated value is

$$\Sigma\Delta\alpha_i = 912.6 \quad 0.1 \text{ s,}$$

it can be concluded that by using the four empirical functions it is possible to give a prognosis for nine years with an accuracy of 12 per cent.

The calculations of the polygon by making use of the monthly trend is shown in Table 6. Here

Table 6. Calculation of the polygon describing inclination by using the relationships for the calendar months

Year	W	$\Delta\alpha_i$	$\sum_1^{12}\Delta\alpha_i$	Year	W	$\Delta\alpha_i$	$\sum_1^{12}\Delta\alpha_i$	Year	W	$\Delta\alpha_i$	$\sum_1^{12}\Delta\alpha_i$
67	196	−5.3		70	147	−9.0		73	435	12.3	
	174	−10.0			189	8.5			443	−17.0	
	177	−10.4			215	−9.6			490	−4.0	
	195	−13.1			223	−9.9			513	23.4	
	208	11.2			246	10.2			516	3.2	
	219	2.9			264	5.7			559	23.6	
	303	−3.2			310	−2.7			687	20.9	
	320	−4.0			354	−4.1			673	−5.0	
	271	−16.6			345	−7.4			708	38.1	
	238	8.5			325	10.6			642	18.6	
	240	23.6			310	26.8			595	39.9	
	240	16.6	20.2		291	17.1	36.2		526	19.5	173.5
68	229	−2.9		71	284	1.2		74	494	16.7	
	224	5.0			293	−1.9			512	−24.0	
	231	−9.3			282	−8.2			505	−3.7	
	214	−10.9			293	−1.9			520	24.2	
	231	10.6			310	8.5			507	3.5	
	256	5.2			311	8.5			552	23.1	
	328	−1.6			379	1.6			631	17.4	
	357	−4.1			484	−4.5			645	−4.9	
	305	−12.4			505	12.7			608	25.6	
	281	9.5			491	14.8			575	16.9	
	260	24.5			470	34.2			520	36.4	
	236	16.6	30.2		467	18.9	83.9		428	18.5	149.7
69	203	−4.8		72	447	13.2		75	346	5.7	
	184	9.0			435	−16.2			314	−4.1	
	194	−10.0			431	−5.2			299	−7.9	
	198	−12.8			412	11.8			297	−1.4	
	204	11.3			486	4.0			305	8.7	
	228	3.5			514	20.8			344	10.5	
	280	−4.6			549	12.3			415	3.9	
	309	−4.0			569	−4.7			431	−4.3	
	266	−17.2			561	19.7			358	−5.7	
	225	8.1			535	15.9			327	10.7	
	190	21.3			486	34.9			293	26.0	
	155	15.7	15.5		461	18.9	125.4		283	17.0	59.1

$$\Sigma\Delta\alpha = 693.7 \ \frac{365.22}{365} = 704 \quad 0.1 \text{ s},$$

the accuracy of the prognosis is then 14.8 per cent. From the connection between the yearly average values of W and v_α we obtain

$$\Sigma\Delta\alpha = 717 \quad 0.1 \text{ s};$$

the accuracy is 11.9 per cent.

Calculations using the water levels on April 1 furnish

$$\Sigma\Delta\alpha = 711 \quad 0.1 \text{ s};$$

with an accuracy of 12.7%.

The comparison of the measured and calculated date is given on Fig. 11.

Computed from the piezometric levels on January 1, and on February 1, 1976, the position of the Tower for December 31, 1976 will be

$$\alpha = 4190 + (0.02724 \cdot 260 - 2.01)12 = 4251$$
$$\alpha = 4190 + (0.02912 \cdot 250 - 2.40)12 = 4249 \text{ resp.}$$

in 0.1 s. According to the calculations related to the period 1967 to 1975, the average difference between the measured and the computed values is 26 per cent, and thus the forecast for the inclination can be given as

$$\alpha = 425'' \pm 2.2''$$

4.3 Calculation of the critical water level

About half of the values of the constant b in equation $v_\alpha = f(\overline{W})$ is negative (see Table 4). It can be hoped rightly that there exists a $W_{\text{crit}} > 0$ piezometric level to which $\Delta\alpha = 0$ belongs. This critical level can be determined by putting

$$\Sigma v_{\alpha_i} \cdot T_i = \Sigma(\alpha_i W_{\text{crit}} + b_i)T_i = 0.$$

i is the serial number of the interval, T_i is their length. According to Table 4, using the time intervals a to d:

$$(0.010747 \cdot W_{\text{cr}} - 5.55)3 + (0.022302 \cdot W_{\text{cr}} + 3.57)4 +$$

$$+ (0.092463 \cdot W_{\text{cr}} - 41.47)2.5 + (-0.002117 \cdot W_{\text{cr}} + 25.77)2.5 = 0,$$

wherefrom

$$W_{\text{cr}} = \frac{41.62}{0.347314} \equiv 120 \text{ cm.}$$

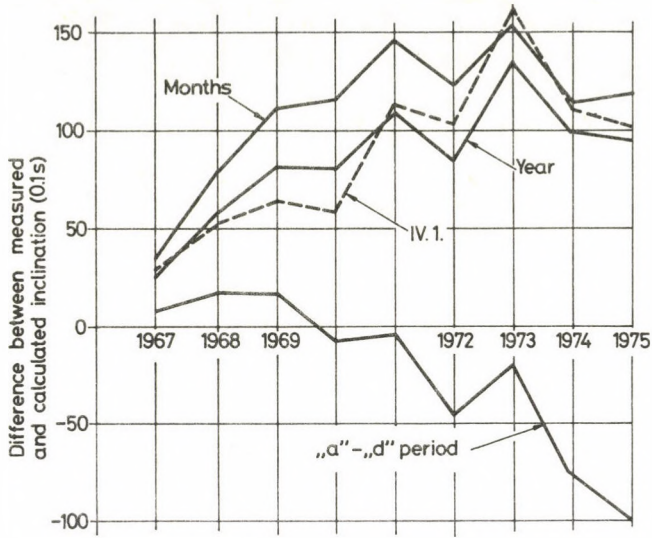With similar considerations, using monthly intervals one gets
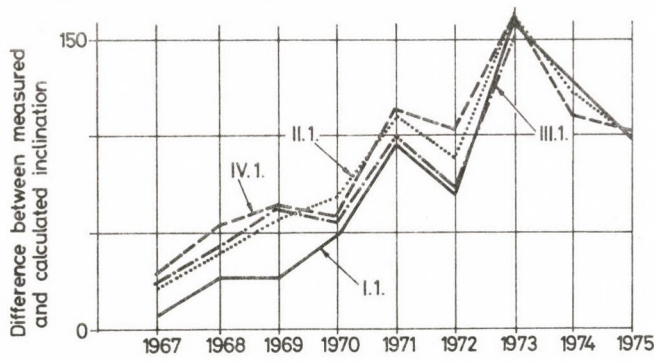
Fig. 11.

$$W_{cr} = \frac{5.4748}{0.027295} = 201 \; cm,$$

from the means of W and v_α

$$W_{cr} = \frac{4.75}{0.031106} = 153 \; cm.$$

Starting from the variations at the beginning of the year:

from January $\qquad W_{cr} = \dfrac{2.01}{0.02724} = \; 74 \; cm,$

February $\qquad W_{cr} = \dfrac{2.40}{0.02912} = \; 82 \; cm,$

$$\text{March} \qquad W_{cr} = \frac{3.09}{0.03068} = 101 \text{ cm,}$$

$$\text{April} \qquad W_{cr} = \frac{2.36}{0.02834} = 83 \text{ cm,}$$

their arithmetic mean $\bar{W}_{cr} = 85$ cm.

Although the final values of the 9 year-prognosis are rather similar (see Fig. 11), but the polygons which belong to the water levels at the beginning of the year are more irregular than the others, therefore it is justified to use a factor of 0.5. Thus

$$W_{cr} = \frac{120 + 201 + 153 + 0.5 \cdot 85}{3.5} = 148 \text{ cm.}$$

Keeping the piezometric level at 148, *the inclination of the tower will not change* in a period of one calendar year, the levels at the beginning and at the end of the year will be identical.

4.4 Other effects

The original shape of the series of the α-values shows a rather irregular polygon.

One of the reasons for the irregularities is likely the limited accuracy of the measurements. It can be, however, easily proved, that other effects are also interfering. By calculating the monthly trends of the inclination the standard deviations σ_f around the best fitting straight lines were also obtained. Their monthly mean values for the period 1967 to 1975 are shown on Fig. 12a. According to this, there are also cyclical elements in the time series of α. It could be ascertained, by analyzing several relationships, that the values a, r and σ_f, which characterize the function $v_\alpha = f(W)$ change continuously during the year; one of the consequencies of this is the bimodality of curve α'.

The autoregression investigations have proven that there is a sharper 12 month-period and a weaker 6-month period in the series of the α-values in contrast to the W-curve having a single period. An interesting result is obtained if the differences of the ordinates of curves α' and W are plotted: the line is a rather regular sinusoidal curve (Fig. 12b).

Comparing the phenomena which were described above, the conclusion can be brought that these are due to the yearly rhythm of the temperature changes. This has a double effect: it induces stresses and deformations in the superstructure and causes changes in the moisture content of the subsoil. It is very likely that the former effect is here stronger and causes that the southern side of the Tower, due to the insolation, expands more than the northern side and, since the Tower leans toward the South, the recorded inclination will be smaller in summer. The effects on both the structure and the subsoil could be separated if not only the inclination but also the differential settlements of the foundation had been measured.
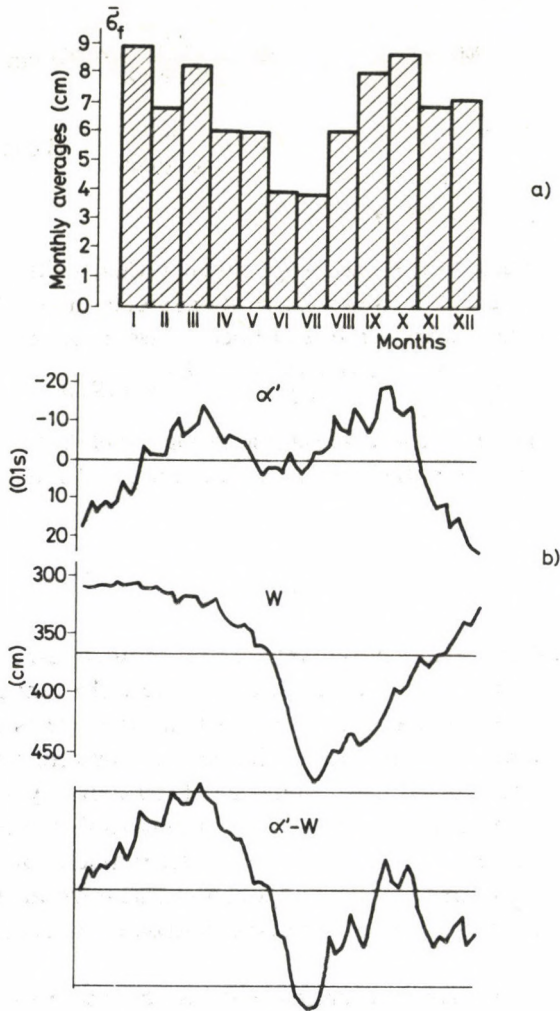
Fig. 12.

It could also be suggested that there is an effect of the precipitations. This forms a considerable amount of surface water, there may be some leakage from the drainage system which may change the moisture content of the soil etc. This effect is in all probability not significant since the measurements did not show anomalies in months with high precipitations. However, it must not be disregarded as is proven by the following.

After calculating the value α to be expected at the end of each time interval (March 31, July 31 etc.) by using the coefficients obtained for the time intervals a to d, the differences between these and the time values will be formed. Then, for each interval, a relationship

$$\alpha_{\text{measured}} - \alpha_{\text{calculated}} = f(\Delta P)$$

can be found, where ΔP is the difference between the effective and mean sum of precipitation in the respective time interval. The tightness of the relationship is different for the intervals; it amounts to

$$
\begin{aligned}
\text{for interval } a \quad & r = -0.232 \\
b \quad & r = -0.287 \\
c \quad & r = +0.416 \\
d \quad & r = +0.141
\end{aligned}
$$

According to this the effect of the precipitations is strongest between August 1 and October 15; the positive sign means that the inclination of the Tower will be greater than expected with increasing amount at precipitation (positive P-anomaly). The calculation with yearly data results in a similar figure ($r = +0.31$).

The effect of wind must not be excluded either. It was observed in Hungary that the majority of chimney stacks tilts toward S—SE; this can be explained partly by the main wind direction (N—NW) and partly by the residual deformation of the building materials, due to the elevated insolation.

In order to demonstrate the consequencies of secondary effects and to prove the results obtained so far and to clarify further the causes of the movement, following investigations seem useful:

— comparison of the movements of the Dome with the leaning of the Tower and with the geohydrological characteristics;

— comparative analysis of the leaning and of the settlement differences measured on the base;

— comparison of the fluctuations of the upper and lower ground water levels;

— investigation of the interaction between leaning, settlement differences and insolation;

— analysis of water pumping elsewhere in the town;

— study of both the direction and intensity of wind.

5. Conclusions

It could be proven unequivocally that the velocity of the inclination is in correlation with the position of the groundwater level and not with the velocity of its fluctuation. Through the arrangement of available data the conclusion could be brought about, that in the period 1967 to 1970 (having high piezometric level) the Tower was in the same position about October 25 as at the beginning of January; on the other hand, in the period 1971 to 1974 (having low piezometric level) the inclination increased rapidly from the beginning of April.

The relationship $v(\alpha) = f(\bar{W})$, determined for different periods, and the relationships $v_\alpha = f(W)$, determined for four water levels at the beginning of the year, served to calculate a critical piezometric level, at which the increment of the inclination

becomes zero. This level is given by

$$W_{cr} = 148 \text{ cm}.$$

If we keep this level constant, the further increase of the tilting will stop.

The introduction of data for the years 1976 and 1977 has not considerably changed the results obtained earlier, indicating thus the persistence of discovered regularities.

NUMERICAL SOLUTION OF EIGENVALUE PROBLEMS
WITH EIGENVALUE PARAMETER
IN THE BOUNDARY CONDITIONS

T. TARNAI*—M. KURUTZ**—G. POPPER***

There are linear problems in the theory of vibration and stability of continuous structures which can be described by differential equations having eigenvalue parameter in the boundary conditions. Applying the finite difference method for solving the problem, an algebraic eigenvalue problem of a lambda-matrix of the same degree as in the original problem is obtained. However, the finitization under the same conditions by a method of Ritz—Galerkin type may increase the degree of the lambda-matrix. A comparison between the mentioned finitizing methods is given by the example of the lateral buckling of a beam hung at both ends.

1. Introduction

It is well-known that for linear problems, under certain restrictions, the finite difference method and the Galerkin method with finite elements are, in general, perfectly equivalent [6]. The Galerkin method with finite elements gives results which are identical to those obtained by the finite difference method.

However, there are linear problems leading to eigenvalue problems with eigenvalue parameter in the boundary conditions for which this statement does not hold. Applying the finite difference method and the Galerkin method with finite elements under the same restrictions for solving these problems, in general, different algebraic eigenvalue problems are obtained.

In the theory of vibration and stability of continuous structures there are problems known for a long time where the boundary conditions are functions of the eigenvalue parameter. In his book Collatz [2] has collected some of such problems.

Although, recently many papers have been published in the topic [4, 7, 10, 12], the theory of differential operators with eigenvalue parameter in the boundary conditions is not worked out so well as that of differential operators whose boundary conditions are independent of the eigenvalue parameter. There are known problems in which the eigenvalues can also be complex numbers. If we want to embed the problem into the theory of Hilbert space then a question is how the selfadjointness is to be

* Dr. T. Tarnai, Hungarian Institute for Building Science, Dávid Ferenc u. 6., H-1113 Budapest, Hungary
** Dr. M. Kurutz, Technical University of Budapest, Dept. of Civil Engineering Mechanics, Műegyetem rkp. 3., H-1111 Hungary
*** Dr. G. Popper, Technical University of Budapest, Dept. of Civil Engineering Mechanics, Műegyetem rkp. 3., H-1111 Budapest, Hungary

defined in order that the spectrum be contained in the reals. Another question is how to give matrix representations of these operators, independent of the eigenvalue parameter, namely, due to the classical theory, all the base functions have to satisfy all the boundary conditions [1]. These mathematical questions have only been partly answered and they have many consequences in the numerical computations.

In this paper, a comparison between the main finitizing techniques, the finite difference method and the finite element method joined with the Galerkin method, is made by the example of the lateral buckling of a beam hung at both ends. This engineering problem can mathematically be written as the eigenvalue problem $A_0 \theta - \lambda A_1 \theta - \lambda^2 A_2 \theta = 0$ of differential operators A_0, A_1, A_2 with boundary conditions linearly containing the eigenvalue parameter λ.

2. Lateral buckling of beams hung at both ends

2.1 Equation of the problem

The differential equation of equilibrium of a laterally buckled thin-walled beam with open constant mono-symmetric cross-section, where the displacements are small, is as follows [11]:

$$EJ_\omega \theta'''' - GJ_t \theta'' + (r - 2t)(M_x \theta')' - (v - t)p\theta - \frac{M_x^2}{EJ_y}\theta = 0 \tag{1}$$

under the boundary conditions

$$\theta''(0) = 0, \tag{2a}$$

$$\theta''(L) = 0, \tag{2b}$$

$$EJ_\omega \theta'''(0) - GJ_t \theta'(0) + (f_0 - t)M_x'(0)\theta(0) = 0, \tag{2c}$$

$$EJ_\omega \theta'''(L) - GJ_t \theta'(L) + (f_L - t)M_x'(L)\theta(L) = 0 \tag{2d}$$

with the notation

x, y, z rectangular coordinates (see Fig. 1),

θ angle of rotation of the cross-section in the $x - y$ plane,

t distance from the centroid to the shear centre,

v distance from the centroid to the point of application of the load,

L span of the beam,

f_0, f_L distances from the centroid to the point of attachment of the rope at the end cross-sections $z = 0$ and $z = L$, respectively,

r cross-sectional radius: $r = J_x^{-1} \int_F y(x^2 + y^2)dF$,

J_x, J_y moments of inertia of the cross-section with respect to the x and y axes,

F area of the cross-section,
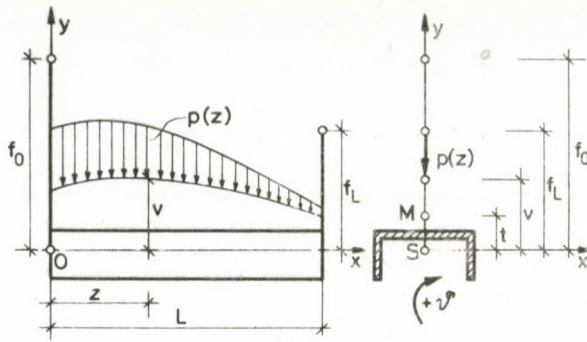
J_t torsional constant of the cross-section,

Fig. 1.

J_ω warping constant of the cross-section,
E modulus of elasticity,
G modulus of elasticity in shear,
p transverse load, considered positive in the negative direction of y,
M_x bending moment in the beam in the $y-z$ plane, considered positive if tensional stresses are in the bottom fibre,
$(.)'$ $= d/dz$ symbol of differentiation with respect to variable z.

The boundary conditions (2a, b) express that the end cross sections are warping free and the boundary conditions (2c, d) express the equilibrium of inner and outer twisting moments in the end cross-sections.

Let λ denote the load parameter. Let p_0 and M_{x0} denote the basic values of the load and the bending moment functions, respectively. By introducing notations

$$\alpha = r - 2t, \qquad \beta = v - t,$$

$$\gamma_0 = f_0 - t, \qquad \gamma_L = f_L - t$$

(1) and (2a–d) assume the following form:

$$EJ_\omega \theta'''' - GJ_t \theta'' - \lambda[-\alpha(M_{x0}\theta')' + \beta p_0 \theta] - \lambda^2 \frac{M_{x0}^2}{EJ_y}\theta = 0 \tag{3}$$

$$\theta''(0) = 0, \tag{4a}$$

$$\theta''(L) = 0, \tag{4b}$$

$$EJ_\omega \theta'''(0) - GJ_t \theta'(0) + \lambda\gamma_0 M'_{x0}(0)\theta(0) = 0, \tag{4c}$$

$$EJ_\omega \theta'''(L) - GJ_t \theta'(L) + \lambda\gamma_L M'_{x0}(L)\theta(L) = 0. \tag{4d}$$

It can be seen that boundary conditions (4c, d) are functions of the parameter λ. Let us introduce the following notations:

$$A_0 \theta = EJ_\omega \theta'''' - GJ_t \theta'', \tag{5}$$

$$A_1 \theta = -\alpha(M_{x0}\theta')' + \beta p_0 \theta, \tag{6}$$

$$A_2\theta = \frac{M_{x0}^2}{EJ_y}\theta. \tag{7}$$

The differential expressions A_0, A_1, A_2 with the boundary conditions (4a–d) denote linear differential operators. Then equation (3) with the boundary conditions (4a–d) may be written as

$$(A_0 - \lambda A_1 - \lambda^2 A_2)\theta = 0. \tag{8}$$

Equation (8) seems to be a quadratic eigenvalue problem where operators A_0, A_1, A_2 are symmetric and the operator A_2 is positive as well.

Let the scalar product of complex functions f, g be defined as

$$\langle f, g \rangle = \int_0^L f(z)\overline{g(z)}\mathrm{d}z.$$

Forming the scalar product of the left hand side of equation (8) and the element θ, considering the boundary conditions (4a–d) and the fact that $M_{x0}(0) = M_{x0}(L) = 0$, we obtain

$$\int_0^L EJ_\omega|\theta''|^2\mathrm{d}z + \int_0^L GJ_t|\theta'|^2\mathrm{d}z - \lambda\left[\alpha\int_0^L M_{x0}|\theta'|^2\mathrm{d}z + \right.$$

$$\left. + \beta\int_0^L p_0|\theta|^2\mathrm{d}z - \gamma_0 M'_{x0}(0)|\theta(0)|^2 + \gamma_L M'_{x0}(L)|\theta(L)|^2\right] - \lambda^2\int_0^L \frac{M_{x0}^2}{EJ_y}|\theta|^2\mathrm{d}z = 0. \tag{9}$$

If λ is an eigenvalue and θ is the corresponding eigenfunction then equation (9) is satisfied. Let us denote the coefficients of λ^i ($i = 0, 1, 2$) in (9) by a, b, c, respectively. Relationship (9) can be considered as a quadratic equation

$$a - \lambda b - \lambda^2 c = 0. \tag{10}$$

Since numbers a, b, c are real and $a \geq 0$, $c \geq 0$ as well, it follows that the discriminant of equation (10) is non-negative: $b^2 + 4ac \geq 0$, consequently the eigenvalue λ is real. *Thus the problem (3, 4a–d) can have only real eigenvalues.*

2.2 The finite difference method

At writing the difference equations we use the order of succession as follows: (4a), (4c), (3), (4d), (4b).

So we obtain a quadratic eigenvalue problem of square matrices:

$$(\mathbf{A}_0 - \lambda\mathbf{A}_1 - \lambda^2\mathbf{A}_2)\mathbf{\theta} = \mathbf{0}. \tag{11}$$

The elements in the first and last rows of matrix $\mathbf{A}_1$ and in the first two and last two rows of matrix $\mathbf{A}_2$ will be zeros. Let us use equidistant subdivision of the interval $[0, L]$ and differences approximating the differentials with error of the same order of

magnitude. In spite of the fact that we apply central difference expressions for equation (3), because of the boundary conditions, the matrices will not be symmetric except matrix A_2 which is diagonal. We mention here, that if the order of magnitude of the errors of the various difference expressions is not required to be the same then matrix A_0 can also be symmetric.

It can be seen that the finite difference method has a quadratic eigenvalue problem of matrices (11) corresponding to the original quadratic eigenvalue problem of differential operators (8). Dependence of the boundary conditions on λ appears mainly in matrix A_1.

2.3 The finite element Galerkin method

Let us denote the quadratic pencil $A_0 - \lambda A_1 - \lambda^2 A_2$ shortly by A. Elements of domain of definition D_A of operator A are functions belonging to class $C^4(0, L)$ and satisfying boundary conditions (4a–d).

Let N be a fixed integer. Let us look for the approximation of the exact solution in the N-dimensional subspace D_A^N of the infinite dimensional space D_A in the form of the linear combination

$$\theta^N = \sum_{i=1}^N a_i \phi_i, \quad \phi_i \in D_A^N \tag{12}$$

where $\{\phi_i\}_{i=1}^N$ is the system of base functions and $\{a_i\}_{i=1}^N$ are the unknown coefficients.

In accordance with the Galerkin principle the error vector $\theta - \theta^N$ has to be orthogonal to the N-dimensional subspace spanned by the base vectors ϕ_1, $\phi_2, \ldots, \phi_N$. This condition leads to a system of linear equations as follows:

$$\sum_{i=1}^N a_i \langle A\phi_i, \phi_j \rangle = 0 \qquad j = 1, 2, \ldots, N \tag{13}$$

where real scalar product is defined:

$$\langle A\phi_i, \phi_j \rangle = \int_0^L A\phi_i \phi_j \, dz, \quad \phi_i, \phi_j \in D_A.$$

Let us use the equidistant subdivision of the interval $[0, L]$:

$$z_0 = 0 < z_1 < z_2 < \ldots < z_n < z_{n+1} = L \tag{14}$$

and search the approximate solution function $\theta^N(z)$ in a piecewise polynomial form

$$\theta^N(z) = \theta_k^N(z), \quad z \in [z_{k-1}, z_k], \quad k = 1, 2, \ldots, n+1.$$

The degree number and the coefficients of the polynomial with respect to section (element) $[z_{k-1}, z_k]$ can be determined from the continuity conditions for the function $\theta^N(z)$. Firstly, let us choose functions satisfying the continuity conditions but not necessarily the boundary conditions. Such a system of functions (not yet base functions) $\{\bar{\phi}_k^0, \bar{\phi}_k^1\}_{k=0}^{n+1}$ belonging to boundary and inner dividing points $\{z_k\}_{k=0}^{n+1}$ can be

$$\bar{\phi}_k^0(z) = \begin{cases} \dfrac{2}{l^2}(z-z_{k-1})^2 - \dfrac{1}{l^4}(z-z_{k-1})^4, & z \in [z_{k-1}, z_k] \\[2mm] 1 - \dfrac{4}{l^2}(z-z_k)^2 + \dfrac{4}{l^3}(z-z_k)^3 - \dfrac{1}{l^4}(z-z_k)^4, & z \in [z_k, z_{k+1}] \\[2mm] 0 & z \notin [z_{k-1}, z_{k+1}] \end{cases}$$

$$\bar{\phi}_k^1(z) = \begin{cases} -\dfrac{1}{l}(z-z_{k-1})^2 - \dfrac{1}{l^2}(z-z_{k-1})^3, & z \in [z_{k-1}, z_k] \\[2mm] (z-z_k) - \dfrac{2}{l}(z-z_k)^2 + \dfrac{1}{l^2}(z-z_k)^3, & z \in [z_k, z_{k+1}] \\[2mm] 0 & z \notin [z_{k-1}, z_{k+1}] \end{cases} \qquad (15)$$

where $l = L/(n+1)$. These functions are shown in Fig. 2. It is easy to see that functions (15) belonging to points $\{z_k\}_{k=2}^{n-1}$ automatically satisfy all the boundary conditions since their value on the first and last elements is zero. In the case of the functions belonging to points z_1 and z_n, respectively, we have to take care of satisfying the boundary conditions, which can modify also the other functions.

Let us satisfy the boundary conditions with the help of functions (15). For this reason let us write the function $\theta^N(z)$ on the first and last elements of the interval, and in order to distinguish it from its final form, let us mark it by a superscript tilde:

$$\tilde{\theta}^N(z) = c_0 \bar{\phi}_0^0 + b_0 \bar{\phi}_0^1 + c_1 \bar{\phi}_1^0 + b_1 \bar{\phi}_1^1, \qquad z \in [z_0, z_1], \qquad (16a)$$

$$\tilde{\theta}^N(z) = c_n \bar{\phi}_n^0 + b_n \bar{\phi}_n^1 + c_{n+1} \bar{\phi}_{n+1}^0 + b_{n+1} \bar{\phi}_{n+1}^1, \qquad z \in [z_n, z_{n+1}]. \qquad (16b)$$

Substituting expressions (16a, b) in boundary conditions (4a–d) we obtain a system of linear equations from which we can express the coefficients belonging to the boundary points by the adjacent coefficients. Thus we have

$$c_0 = \frac{A_0 c_1 + B_0 b_1}{F_0}, \qquad c_{n+1} = \frac{A_L c_n + B_L b_n}{F_L},$$

$$b_0 = \frac{C_0 c_1 + D_0 b_1}{F_0}, \qquad b_{n+1} = \frac{C_L c_n + D_L b_n}{F_L} \qquad (17)$$

in which

$$A_0 = A_L = -\frac{12EJ_\omega}{l^2} + 2GJ_t,$$

$$B_0 = -B_L = -\frac{6EJ_\omega}{l} - GJ_t l,$$

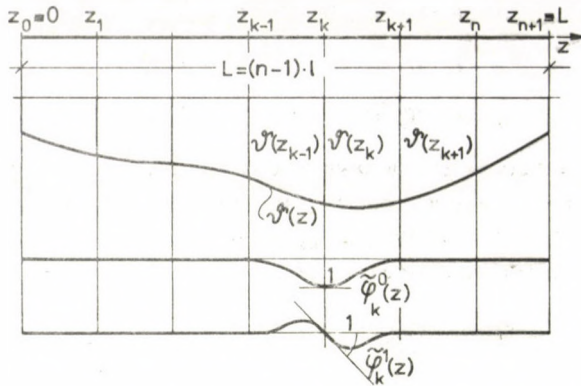$$C_0 = \frac{48EJ_\omega}{l^3} + 2\lambda\gamma_0 M'_{x0}(0).$$

Fig. 2.

$$C_L = -\frac{48EJ_\omega}{l^3} + 2\lambda\gamma_L M'_{x0}(L),$$

$$D_0 = -\lambda\gamma_0 l M'_{x0}(0),$$

$$D_L = \lambda\gamma_L l M'_{x0}(L),$$

$$F_0 = \frac{24EJ_\omega}{l^2} + 4GJ_t + 2\lambda\gamma_0 l M'_{x0}(0),$$

$$F_L = \frac{24EJ_\omega}{l^2} + 4GJ_t - 2\lambda\gamma_L l M'_{x0}(L). \tag{18}$$

Replacing c_0, c_{n+1}, b_0, b_{n+1} in (16a, b) by expressions (17) we have

$$\tilde{\vartheta}^N_{0,1}(z) = \frac{1}{F_0}(A_0 c_1 + B_0 b_1)\tilde{\phi}^0_0 + \frac{1}{F_0}(C_0 c_1 + D_0 b_1)\tilde{\phi}^1_0 + c_1\tilde{\phi}^0_1 + b_1\tilde{\phi}^1_1,$$

$$\tilde{\vartheta}^N_{n,n+1}(z) = \frac{1}{F_L}(A_L c_n + B_L b_n)\tilde{\phi}^0_{n+1} + \frac{1}{F_L}(C_L c_n + D_L b_n)\tilde{\phi}^1_{n+1} + c_n\tilde{\phi}^0_n + b_n\tilde{\phi}^1_n. \tag{19}$$

Since F_0 and F_L contain parameter λ, they cannot be in the denominator. Multiplying (19) by $F_0 F_L$, we obtain the approximate function on the first and last elements, respectively, in the form:

$$\theta^N_{0,1}(z) = c_1\phi^0_1 + b_1\phi^1_1,$$

$$\theta^N_{n,n+1}(z) = c_n\phi^0_n + b_n\phi^1_n \tag{20}$$

where $\theta^N_{0,1}(z) = F_0 F_L\tilde{\vartheta}^N_{0,1}(z)$ and $\theta^N_{n,n+1}(z) = F_0 F_L\tilde{\vartheta}^N_{n,n+1}(z)$, and ϕ^0_1, ϕ^1_1 and ϕ^0_n, ϕ^1_n are the base functions belonging to points z_1 and z_n, respectively, satisfying the continuity conditions and the boundary conditions:

$$\phi^0_1 = F_L(A_0\tilde{\phi}^0_0 + C_0\tilde{\phi}^1_0 + F_0\tilde{\phi}^0_1),$$

$$\phi_1^1 = F_L(B_0 \bar{\phi}_0^0 + D_0 \bar{\phi}_0^1 + F_0 \bar{\phi}_1^1),$$

$$\phi_n^0 = F_0(A_L \bar{\phi}_{n+1}^0 + C_L \bar{\phi}_{n+1}^1 + F_L \bar{\phi}_1^0),$$

$$\phi_n^1 = F_0(B_L \bar{\phi}_{n+1}^0 + D_L \bar{\phi}_{n+1}^1 + F_L \bar{\phi}_n^1). \tag{21}$$

These special base functions are shown in Fig. 3. It is important to see that not only the functions belonging to points z_1 and z_n are modified by satisfying the boundary conditions but all the other functions $\bar{\phi}_k^0$, $\bar{\phi}_k^1$, too.

Thus the solution is obtained in the form

$$\theta^N(z) = \sum_{j=1}^n (c_j \phi_j^0 + b_j \phi_j^1), \qquad \phi_j^0, \phi_j^1 \in D_A^N \tag{22}$$

where $N = 2n$ and the base functions contain the second power of parameter λ.

The Galerkin principle with these base functions leads to the homogeneous set of linear equations as follows:

$$\left\langle \left[EJ_\omega \left\{ \sum_{j=1}^n (c_j \phi_j^0 + b_j \phi_j^1) \right\}'''' - GJ_t \left\{ \sum_{j=1}^n (c_j \phi_j^0 + b_j \phi_j^1) \right\}'' + \right. \right.$$

$$+ \lambda \alpha \left\{ M_{x0} \left(\sum_{j=1}^n (c_j \phi_j^0 + b_j \phi_j^1) \right)' \right\}' - \lambda \beta p_0 \sum_{j=1}^n (c_j \phi_j^0 + b_j \phi_j^1) -$$

$$\left. \left. - \lambda^2 \frac{M_{x0}^2}{EJ_y} \sum_{j=1}^n (c_j \phi_j^0 + b_j \phi_j^1) \right], \phi_i^0 \right\rangle = 0,$$

$$\left\langle \left[EJ_\omega \left\{ \sum_{j=1}^n (c_{ij} \phi_j^0 + b_j \phi_j^1) \right\}'''' - GJ_t \left\{ \sum_{j=1}^n (c_j \phi_j^0 + b_j \phi_j^1) \right\}'' + \right. \right.$$

$$+ \lambda \alpha \left\{ M_{x0} \left(\sum_{j=1}^n (c_j \phi_j^0 + b_j \phi_j^1) \right)' \right\}' - \lambda \beta p_0 \sum_{j=1}^n (c_j \phi_j^0 + b_j \phi_j^1) -$$

$$\left. \left. - \lambda^2 \frac{M_{x0}^2}{EJ_y} \sum_{j=1}^n (c_j \phi_j^0 + b_j \phi_j^1) \right], \phi_i^1 \right\rangle = 0, \qquad i = 1, 2, \ldots, n. \tag{23}$$

Considering the fact that both operator pencil A and the base functions ϕ_i^0, ϕ_i^1 contain λ^2, after forming the scalar product, we arrive at a sixth degree eigenvalue problem of square matrices of order $2n$:

$$(\mathbf{A}_0 - \lambda \mathbf{A}_1 - \lambda^2 \mathbf{A}_2 - \lambda^3 \mathbf{A}_3 - \lambda^4 \mathbf{A}_4 - \lambda^5 \mathbf{A}_5 - \lambda^6 \mathbf{A}_6)\boldsymbol{\theta} = \mathbf{0}. \tag{24}$$

In the special case, where the load p is constant and the distances between the centroid and the point of attachment of the rope at both end cross-sections are the same ($f_0 = f_L$) and thus $F_0 = F_L$, the sixth degree eigenvalue problem (24) is reduced to a fourth degree one.

It can be seen that the Galerkin method, where the base functions satisfy all the boundary conditions, has a sixth (fourth) degree eigenvalue problem of matrices (24)
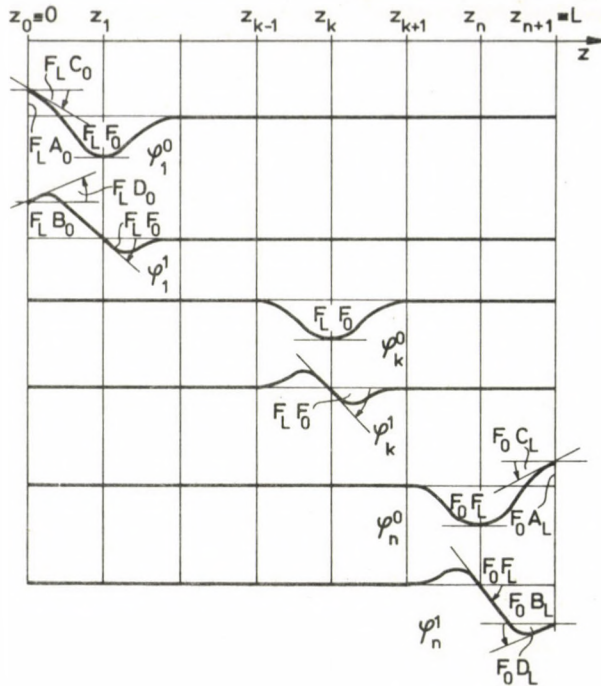
Fig. 3.

corresponding to the original quadratic eigenvalue problem of differential operators (8).

It should be noted that in the case of a similar problem the Rayleigh—Ritz method with base functions satisfying all the boundary conditions leads to an eigenvalue problem higher degree than the original one. This fact was discovered by Falk [5] and was applied e.g. by Zimmermann [14] and Kelkel [8].

2.4 The extended Galerkin method

In the eigenvalue problem (3, 4a–d), (4a) and (4b) are the essential boundary conditions but (4c) and (4d) are the natural boundary conditions. If we use base functions satisfying the essential boundary conditions and not necessarily the natural boundary conditions then the quadratic pencil of linear operators in (3) can be modified by the natural boundary conditions (4c, d). The extended Galerkin statement [3] can be written for functions θ and u satisfying the essential boundary conditions:

$$\int\limits_0^L \left\{ EJ_\omega \theta'''' - GJ_t \theta'' - \lambda [-\alpha (M_{x0} \theta')' + \beta p_0 \theta] - \lambda^2 \frac{M_{x0}^2}{EJ_y} \theta \right\} u \, dz -$$

$$- \{ EJ_\omega \theta'''(L) - GJ_t \theta'(L) + \lambda \gamma_L M'_{x0}(L) \theta(L) \} u(L) +$$

$$+ \{ EJ_\omega \theta'''(0) - GJ_t \theta'(0) + \lambda \gamma_0 M'_{x0}(0) \theta(0) \} u(0) = 0. \tag{25}$$

Integrating the first term by parts, we obtain

$$\int\limits_0^L EJ_\omega \theta'' u'' dz + \int\limits_0^L GJ_t \theta' u' dz - \lambda [\alpha \int\limits_0^L M_{x0} \theta' u' dz +$$

$$+ \beta \int\limits_0^L p_0 \theta u \, dz + \gamma_L M'_{x0}(L) \theta(L) u(L) - \gamma_0 M'_{x0}(0) \theta(0) u(0)] -$$

$$- \lambda^2 \int\limits_0^L \frac{M_{x0}^2}{EJ_y} \theta u \, dz = 0. \tag{26}$$

If we consider the interval $(0, L)$ as single element then base functions can be e.g.: $\phi_1 = 1$, $\phi_2 = z - L/2, \phi_{i+2} = \sin i\pi z/L \, (i = 1, 2, \ldots)$. When the technique of finite elements is used then the spline functions can be of an order lower than in the previous Section (third degree instead of fourth degree). Thus we arrive at a problem

$$(\mathbf{A}_0 - \lambda \mathbf{A}_1 - \lambda^2 \mathbf{A}_2) \boldsymbol{\theta} = \mathbf{0}. \tag{27}$$

It may be seen that the extended Galerkin method has a quadratic eigenvalue problem of symmetric square matrices (27) corresponding to the original quadratic eigenvalue problem of symmetric differential operators (8). Dependence of the boundary conditions on λ appears mainly in matrix $\mathbf{A}_1$.

3. Numerical solution of the algebraic eigenvalue problems

The algebraic eigenvalue problems (24) and (27) are special cases of the generalized eigenvalue problem of lambda-matrix of order n and degree m

$$(\mathbf{A}_0 + \mathbf{A}_1 \lambda + \mathbf{A}_2 \lambda^2 + \ldots + \mathbf{A}_{m-1} \lambda^{m-1} + \mathbf{A}_m \lambda^m) \boldsymbol{\theta} = 0 \tag{28}$$

where $\mathbf{A}_0, \mathbf{A}_1, \ldots, \mathbf{A}_m$ are real square matrices all of order n and either $\mathbf{A}_0$ or $\mathbf{A}_m$ is supposed to be nonsingular [9].

If $\mathbf{A}_m$ is non-singular, the generalized eigenvalue problem (28) can be reduced to the special eigenvalue problem of the hypermatrix

$$\begin{bmatrix} -A_m^{-1}A_{m-1} & -A_m^{-1}A_{m-2} & \cdots & -A_m^{-1}A_1 & -A_m^{-1}A_0 \\ I & 0 & \cdots & 0 & 0 \\ 0 & I & \cdots & 0 & 0 \\ \vdots & \vdots & \vdots & \vdots & \vdots \\ 0 & 0 & \cdots & I & 0 \end{bmatrix} \tag{29}$$

i.e. of the matrix of order $m \times n$ with constant elements. If A_0 is non-singular, a hypermatrix of similar form to (29) can be obtained after introducing a new variable $\kappa = 1/\lambda$.

The hypermatrix (29) is, in general, very badly balanced that is, the corresponding rows and columns have very different norms. Hence before calculating its eigenvalues and eigenvectors it is very important to balance it.

The solution of the standard eigenvalue problem of matrix (29) has been accomplished by a program composed of procedures balance, elmhes, elmtrans, hqr2, and balbak published in Wilkinson—Reinsch [13].

4. Numerical example

Let us consider the steel I beam which has been analysed in [11]. The beam (Fig. 4) is hung at both ends by vertical ropes attached to the upper flange of the beam and is loaded by uniformly distributed forces acting along the centroidal axis of the beam. The data of the beam are the following:

$$J_y = 3.576 \times 10^3 \ cm^4, \qquad v = 0 \ cm,$$

$$J_t = 1.48 \times 10^2 \ cm^4, \qquad f_0 = f_L = 48.16 \ cm,$$

$$J_\omega = 7.364 \times 10^6 \ cm^6, \qquad E = 2.05947 \times 10^7 \ N/cm^2,$$

$$t = 19.44 \ cm, \qquad G = 7.94367 \times 10^6 \ N/cm^2,$$

$$r = -5.22 \ cm, \qquad p_0 = 9.807 \times 10^3 \ N/cm.$$

$$L = 1.25 \times 10^3 \ cm,$$

The case will be examined where the models have three degrees of freedom. This means that in the case of the finite difference method three internal grid points are taken into account and in the case of the (extended) Galerkin method three terms of the series of the displacement function are taken into account.
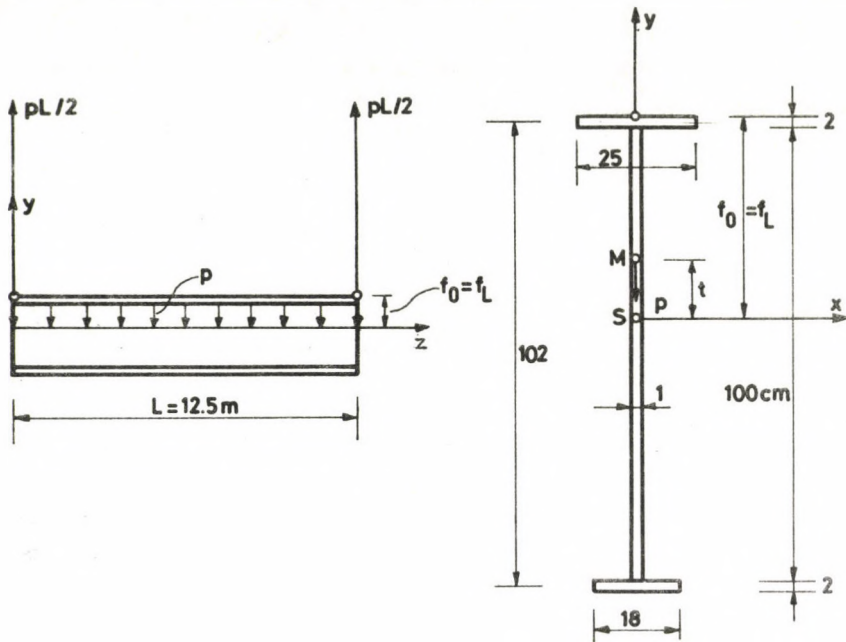
Fig. 4.

4.1. The finite difference method

Using three internal grid points and the four boundary points corresponding to the four boundary conditions, we obtain a quadratic eigenvalue problem of square matrices of order 7. The eigenvalues of this problem are found to be

$$\lambda_1 = 0.000\,000\,00,$$
$$\lambda_2 = +1.295\,388\,25 \times 10^{-2},$$
$$\lambda_3 = -6.459\,504\,84 \times 10^{-3},$$
$$\lambda_4 = +1.948\,567\,69 \times 10^{-1},$$
$$\lambda_5 = -3.236\,827\,31 \times 10^{-2},$$
$$\lambda_6 = +5.731\,911\,57 \times 10^{-2},$$
$$\lambda_7 = -1.088\,715\,81 \times 10^{-1},$$
$$\lambda_8 = -1.878\,914\,73,$$
$$\lambda_9 = \lambda_{10} = \lambda_{11} = \lambda_{12} = \infty,$$
$$\lambda_{13} = -7.037 \times 10^{-1} + i\,7.105 \times 10^{-1},$$
$$\lambda_{14} = -7.037 \times 10^{-1} - i\,7.105 \times 10^{-1}.$$

Analysing these results, we have found that the eigenvalues λ_1 to λ_6 are correct approximations of the eigenvalues of the original problem. However, the eigenvalues λ_7 to λ_{14} are false results, they are not approximations of the eigenvalues of the original problem, their existence is a consequence of the method.

4.2. The Galerkin method

Using either finite elements or the whole interval $(0, L)$ as single element, the Galerkin method results in many false eigenvalues, for example complex numbers not having any physical meaning. Similarly to the finite difference method, the appearance of the false solutions is due to the method itself.

The fact, that in this example the Galerkin method gives also false eigenvalues, was numerically illustrated earlier in [11] and therefore numerical details are omitted here. We only mention that, in the case of three degrees of freedom by the Galerkin method, we obtain 18 eigenvalues from which 6 ones are correct approximations and 12 ones are false.

4.3. The extended Galerkin method

Considering the interval $(0, L)$ as single element and using base functions $\phi_1 = 1$, $\phi_2 = z - L/2$, $\phi_3 = \sin(\pi z/L)$, we have obtained the following eigenvalues:

$$\lambda_1 = 0.000\,000\,00,$$

$$\lambda_2 = +1.428\,711\,88 \times 10^{-2},$$

$$\lambda_3 = -5.881\,827\,12 \times 10^{-3},$$

$$\lambda_4 = +1.348\,126\,00 \times 10^{-1},$$

$$\lambda_5 = -2.272\,187\,58 \times 10^{-2},$$

$$\lambda_6 = +4.195\,927\,02 \times 10^{-1}.$$

It can be seen that all the eigenvalues are real in agreement with the statement in Section 2.1.

5. Conclusions

When one solves a complete eigenvalue problem, and has a lot of solutions, many numbers, it is important to know what are the correct and what are the false values. In the case of the buckling problem treated here, the extended Galerkin method seems to be the only one among the examined methods, in which every eigenvalue is an approximation of the eigenvalues of the original problem and thus this method does not result in false solution.

In this paper some of the theoretical possibilities of the numerical solution of eigenvalue problems with eigenvalue parameter in the boundary conditions were mainly treated. A detailed numerical analysis of the problem will be published elsewhere.

References

1. Akhiezer, N. I.—Glazman, I. M.: *Theory of linear operators in Hilbert space.* Vol. 1. (in Russian). Izd. "Vishcha Shkola", Khar'kov 1977
2. Collatz, L.: *Eigenwertaufgaben mit technischen Anwendungen.* Akademische Verlagsgesellschaft, Leipzig 1949
3. Connor, J. J.—Brebbia, C. A.: *Finite Element Techniques for Fluid Flow.* Newnes-Butterworths, London 1976
4. Evans, W. D.: A Non-Self-Adjoint Differential Operator in $L^2[a, b]$. *Quart. J. Math. Oxford* (2) **21** (1967), 371–383
5. Falk, S.: Das Verfahren von Rayleigh—Ritz mit hermiteschen Interpolations-polynomen. *ZAMM* **43** (1963), 149–166
6. Finlayson, B. A.: *The Method of Weighted Residuals and Variational Principles.* Academic Press, New York 1972
7. Fulton, Ch. T.: Two-Point Boundary Value Problems with Eigenvalue Parameter Contained in the Boundary Conditions. *Proc. of the Royal Society of Edinburgh* **77A** (1977), 293–308
8. Kelkel, K.: Selbstadjungiertheit und Volldefinitheit bei Eigenwertaufgaben der Schwingungslehre, die den Eigenwert (Eigenfrequenz) in den Randbedingungen enthalten. *ZAMM* **58** (1978), T149–T151
9. Popper, Gy.—Gáspár, Zs.: The solution of the algebraic eigenvalue problem by partitioning. EUROMECH 112 Mátrafüred (Hungary) 21–23, February 1979. *Bracketing of eigenfrequencies of continuous structures.* Akadémiai Kiadó (1980), 399–413
10. Schneider, A. A.: Note on Eigenvalue Problems with Eigenvalue Parameter in the Boundary Conditions. *Math. Z.* **136** (1974), 163–167
11. Tarnai, T.: Variational Methods for Analysis of Lateral Buckling of Beams Hung at Both Ends. *Int. J. Mech. Sci.* **21** (1979), 329–337
12. Walter, J.: Regular Eigenvalue Problems with Eigenvalue Parameter in the Boundary Condition. *Math. Z.* **133** (1973), 301–312
13. **Wilkinson, J. H.—Reinsch, C.:** *Linear Algebra,* Handbook for Automatic Computation, Volume II., Springer 1971
14. Zimmermann, R.: Ritzsches Verfahren für Aufgaben mit Eigenwerten in den Randbedingungen. *ZAMM* **50** (1970), 315–316

BOOK REVIEWS

MÓR KORACH–ERIKA KLIMENT: *Chemical Engineering as a Science*. Redaction and postscript by Pál Juhász Nagy, Akadémiai Kiadó, Budapest 1982. 170 pp.

Nearing the end of his career, Academician Mór Korach with his co-worker undertook to compile this comprehensive work based on his widely extended experience and chemical engineering studies. He meant to speak to all those interested in scientific work, in scientific mentality, and even in regularities of the social medium inducing and surrounding science. Once a professor in Bologna, then in Budapest, director of an industrial research laboratory in Faenza, and of a research institute in Budapest, director of the Chemical Engineering Research Institute of the Hungarian Academy of Sciences, he has solved several industrial problems, elaborated inventions, his work is intended as an orientation from the observation tower of chemistry, rather than being concerned with certain branches of chemical technology. This work reflects systems approaching a scientific approach, relevant to still actual questions of "Science of Sciences".

Rather than to present new principles or methods, Mór Korach considered it as a goal of his book to recapitulate engineering experience of a life, hoping "to have outlined of some regularities to unfold, beyond the rather chaotic literature of chemical engineering, in the chemical industry itself". He does not only look back to the past and transmit his generalizable experience, the recapitulated regularities of chemical technology, but he has confidence in future, as written in the preface:

"Looking forward to a future in the evening of my life, I realize the to-be representants of complex sciences as members of a well-attuned, excellent orchestra who are able to play variations even without a conductor, or to create new music, since each musician has a command of his instrument. They would always play something different. They could improvise like Indian orchestras. Namely I am convinced in our scientific circulation a higher-order human community will develop."

The book comprises seven chapters, with preface, postscript, and references. Chapter 1 is concerned with the terminology of chemical engineering; with concepts of technique and technology; fields, development and subregions of chemical engineering. Chapter 2 presents epistemology background of chemical engineering, discussing, among others, the metrological significance of material reality, solid state and invariants. The next chapter is spent on the theoretical fundamentals of chemical engineering. It is followed by the chapter on fundamental and evolutional laws of chemical engineering, then by that on relationships and controversies between chemical engineering and other sciences. A separate part is devoted to the application of theoretical and natural sciences in chemical engineering. The chapter on the methodology of chemical engineering is of special interest.

Part of the theoretical chemical engineering works have already been incorporated into university education as subject matter, and are a guideline in chemical research. In both fields his activity has been of pioneering importance, updating chemical technology and setting out new ways for its development. We as his former co-workers find a special delight in the appearance of this book with the contribution of Mrs. Erika Kliment-Kisdálnoki, as an overall synthesis of Korach's activities. Thanks are due to Mr. Pál Juhász Nagy for his efforts in editing the book.

I hope the confidence of Korach in the future of chemical engineering is right, and this book will be read with interest not only by those concerned with teaching and research in chemical engineering, but also by those active in other fields of science, enjoying the irradiated practical philosophy, the colourful expressions and metaphores.

K. Polinszky

Proceedings of an International Symposium on Absorbed specific energy and/or strain energy density criterion in memory of the late Professor László GILLEMOT

The Publishing House of the Hungarian Academy of Sciences, in common with the Martinus Nijhoff Publishers Co., has published the lectures at the international symposium in commemoration of the late László Gillemot, Academician, in his special scientific fields of activity, specific contraction work and strain energy density criterion, organized upon the initiative of Professor G. C. Sih, at Lehigh University (Betlehem, Pennsylvania, U.S.A.) by Section VI of Technical Sciences of the Hungarian Academy of Sciences.

Lectures were classified into seven groups.

The first group comprises lectures on conditions of crack propagation, of the start of crack propagation.

The second group was concerned with metal fracture phenomena, presenting some interesting tests to illustrate details of this much debated field, far from being reassuringly known.

The third group recapitulates lectures on the fracture of materials recently getting into the foreground of interest, such as plastics, concrete, and rubber-like materials.

The only lecture in the fourth group on photo-elasticity has been spent on applying a photoelastic coat of lacquer on the surroundings of a crack in a thin metal sheet to measure displacements controlling the strain energy, and comparing the results to those obtained by the finite element method.

Short lectures in the fifth group discuss fracture as a consequence of energy density as a controlling criterion.

In the sixth group, short lectures on fatigue failure are found.

The seventh, last group presents some concise reports on experimental and analytic work.

The thirty-three professional lectures in this volume are seen to embrace a wide scope of fracture mechanisms and of the eliciting loading conditions. Lecturers, that is, authors are eminent specialists of these problems, among them G. C. Sih (Lehigh University, U.S.A.), T. Yakobori (Tohoku University, Japan), P. S. Theokaris (Athens National Technical University, Greece), H. P. Stüwe (Erich-Schmid Institut für Festkörperphysik, Austria).

The lively interest raised by the lectures at the Symposium, and the success of the published volume show that it was worth-while organizing this Symposium in Budapest, attended by the internationally most outstanding specialists, giving Hungarian specialists an opportunity both to present their achievements, and to personally meet leading authorities of this profession, to discuss, exchange ideas with those setting the trend of development. Lectures by Hungarian specialists testify it as being reasonable to investigate this subject also in this country, giving rise to internationally appreciable achievements.

Last but not least, this successful meeting held upon an initiative from abroad in memory of the late Prof. László Gillemot added both to his esteem and to the acknowledgement of Hungarian engineering science.

J. Prohászka

ATTILA J. ROOS: *Elektrotechnik anschaulich: Resultierende*, 1982 Roos, Germering BRD, 128 Seiten

Das Buch behandelt die anschaulichen graphischen Verfahren der Elektrotechnik. Die Größen, die sich zeitlich sinusförmig ändern, können mit den Resultierenden niedergeschrieben werden. Die Zeigerdiagramme sind wichtige Bestandteile der Grundlagen der Elektrotechnik.

Das Buch behandelt mehr als 100 Probleme. Die farbigen Bilder, die viele Testfragen und Antworten machen das Buch sehr gut angepaßt für das selbstständige Studium. Für das Verständnis sind elementare algebraische, geometrische und physikalische Kenntnisse genügend.

Dieser Leitfaden kann man für Studenten der Ingenieurschulen und elektrotechnischen Hochschulen empfehlen.

K. Géher

HANS NEUMANN–KLAUS SCHÄFER: *Elektrische und elektronische Meßtechnik.* Akademie-Verlag Berlin 1982, 194 pages

Disregarding simple measurements, the electronic and electrical methods have obtained a leading role in almost every field of the measuring technics. The elements of a typical measuring system are: some kind of sensor, electrical measuring instrument and display or data processing device.

Beside the very comprehensive encyclopedic works made for experts or the monographs discussing certain questions of detail there can hardly be found any such shorter survey, which brings the whole topic to the younger student nearer or to the not professional inquirer without submerging

excessively into the details. The little book, which appeared in the series entitled "Wissenschaftliche Taschenbücher" of the publisher, tries to retrieve this lack.

After discussing the idea of measuring and electrical basic instruments, the presentation of the principles of the bridges and compensators follows. The second half of the book surveys the electronic measuring technology with the same compactness.

The extremely limited volume gives no possibility for much more than to disclose the treasure of the knowledge of the technically educated man. However, this is accomplished on a high, modern level, and it is especially pleasing, that a relatively great part of the last chapter is devoted to the digital technology.

I. P. Valkó

ANDRÁS AMBRÓZY: *Electronic Noise.* Publishing House of the Hungarian Academy of Sciences, Budapest and McGraw-Hill Inc., New York 1982, 28 pages

Many books have been published on electronic noises, but they have not generally been engaged in the whole field. They are either excessively immersed in the mathematical formalism, or they treat noise as a primary physical phenomenon from the point of wiev of the natural scientist, or by heuristically treating the problem of noise reduction, they mainly contain solutions in electric circuits.

The present book of András Ambrózy is free from these onesidednesses. It supplies adequate spaces for the mathematical apparatus as well, as for the physical background and for the practical standpoints of the electronic engineer. Thus, in spite of the high level of the treatment of this topic, it is not necessary to have profound preliminary studies: the older specialist already remembering with difficulty his studies at the university and the student, who has not finished it yet can equally make use of it.

The first chapter gives the explanation of the basic ideas, the second one discusses the most important distribution types and relating mathematical expressions, and in the third one the time and frequency domain characteristics of stochastic signals can be found.

The next chapter contains the physical causes of the origin of noise.

The fifth chapter reviews the noise parameters of linear networks, the sixth chapter treats the noise of bipolar and field effect transistors, also keeping in mind the special circumstances of the integrated

circuit. The next chapter discusses the modifications of noise caused by nonlinear transfer mechanisms. The last chapter is dedicated to the methods for measuring the noise. One or two completely elaborated practical examples are attached to each chapter as well as an abundant literature. The style of the book is clear, the structure of it is logical, therefore, the study of it is not exhausting, although it sticks to scientific exactness.

The original work appeared some years ago in Hungarian (and was sold out very quickly). The author—who have incorporated the results of his own research into the material—has revised the English edition and has brought it up to date.

The book can equally be recommended to electric engineers, in general, and also to those, who want to have a guideline in this field for a more profound investigation.

I. P. Valkó

EDELMANN CHRISTIAN: *Druckmessung und Druckerzeugung.* **Wissenschaftliche Taschenbücher.** (Akademie-Verlag. Berlin 1982) 181 pages. Size 11×19 cm.

The booklet describes the methods available for generation and measurement of pressure, especially of very low pressures (high vacuum). A summary of physics and physical chemistry of gases and vapors covering 35 pages serves as an introduction, needed for the explanation of the very different physical principles of pressure measurement instrumentation.

Measurement of low pressures covers 60 pages. Besides mechanical manometer instruments based on heat conduction and friction, radiometer- and ionization manometers are presented, following by mass-spectrometers for the measurement of partial pressure. Generation of low pressures and its instrumentation covers 45 pages. Beside the description of different types of vacuum pumps, combinations of these are discussed, and some problems of pipe-connections and the detecting of leakages are mentioned. The generation and measurement of high pressures is dealt with far shorter. (15 pages). Thus the reader has the impression that this field is outside of the authors range of interest. No mention is made about the safety devices necessary in operating high pressure apparatus.

The booklet is a useful summary of the physical basis of measuring and generating pressure but is greatly limited in dealing with practical construction and maintenance of pressurizing and

pressure measurement apparatus. The figures are extremely simplified, no pictures of actual instruments are shown at all. So the booklet may be a guide for making up a concept for an experimental procedure but none for the assembly of a measuring device and its maintenance.

Fr. Thamm

ATTILA J. ROOS: *Operations in Electrical Engineering I. Resultants;* 1982 by ROOS, D-8034 Germering, 64 pages

A series of manuals will be published under the title "Operations in Electrical Engineering". The title of the first volume is: "Resultants" and it gives a detailed discussion of the graphical representation of sine functions for students of electrical engineering colleges. The clear understanding of rotating phasors is very important in basic electrical engineering. The book presents a systematic introduction into the subject for almost a hundred problems. Test questions, answers and applications, coloured figures and text help the students in the learning procedure. In order to understand the book, elementary algebra, geometry and physics are sufficient.

K. Géher

ABSTRACTS

Jankó, L.: *Stresses due to slow deformation and shrinkage of prestressed concrete composite girders having adhesive insert* (Mélyépítéstudományi Szemle, Vol 32, 1982, p. 14.)
The most popular procedures concerning the determination of additional stresses resulting from slow deformation and shrinkage of prestressed concrete composite girders having adhesive insert are described and compared.

Lámer, G.: *Dynamic action of the travelling load on continuous girder* (Mélyépítéstudományi Szemle, Vol. 32, 1982, p. 24.)
Under the influence of a force travelling with uniform speed along a two support beam, this one performs bending vibrations. Dynamic test of a continuous girder having a concentrated load performing a steady motion is described. The development of the critical speed as well as the necessity of testing dynamic stability of bridges constructed with 10 spans are shown on appropriate examples.

Márkus, Gy.: *Antimetrically loaded circular plates having spring mounting* (Mélyépítéstudományi Szemle, Vol. 32. 1982, p. 49.)
An analytical solution is provided by the paper for calculating round plates having spring mounting, loaded antimetrically. This method of procedure affords possibility of economizing building materials in case of subsoils having great load bearing capacity.

Jankó, L.: *Elastic load-capacity response of cracked, reinforced concrete beam girders* (Mélyépítéstudományi Szemle, Vol. 32. 1982, p. 106.)
The procedure described in this paper provides a method for computing stress and deformation conditions after cracking of prefabricated beam girders co-operative together with reinforced concrete monolithic slabs. The method of computation is exposed in detail, as well as the stresses of the compression flange as function of the loading process.

Mistéth, E.: *System technical evaluation of networks and establishments made by building engineer* (Mélyépítéstudományi Szemle, Vol. 32, 1982, p. 123.)
The optimization should be carried out according to several points of view, when designing installations and qualifying a work. The most important complex methods of evaluation and the mode of their appreciation are discussed in the paper.

Dulácska, E.: *Test of the stability of reinforced concrete shells of hyperboloid of revolution for cooling towers* (Mélyépítéstudományi Szemle, Vol. 32, 1982, p. 281)
This paper deals with the special relationships of the test of stability of reinforced concrete shells. All the possible forms of buckles of hyperboloid shells of revolution are discussed, together with initial errors to be considered and with the necessary safety factor. The course of the test is illustrated by an example of actual size and real ratio.

Bognár, L.: *Dynamic test of floor discs* (Mélyépítéstudományi Szemle, Vol. 32, 1982, p. 312)
This paper presents relationships allowing exact description of stresses arising in the environment of the junction of floor discs and the bracing walls. Starting from the disc formula it gives the solution for three practical cases. Further solutions may be obtained by using of the three basic cases.

Gábor, P.: *Construction of reinforced concrete highway bridges, taking into account considerations for probability calculation* (Mélyépítéstudományi Szemle, Vol. 32, 1982, p. 368)
The most important points of view of constructing up-to-date, economic and safe bridges are surveyed. The paper deals with the durability, the traffic arrangements, as well as with some problems of the design work, the execution and maintenance.

Varga, L.: *Effects of line load working inside an endless, cylindrical hole* (Mélyépítéstudományi Szemle, Vol. 32, 1982, p. 399)
A symmetrically situated, linear radial load works upon the inside surface of an endless hole having straight axis and circular cross-section. The influences of various load cases are analysed and the non-dimensional multiplicators of the required quantities are provided on a diagram.

. assné, Szücs R.: *Membrane cone-shaped shells having linearly alternating thickness* (Mélyépítéstudományi Szemle, Vol. 32, 1982, p. 409)

Cone-shaped shells having linearly alternating thickness often occur in engineering practice, formulae worked out for their calculation, however, are none. This article renders help for precise reckoning of the structure, in order to simplify shuttering work, and provides formulae of calculation for the commonest load cases in membrane stress state.

Benedek, A.: *Computation of anchored diaphragm walls* (Mélyépítéstudományi Szemle, Vol. 32, 1982, p. 500)
Supporting working pits of Dunakiliti river barrage is planned making use of anchored reinforced concrete diaphragm walls. Various solutions for calculation are analysed with the consideration of the problems of grouting.

Szilvágyi, L.: *Thest of annular foundation body having eccentric load* (Mélyépítéstudományi Szemle, Vol. 32, 1982, p. 515)
Annular solution is used for the foundations of tower-like buildings with high centre of gravity. The article deals with the planning of annular foundation bodies, as well as the general geotechnical calculations necessary to dimensioning.

Czap, Z.: *Examination of a beam resting upon combined half-space* (Mélyépítéstudományi Szemle, Vol. 32, p. 532)
The paper deals with the influence exerted by the dimensions, location and building technology of Underground Railway tunnels on the subsidence of surface, on the basis of a series of finite-element testing. Approximate values are given for the probable magnitude of the subsidences and for the form of the sinking trough.

Kollár, L.: *A paradoxical phenomenon of the shell buckle* (Mélyépítéstudományi Szemle, Vol. 32, p. 558)
In the paper the buckle of the shells of revolution under the influence of internal overpressure is discussed, as well as the behaviour beyond critical stress of shells of revolution and the use of air tent in the meantime.

Holló, E.:—Siklóssy, P.: *Nuclear power plant diagnostics* (VEIKI Közlemények 1982, p. 29)
Our Institute is the designer, partial supplier and executor of the vibration diagnostical system for block 1 in the Paks Nuclear Power Plant. In the treatise the major characteristics of the primary-circuit part, the experience gained during the time of designing, location and commissioning, some results of the measurements conducted during the hot trial run of block 1 as well as the future goal setting of research and development are summarized.

Horváth, Gábor L.: *Possibilities of activity reduction in nuclear power plants* (VEIKI Közlemények 1982, p. 51)
For the calculation of the amount of radioactive wastes in nuclear power plants as well as of the activity of the corrosion products activated on the technological system surfaces outside the active zone the programme system RADSYS-RADTRAN has been developed. In the physicochemical theory, on which the activation calculation is based, we have considered the transport of material both in solved and particle form. The above-mentioned theory presents explanation to the differences between the existing models. The contamination can be reduced by using a particle filter operating at primary-circuit working temperatures. According to our calculation results, without this filter the contamination of the system surfaces by

corrosion products is mostly influenced by the pH. The second part of the programme calculates the dynamics of the arising of radioactive wastes and offers the possibility of detecting the factors mostly influencing the arising wastes.

Pammer, Z.—Szabó, L.: *Solution of elastic/plastic strength tasks with the finite-elements method* (VEIKI Közlemények 1982, p. 191)

The up-to-date strength calculation processes require the consideration of the non-elastic material properties. As a result, in designing machine elements more economic material utilization can be realized, Beside this a more precise determination of the stress and expectable, life of the mechanisms is achievable with the consequence that the safety of the nuclear power plant equipment can be increased. In this paper the finite-elements programme system suitable for solving elastic/plastic problems, developed for the above purposes, is described. A brief survey of the theoretical fundamentals associated with the programme is given and on two rather simple examples the application possibilities illustrated.

CONTENTS
VOLUME 17, NUMBERS 3-4

NOTICE TO CONTRIBUTORS

Papers in English* are accepted to the condition that they have not been previously published or accepted for publication.

Manuscripts in two copies (the original type-written copy plus a clear duplicate one) complete with figures, tables, and references should be sent to the

Acta Technica
Münnich F. u. 7. I. 111A
Budapest, Hungary
H-1051

Although every effort will be made to guard against loss, it is advised that authors retain copies of all material which they submit. The editorial board reserves the right to make editorial changes.

Manuscripts should be typed double-spaced on one side of good quality paper with proper margins and bear the title of the paper and the name(s) of the author(s). The full postal address(es) of the author(s) should be given in a footnote on the first page. An abstract of 50 to 100 words should precede the text of the paper. The paper should not exceed 25 pages including tables and references. The approximate locations of the tables and figures should be indicated on the margin. An additional copy of the abstract is needed. Russian words and names should be transliterated into English.

References. Only papers closely related to the author's work should be referred to. The citations should include the name of the author and/or the reference number in brackets. A list of numbered references should follow the end of the manuscript.

References to periodicals should mention: (1) name(s) and initials of the author(s); (2) title of the paper; (3) name of the periodical; (4) volume; (5) year of publication in parentheses; (6) number of the first page. Thus: 5. Winokur, A., Gluck, J.: Ultimate strength analysis of coupled shear walls. American Concrete Institute Journal 65 (1968), 1029.

References to books should include: (1) author(s) name; (2) title; (3) publisher; (4) place and year of publication. Thus: Timoshenko, S., Gere, J.: Theory of Elastic Stability. McGraw-Hill Company, New York, London 1961.

Illustrations should be selected carefully and only up to the necessary quantity. Black-and-white photographs should be in the form of glossy prints. The author's name and the title of the paper together with the serial number of the figure should be written on the back of each print. Legends should be brief and attached on a separate sheet. Tables, each bearing a title, should be self-explanatory and numbered consecutively.

Authors will receive proofs must be sent back by return mail.

Authors are entitled to 50 reprints free of charge.

* Hungarian authors should send their papers also in Hungarian.

Periodicals of the Hungarian Academy of Sciences are obtainable at the following addresses:

AUSTRALIA
C.B.D. LIBRARY AND SUBSCRIPTION SERVICE
Box 4886, G.P.O., *Sydney N.S.W. 2001*
COSMOS BOOKSHOP, 145 Ackland Street
St. Kilda (Melbourne), Victiria 3182

AUSTRIA
GLOBUS,Höchstädtplatz 3, *1206 Wien XX*

BELGIUM
OFFICE INTERNATIONAL DE LIBRAIRIE
30 A venue Marnix, *1050 Bruxelles*
LIBRAIRIE DU MONDE ENTIER
162 rue du Mindi, *1000 Bruxelles*

BULGARIA
HEMUS, Bulvar Ruszki 6, *Sofia*

CANADA
PANNONIA BOOKS, P.O. Box 1017
Postal Station "B", *Toronto, Ontario M5T 2T8*

CHINA
CNPICOR, Periodical Department, P.O. Box 50
Peking

CZECHOSLOVAKIA
MAD'ARSKÁ KULTURA, Národní třida 22
115. 66 Praha
PNS DOVOZ TISKU, Vinohradská 46, *Praha 2*
PNS DOVOZ TLAČE, *Bratislava 2*

DENMARK
EJNAR MUNKSGAARD, Norregade 6
1165 Copenhagen K

FEDERAL REPUBLIC OF GERMANY
KUNST UND WISSEN ERICH BIEBER
Postfach 46, *7000 Stuttgart 1*

FINLAND
AKATEEMINEN KIRJAKAUPPA, P.O. Box 128 *SF-00101 Helsinki 10*

FRANCE
DAWSON-FRANCE S. A., P. 40, *91121 Palaiseau*
EUROPÉRIODIQUES S. A., 31 Avenue de Versailles, *78170 La Celle St. Cloud*
OFFICE INTERNATIONAL DOCUMENTION ET
LIBRAIRIE,48 rue Gay-Lussac
75240 Paris Cedex 05

GERMAN DEMOCRATIC REPUBLIC
HAUS DER UNGARISCHEN KULTUR
Karl Liebknecht-Straße 9, *DDR-102 Berlin*
DEUTSCHE POST ZEITUNGSVERTRIEBSAMT Straße der
Pariser Kommüne 3 4, *DDR-104 Berlin*

GREAT BRITAIN
BLACKWELL'S PERIODICALS DIVISION
Hythe Bridge Street, Oxford OXI 2ET
BUMPUS, HALDANE AND MAXWELL LTD.
Cowper Works, *olney, Bucks MK46 4BN*
COLLET'S HOLDINGS LTD., Denington Estate *Wellingborough, Northants NN8 2QT*
WM. DAWSON AND SONS LTD., Cannon House *Folkstote, Kent CT19 5EE*
H. K. LEWIS AND CO., 136 Gower Street
London WC1E 6BS

GREECE
KOSTARAKIS BROTHERS INTERNATIONAL
BOOKSELLERS, 2 Hippokratous Street, *Athens-143*

HOLLAND
MEULENHOFF-BRUNA B. V., Beulingstraat 2,
Amsterdam
MARTINUS NIJHOFF B.V.
Lange Voorhout 9—11, *Den Haag*

SWETS SUBSCRIPTION SERVICE
347b Heereweg, *Lisse*

INDIA
ALLIED PUBLISHING PRIVATE LTD., 13/14
Asaf Ali Road,*New Delhi 110001*
150 B-6 Monunt Road, *Madras 600002*
INTERNATIONAL BOOK HOUSE PVT. LTD.
Madame Cama Road, *Bombay 400039*
THE STATE TRADING CORPORATION OF INDIA LTD.,
Books Import Division, Chanralok 36 Janpath, *New Delhi 110001*

ITALY
INTERSCIENTIA, Via Mazzé 28, *10149 Torino*
LIBRERIA COMMISSIONARIA SANSONI, Via Lamarmora 45,
50121 Firenze
SANTO VANASIA, Via M. Macchi 58
20124 Milano
D. E. A., Via Lima 28, *00198 Roma*

JAPAN
KINOKUNIYA BOOK-STORE CO. LTD.
17-7 Shinjuku 3 chome, Shinjuku-ku, *Tokyo 106-91*
MARUZEN COMPANY LTD., Book Department, P.O. Box
5050 Tokyo International, *Tokyo 100-31*
NAKUA LTD. IMPORT DEPARTMENT
2-30-19 Minami Ikebukuro, Toshima-ku, *Tokyo 171*

KOREA
CHULPANMUL, *Phenjan*

NORWAY
TANUM-TIDSKRIFT-SENTRALEN A.S., Karl Johansgatan
41 43, 1000 Oslo

POLAND
WEGIERSKI INSTYTUT KULTURY, Marszalkowska 80,
00-517 warsawa
CKP-I W, ul. Towarowa 28,*00-958 Warszawa*

ROUMANIA
D.E.P., *Bucuresti*
ILEXIM,Calea Grivitei 64-66, *Bucuresti*

SOVIET UNION
SOJUZPECHAT — IMPORT, *Moscow*
and the post offices each town
MEZHDUNARODNAYA KNIGA, *Moscow G-200*

SPAIN
DIAZ DE SANTOS, Lagasca 95, *Madrid 6*

SWEDEN
GUMPERTS UNIVERSITETSBOKHANDEL AB
Box 346, *40125 Göteborg 1*

SWITTZERLAND
KARGER LIBRI AG, Petersgraben 31, *4011 Basel*

USA
EBSCO SUBSCRIPTION SERVICES
P.O. Box 1943, *Birmingham, Alabama 35201*
F.W. FAXON COMPANY, INC.
15 Soutwest Park, *Westwood Mass. 02090*
READ-MORE PUBLICATIONS, INC.
140 Cedar Street, *New York,N.Y. 10006*

YUGOSLAVIA
JUGOSLOVENSKA KNJIGA,Terazije 27, *Beograd*
FORUM,Vojvode Mišića 1, *21000 Novi Sad*